(5.)

Coastal Studies Institute
Center for Wetland Resources
Louisiana State University
Baton Rouge, Louisiana 70803

Technical Report No. 238

# DOCUMENTATION AND ANALYSIS OF COASTAL PROCESSES, NORTHEAST COAST OF BRAZIL

By J. N. Suhayda, S. A. Hsu, H. H. Roberts, and A. D. Short

August 1977

Coastal Studies Institute

Center for Wetland Resources

Louisiana State University

Baton Rouge, Louisiana 70803

⑨

⑭ $TR-238$

Technical Report No. 238

⑥ # DOCUMENTATION AND ANALYSIS OF COASTAL PROCESSES, NORTHEAST COAST OF BRAZIL.

⑩ By J. N. Suhayda, S. A. Hsu, H. H. Roberts, and A. D. Short

Joseph    Harry    Andrew

⑮ $N00014-75-C-0192$

⑪ August 77

⑫ 107 p.

086 700

# ABSTRACT

A multidisciplinary investigation was conducted during June and July 1975 to acquire data that would set a basic framework of the physical processes controlling morphology of the northeast coast of Brazil. Detailed field data were taken at two sites along the coast: Aracaju, Sergipe, and Suape, Pernambuco. Analysis of the data and long-term broad-scale data supplied by cooperating Brazilian agencies was conducted for two purposes: to delineate the physical processes and morphology of the coast and to investigate under field conditions the mechanics of specific important coastal processes.

The northeast coast of Brazil is located on the trailing edge of the South American continental land mass and consists of a broad coastal plain recently drowned by the Holocene rise in sea level. Long, linear depositional forms, barrier beaches, and stone reefs dot the coastline. The lithified stone reefs (beach-rock reefs) occur at various distances from the shoreline and greatly affect nearshore waves and currents; many small harbors along the coast result. At Aracaju the coastline was formed by a progradation process that has recently been reversed, so that dune migration and shoreline erosion are now occurring. The stone reefs were formed in a marine environment, and the cementation process may be continuing in several places contemporaneously.

Physical processes affecting these morphologic features were studied in detail. Atmospheric shear velocity measurements indicate that the aerodynamic drag coefficient varies greatly from the offshore region, across the nearshore and beach environments, to the dune field. Beach dynamics are shown, by a study of the formation of an alongshore bar and accompanying processes, to depend greatly upon the action of long-period wave components in the surf zone. The stone reefs cause a decrease of up to 90 percent in wave heights as a result of induced breaking and wave reflection. The amount of decrease varies during a single tidal cycle from 50 percent to 90 percent. Circulation in back-reef lagoons varies greatly in pattern and intensity over a tidal cycle.

iii

## ACKNOWLEDGMENTS

iv

CONTENTS

FIGURES

TABLES

# I.   INTRODUCTION

As part of a 3-year investigation of physical processes in a high-energy coastal environment, a field study was conducted by Coastal Studies Institute (CSI) personnel during June and July 1975 on the northeast coast of Brazil.  The study represented a major effort by the Institute to move toward its long-standing goal of understanding the variability of coastal processes associated with different environmental settings on a worldwide basis.  Because in nature physical processes and coastal morphology are a closely integrated dynamic system, this study was interdisciplinary; it focused upon the aerodynamics, hydrodynamics, geology, and morphology of the study area.  Two types of studies were conducted:  broad-scale descriptive documentation of the coastal processes and morphology; and detailed analytic investigations of specific processes and sites.

The Brazil study has followed several Institute interdisciplinary investigations of coastal processes.  Project SALIS (Sea-Air-Land Interaction System), conducted by the Institute on Santa Rosa Island, Florida, during 1971, was a first attempt at a systematic multidisciplinary study in the nearshore environment.  That study (Sonu et al., 1973) resulted in significant progress toward the understanding of a sandy, moderate-energy coast dominated by a diurnal land-breeze/sea-breeze wind system. Subsequent interdisciplinary studies have been conducted by CSI on the arctic coast of Alaska, in 1972 (Wiseman et al., 1973), and on a reef coast in the trade winds (Grand Cayman, 1972; Barbados, West Indies, 1973) (Roberts et al., 1975).  The Brazil project was designed to investigate a high-energy barrier and beach system.  The northeast coast of Brazil was selected because strong, persistent onshore winds are present, wave action exceeds 1 meter much of the year, sediment supply is abundant, and morphologic characteristics are highly variable.  A reconnaissance of the field site was conducted during January 1974 (Wright et al., 1974).

Contained within the broad objective of the Brazil high-energy barrier study were specific goals in aerodynamics, hydrodynamics, and morphodynamics.  The objective of the aerodynamics study (conducted by S. A. Hsu) was to investigate the aerodynamic roughness of the air-sea and air-land interfaces from offshore to the beach zone, including the study of the relationship between atmospheric turbulent flux of momentum and wave-spectra modification, sediment transport on dunes, and verification of an equation for dynamic roughness.  The objectives of the hydro-dynamics studies (J. N. Suhayda, H. H. Roberts) were to determine the synoptic pat-terns of nearshore waves and currents on a high-energy beach, the alongshore varia-tion of surf-zone infragravity waves, and the effect of a cemented offshore barrier on nearshore wave and current action.  The morphodynamics and geologic studies (H. H. Roberts and A. D. Short) had as objectives the characterization of sedimentary patterns of a beach-ridge and swale complex and the morphodynamics of a beach-ridge plain, description of sedimentary patterns associated with a barrier/lagoon system, and understanding of the formation of cemented offshore beach-rock barriers.

This report is organized along lines of scientific disciplines.  Section II presents the results of meteorological studies.  Section III presents the results of the oceanographic studies, and Section IV presents the morphologic results.  The major results of the study are summarized in Section V.

1

## The Northeast Coast of Brazil

The study area extends a distance of 700 km along the northeast coast of Brazil between Salvador and Recife. This area, shown in Figure 1, lies between latitudes 8°S and 13°S. The regional characteristics of the coast are determined by its location on a trailing edge of the South American continent crustal block (Inman and Nordstrom, 1971). These characteristics are a broad coastal plain, high river discharge, abundant sediment supply, and absence of coastal mountain ranges. The shelf, however, is not broad; its average width (∿30–40 km) is approximately one-half the world average. These general characteristics of the coast were determined by the sequence of tectonic events that developed the Atlantic Ocean.

The tectonic configuration of the Brazilian continental margin was established during the Early Cretaceous (Campos et al., 1974) in response to the Wealdian Reactivation, an intense tectonism that affected the present coastal areas after the region had been stable since the early Paleozoic. These processes, operating along Precambrian lines of crustal weakness, developed a gravity-faulting pattern that controlled the pattern of what was to become the Brazilian and African coastlines. The initial stage of the process is shown in Figure 2A. The existing continental land mass was Gondwanaland, as shown in the figure. Faulting and the development of a rift valley occurred, and spreading of the land masses that were to become the South American and African continents was initiated. During an early stage in the formation of the coast, a Proto Atlantic Gulf developed, and the present coastline of Brazil become evident, as shown in Figure 2B. Later, during the Upper Cretaceous, the Gulf opened and the Atlantic Ocean basin became fully developed, as shown in Figure 2C. The Brazilian shelf then became subject to oceanographic and meteorological processes.

In gross character the present coast from Salvador to Recife is a sandy, wave-built depositional feature: the coastline is composed almost entirely of coastal beaches and barrier formations. On a regional scale the coast is aligned to face the prevailing southeasterly waves. In detail, however, the coast is relatively irregular, and numerous low-amplitude (i.e., not extremely protruding) headlands alternate with arcuate embayments and small inlets. These local irregularities cause local variations in the degree of wave refraction and exposure to the prevailing waves and, hence, in the strength of wave forces near the shoreline. As a consequence of variations in (a) nearshore wave energy and, more importantly, (b) proximity to a sediment source, some sections of the coast are characterized by rapidly prograding beach-ridge plains, whereas erosion prevails along other sections. Overall, much of the coastline appears to be relatively stable. Offshore slopes fronting the coast are moderately steep and linear to slightly convex in profile; slopes from the shoreline to the 100-meter contour range from 0°4' to 0°38' and average 0°15'.

The northeast coast of Brazil differs significantly from typical barrier coasts (such as the eastern coast of the U.S.) in the sense that extensive modern cemented beach rock prevails in varying degrees along the entire length of the coastal region. This beach rock is responsible for the existence of broad bands of lithified beach sand in intertidal zones, of impermeable layers beneath active beach sands, of cemented headlands and inlet-mouth bars, and of long, linear "reefs" ("recifes") of carbonate-cemented sandstone that parallel the coast in the nearshore region. The presence of this beach rock appreciably affects wave breaking and wave-energy dissipation, as well as the response characteristics of the beach.
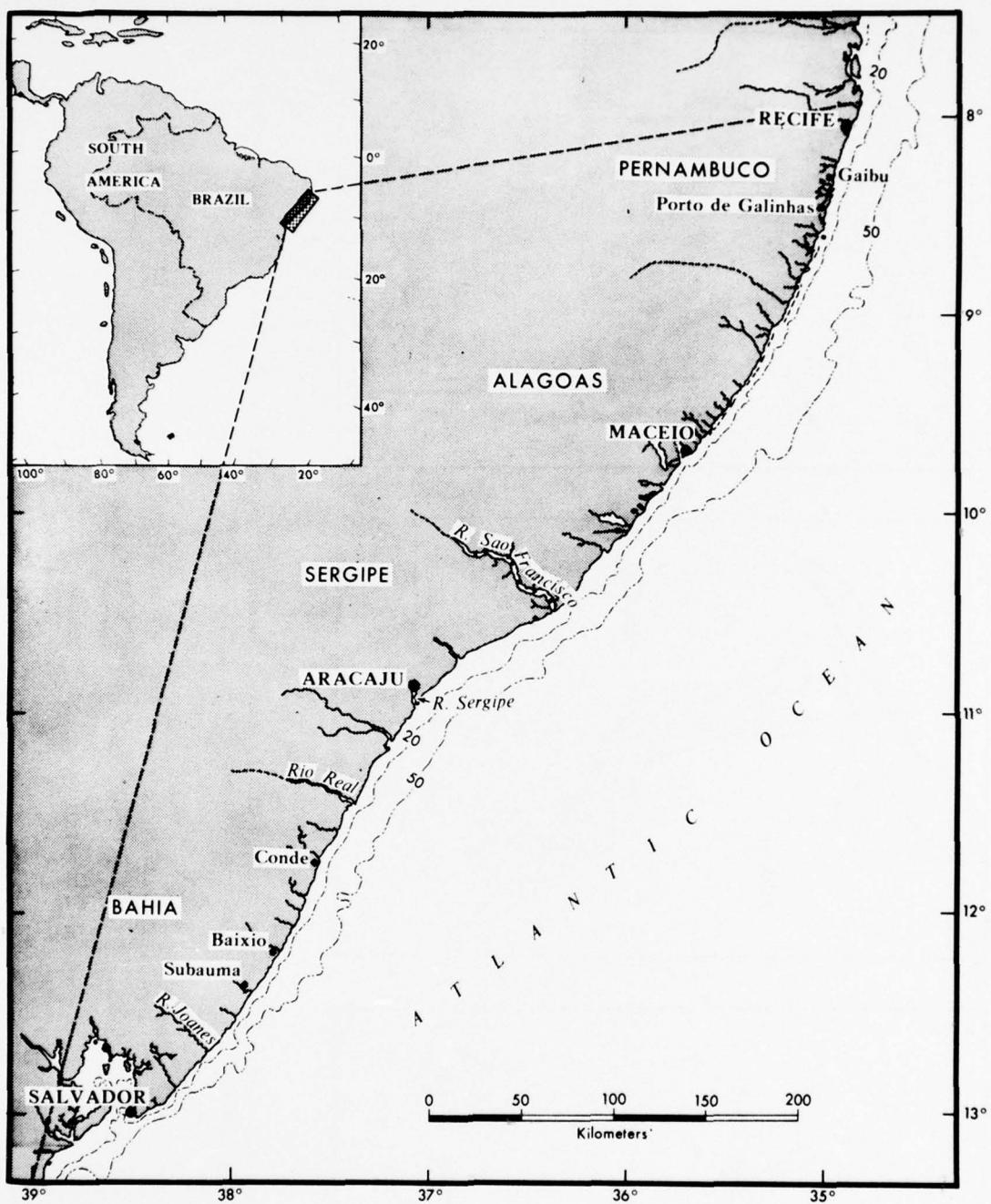
Figure 1. Location map showing the northeastern coast of Brazil. Detailed studies were conducted near Aracaju and Recife.

3
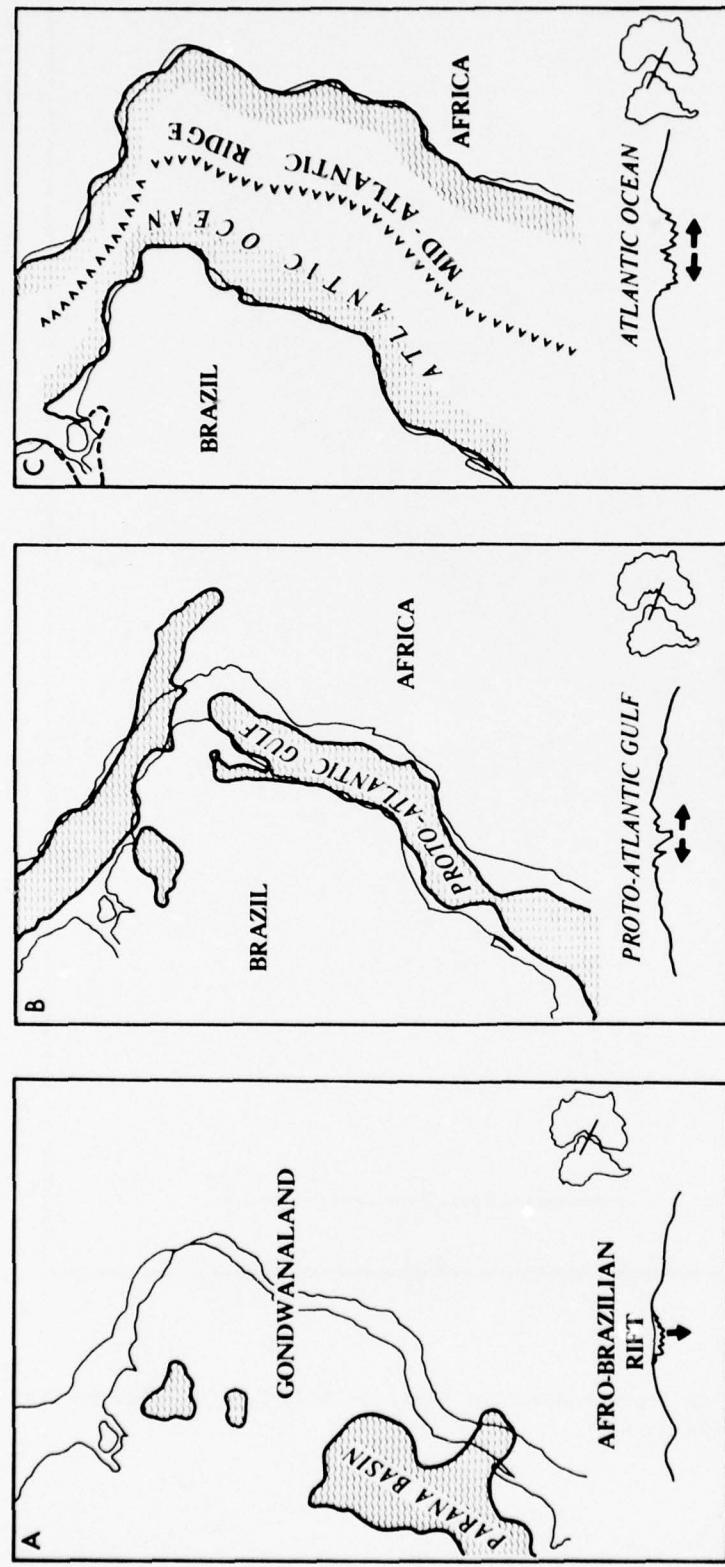
Figure 2. Development of the Atlantic Ocean through the process of sea-floor spreading. The stages shown are Early Cretaceous (A), Middle Cretaceous (B), and Late Cretaceous (C).

Monthly wind roses for the region indicate that southeasterly winds are dominant. Wind velocities rarely exceed 20 m/sec; severe storms of hurricane force are virtually nonexistent. Directions of average coastal currents in the offshore zone are variable. Currents generally set to the south from September through May and to the north during the winter months of June through August.

Tides are semidiurnal and have a moderate range. The average annual mean and spring tidal ranges at Salvador and Recife are 1.63 meters and 2.17 meters, respectively. The east coast of Brazil is dominated by moderate- to high-energy waves that arrive almost exclusively from the southeast, where they are generated by the southeasterly trades and storms in the higher latitudes of the South Atlantic. The results of wave observations made by Petrobras (the Brazilian national oil company) on offshore platforms in the vicinity of Aracaju are summarized in Figure 3. The frequency distribution of significant and maximum wave height is shown in Figure 3A; the frequencies of significant periods are indicated in Figure 3B; and Figure 3C shows the directional frequency of occurrence of all waves. The most frequently occurring significant waves have heights of about 1 meter and periods of 7.5 sec; however, wave heights in excess of 2.5 meters are not uncommon (Fig. 3A). The nearshore wave power is determined by the effects of refraction, shoaling, and frictional attenuation on waves. Estimates of the resulting nearshore wave power and breaker heights (height = 1 meter; period = 7.5 sec) were made using the Institute's comprehensive wave refraction computer program (Wright and Coleman, 1973). Figure 4 shows the spatial variations in nearshore wave power, longshore power, and breaker height along the coast between Salvador and Recife.

## Field Sites and Instruments

Two field sites were occupied during the study. One was located at Aracaju, in the state of Sergipe (Fig. 5), and the other was at Suape, in the state of Pernambuco, near Recife (Fig. 6). The Aracaju site consisted of a river and beach-ridge complex having well-developed alongshore bars. The Suape site consisted of a river/lagoon complex formed by a long beach-rock barrier.

The city of Aracaju (see Fig. 5), located in the approximate center of the Sergipe coast, is a major site of Petrobras petroleum production: production and drilling platforms are situated a short distance offshore from Aracaju. Because of the availability of these platforms for mounting instruments and the cooperation and logistic support of Petrobras, Aracaju was the preferred location for several detailed investigations.

The active beach between Aracaju and Rio Vasa Barris is composed of "dirty" fine sand containing a significant percentage of silt and is extremely flat. The flat foreshore is responsible for a broad breaker zone. The subaerial beach is relatively featureless, lacking rhythmic topography and a wave-built berm. The flat beach is about 150 meters wide at low tide and is almost completely transgressed at high tide. The beach is backed by a relatively straight scarp at the foot of the foredune. Behind the foredune a broad expanse of irregular dune topography is common.

Extensive and impressive beach-rock formations are found along the coast of Pernambuco State. Recife, the principal city of this state, derives its name from these formations ("recife" is the Portuguese word for "reef"). The second field site was located at Suape, shown in Figure 6. The coastal system at Suape consists of a beach-rock barrier that has enclosed a lagoon and river mouth as a result of the erosion of unconsolidated sand between the barrier and the present-day shoreline. In several places along the Pernambuco coast long, linear beach-rock bars
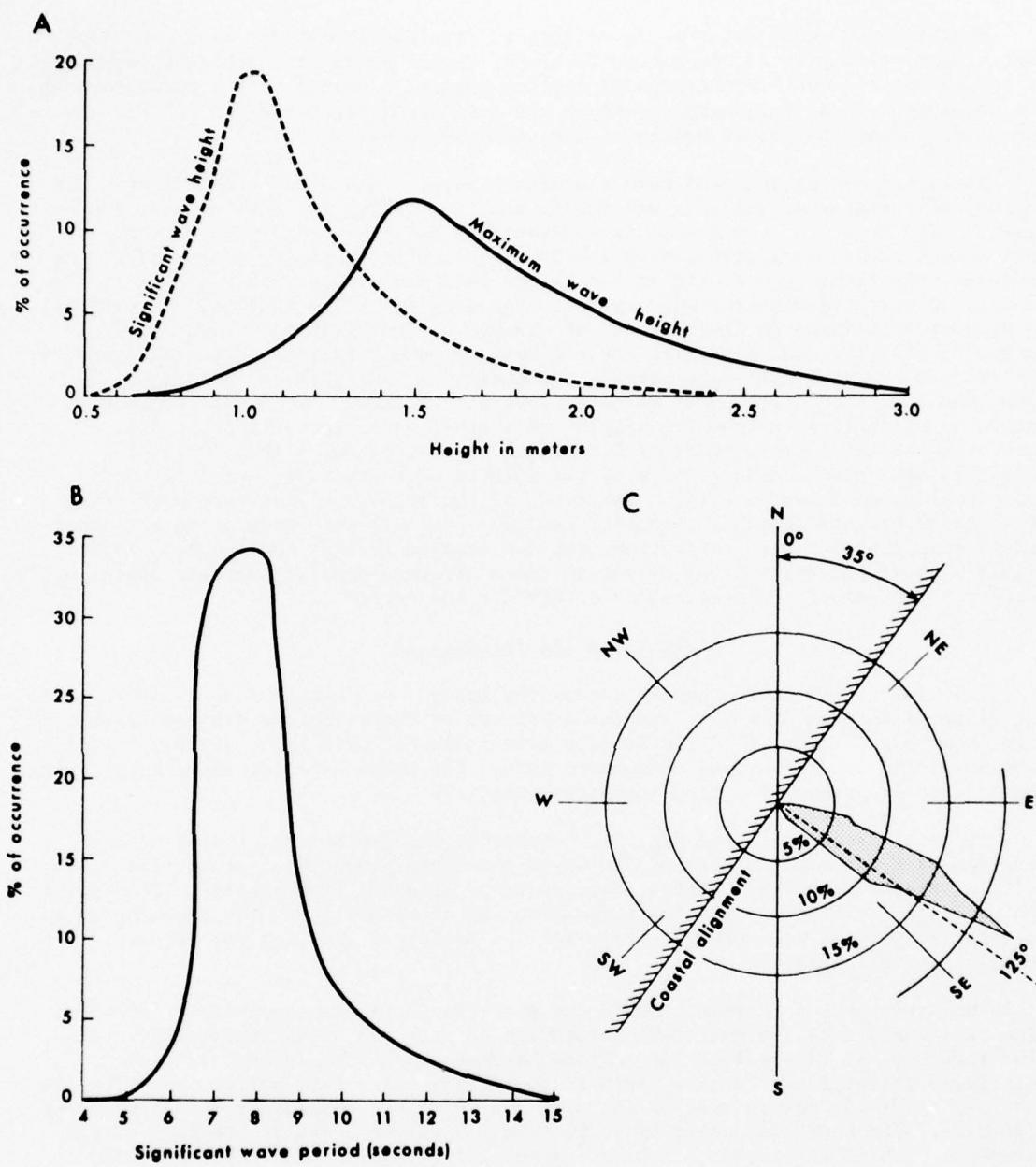
Figure 3. Deepwater wave characteristics for the coast of Sergipe. A. Frequency distribution of significant and maximum wave height. B. Frequency distribution of significant period. C. Directional frequencies.

6
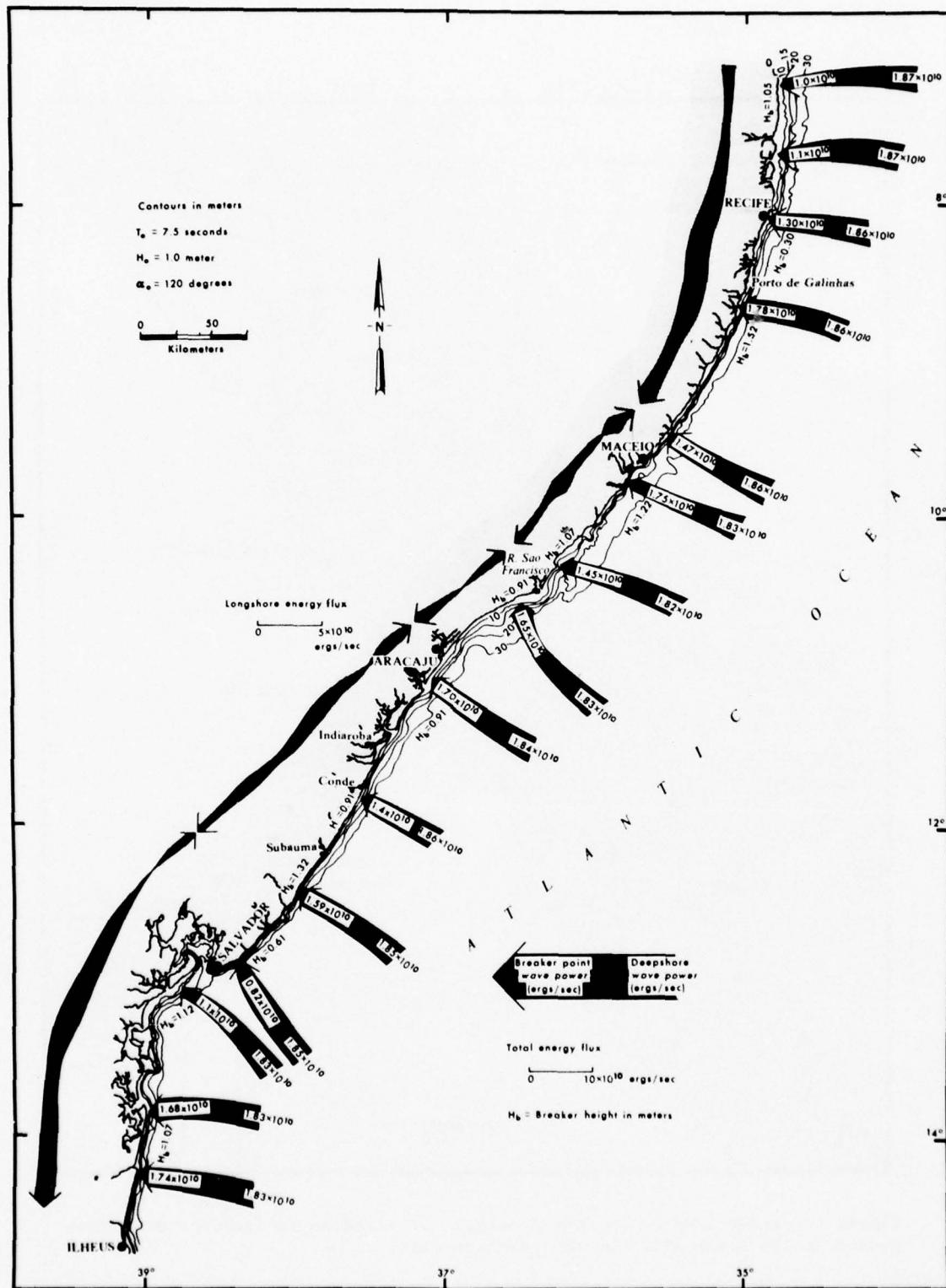
Figure 4. Spatial variations in the nearshore wave power, longshore power, and breaker height along the northeast coast. Convergence zones of littoral drift are indicated at points north of Salvador, at Aracaju and Rio Sao Francisco, and north of Maceio.

7
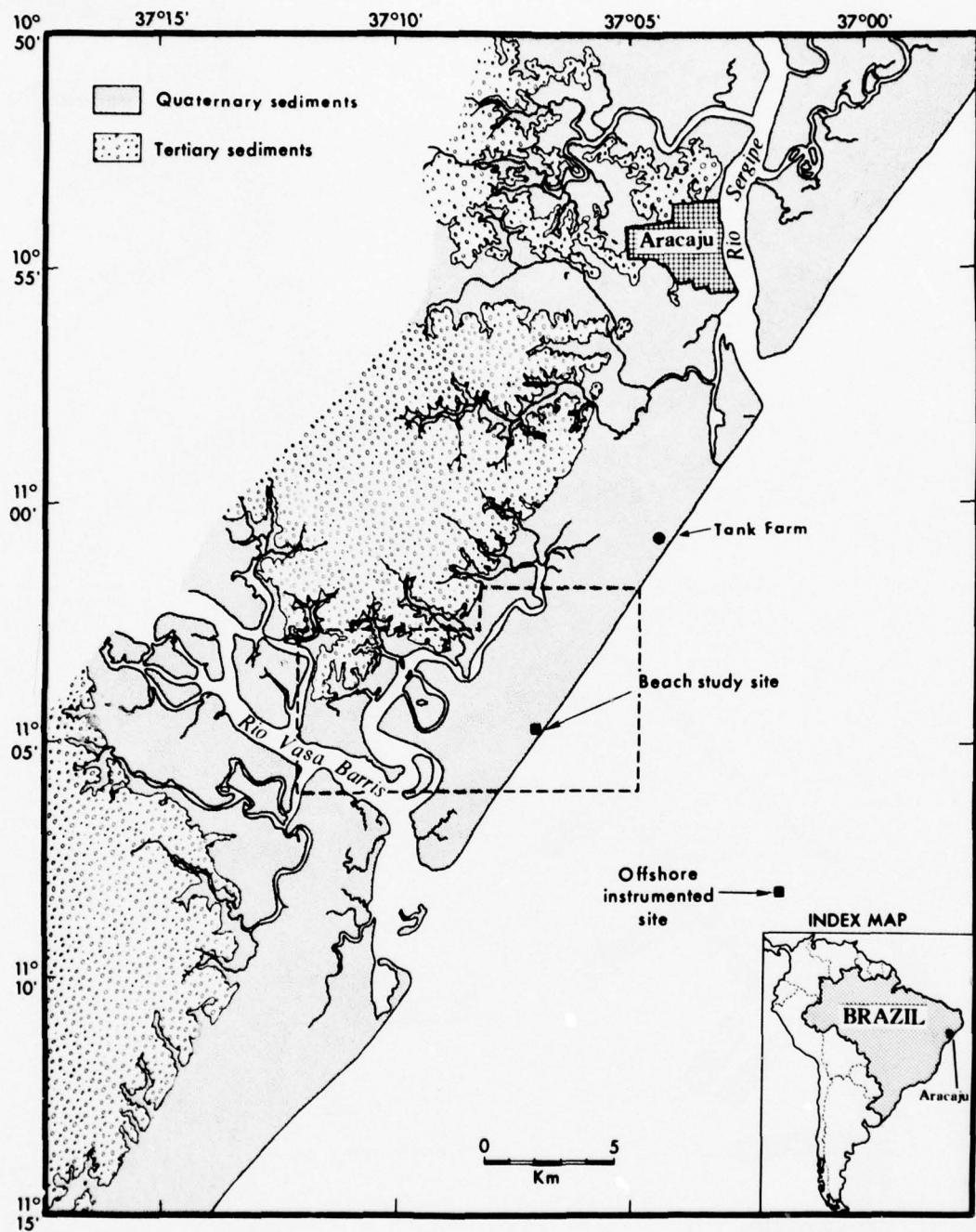
Figure 5.  Field study area near Aracaju.  Detailed investigations were conducted at the beach site and the offshore site.

8
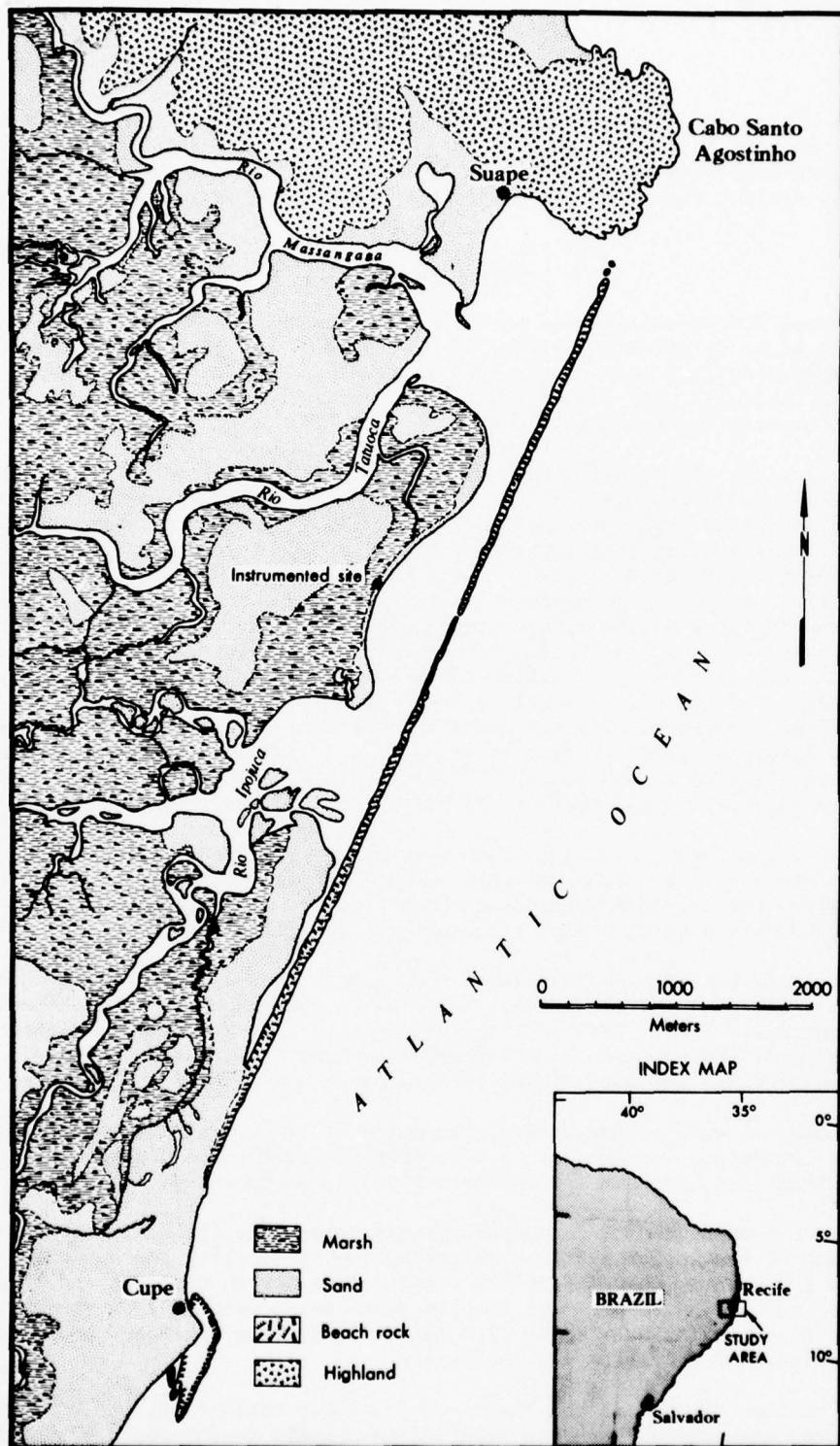
Figure 6.  Field study site south of Recife at Suape.  Instrumented
beach site is indicated shoreward of break in beach-rock barrier.

9

parallel the coast both in the nearshore region and offshore, where they are sub-
merged. In some locations there are as many as four successive bands of beach rock.
These beach-rock bars are highly effective in dissipating incident wave energy and
generally protect the subaerial beach from normal wave activity.

## Field Experiments

Several individual studies were conducted in which data were acquired during
the field program, including primarily CSI research and also cooperative programs.
These experiments are summarized in Table 1. The major field instruments used are
listed in Table 2. Data used in this study were also acquired from the files of
several cooperating Brazilian agencies.

The initial aerodynamic field experiments were conducted in the Aracaju area.
An air-sea interaction station was in operation for about a week. Instruments
designed to monitor wind profiles and oceanographic parameters were installed on an
offshore oil rig located in water approximately 30 meters deep, shown in Figure 5.
Meteorological and oceanographic sensors were set up as far away from the platform
as possible. After the offshore study was completed, the wind profile register
system was deployed on the beach, over the dune, and in the swale area at the
onshore site (Fig. 5) to investigate the air flow characteristics over these coastal
features. In addition, an acoustic radar was in operation for about 10 days in the
study area. We obtained regional weather maps covering the tenure of the Brazil
studies from Petrobras, from the Brazilian Air Force weather station in Recife, and
from the agrometeorological station in Aracaju. These weather maps covered north-
eastern Brazil from the surface to 500 mb and incorporated U.S. meteorological
satellite information and surface and pilot balloon observations.

At the platform oceanographic measurements were made of shelf waves, tides, and
near-surface currents. Tide and near-surface currents were measured continuously
for 6 days. Wave records were taken once a day for 3 days. These measurements were
made to indicate several scales of oceanographic motion.

Nearshore wave and current measurements were made at various distances along
the beach site on the Aracaju coast (Fig. 5) to determine the alongshore variations
of infragravity waves. Three water-level pressure sensors and two current meters
were deployed. The signals were low-pass-filtered (30-sec time constant) to bring
out strong current and water-level variations at a period of about 1 min.

A study of wave action behind (shoreward of) a partially submerged barrier was
conducted at Suape, Pernambuco. A wave pressure sensor was placed near the shore-
line inshore of a break in the offshore barrier, as shown in Figure 6.

The dune and beach-ridge morphology was determined initially by using a de-
tailed map of the region that was prepared from 1966 aerial photographs; second, by
making a 1.5-km-long survey from the beach inland across the dune and ridge field;
third, by collecting 26 sediment samples at selected points along the survey line;
and fourth, by taking four cores (1.3 meters deep) from the beach and a swale for
later analysis of sedimentary structures.

To monitor changes in the beach and inner-bar morphology, two beach grids were
established at Aracaju. One was located immediately to the south of the Petrobras
tank farm and measured 200 x 150 meters. The second grid (450 x 200 meters) was
located at the main study site, approximately 6 km farther south. At each grid
beach stakes were set up 50 meters apart along the beach and at 10-meter spacings

10

down the beach. The tank farm grid was surveyed on 10-13 June and 3 July. The main-site grid was surveyed on 8-15, 17, and 20-23 June and 1 July. In addition, a set of 30 beach sand samples was collected at the main grid on 2 July. These were analyzed for texture characteristics.

Two sets of air photographs, taken at 1,200 meters and 9,000 meters, were used to analyze the spatial distribution and plan-view geometry of coastal landforms at the Suape location.

Table 1

Field Experiments Conducted and/or Data Sets Acquired

| Investigation or Experiment | Site |
| --- | --- |
| Air-sea interaction | Aracaju/Offshore |
| Boundary layer / micrometeorology | Aracaju/Onshore |
| Weather data for June / Agriculture Station | Aracaju |
| Atmospheric boundary layer / mesoscale | Aracaju/Onshore |
| Weather maps / Brazilian Air Force | Recife |
| Shelf waves and currents | Aracaju/Offshore |
| Nearshore currents / waves | Aracaju/Onshore |
| Lagoon wave action | Suape |
| Wave-current climate data / Petrobras | Aracaju |
| Sediment transport date / DIPER | Suape |
| Morphology of alongshore bars | Aracaju |
| Dune-swale sediment and morphology study | Aracaju |
| Aerial photos / DIPER, Petrobras | Aracaju/Suape |
| Dune-swale sediment and morphology study | Aracaju |
| Beach rock studies | Maceio/Suape |
| Lagoon morphodynamics | Suape |
| Geologic-geophysical data / DIPER | Suape |
| Aerial photos / DIPER, Petrobras | Aracaju, Suape |

11

Table 2

Major Equipment Used in Brazil Study

| Item | Manufacturer | Use |
|------|--------------|-----|
| Meteorology | | |
| 1. Anemometer | Climet Instruments | Wind speed and direction |
| 2. Wind profile register | Thornthwaite Associates | Wind speed at six levels |
| 3. Microbarograph | Weathermeasure | Atmospheric pressure |
| 4. Atmospheric profiler | Aerovironment | Acoustic sounder / structure in lower atmosphere |
| Oceanography | | |
| 1. Q-15 current meter | Marine Advisers | Current speed and direction (2D) |
| 2. Ducted meter | CSI | Current speed (1D) |
| 3. Pressure water level gage | CSI | Waves/tides |
| 4. Wave staff | CSI | Capacitance wire/waves and tides |
| 5. RS-5 salinometer | Beckman Instruments | Salinity and temperature |
| 6. Digital flowmeter | General Oceanics | Counter/current speed |
| Geomorphology | | |
| 1. Fathometer | Raytheon Model 731 | Echo sounder |
| Geology | | |
| 1. Coring rig | CSI | Core samples |

## II.  ATMOSPHERIC PROCESSES

### Introduction

Coastal meteorology is an integral part of the total-systems approach to under-
standing coastal environments.  This section is devoted to the investigation of
atmospheric processes in the study area.  Particular emphasis, however, is placed
upon boundary-layer meteorological research, namely air-sea and air-land inter-
actions.  Specific experiments to determine the momentum flux at the air-sea-land
interfaces were conducted and are discussed in detail.

Some review of the general synoptic meteorology, particularly the weather sys-
tems that affect the northeast coast of Brazil, may be helpful.  From the experi-
mental standpoint, one also needs to know what the larger scale atmospheric effect
is during the period of field experiments.  Therefore, this chapter is organized as
follows:  general synoptic meteorology, eolian sand transport, and air-sea inter-
action.  Specific applications from this study are discussed in appropriate sections.

### General Synoptic Meteorology

The mean circulation and the synoptic perturbations over the southern tropical
zone of South America are poorly known (see, e.g., Taljaard, 1972).  This circum-
stance can be ascribed mainly to the lack of upper-air sounding stations over the
vast area, particularly the Amazon Basin.  On the temporal scale, this deficiency is
a critical factor in some regional studies.  For example, lack of a sufficient
period of record of upper-air observations necessitated using only a single year's
complete reporting network in the investigation of precipitation characteristics in
the northeastern Brazil dry region (Ramos, 1975).  Nevertheless, some general
knowledge may be obtained from the literature.  The following discussion is based
mainly on Taljaard's (1972) analysis of synoptic meteorology.

Low-level circulation conditions in summer (December to February) and in winter
(June to August), which were obtained from the monthly resultant winds during 1968-
70 at ten stations east of the Andes and taken in conjunction with longer series of
observations at Lima, Guayaquil, Recife, Fernando Noronha, and stations farther
south in Chile and Argentina, are shown in Figure 7.  These results represent mainly
the 850-mb flow, but 700-mb winds have also been taken into account.

A first impression is that circulation is very similar in summer and in winter.
In both seasons the ridge associated with the Atlantic anticyclone stretches west-
ward over the continent; its axis is along 15°-20°S.  The important difference is
that in winter steady southeasterlies blow across the equator, whereas in summer
less constant easterlies blow more or less parallel to the equator.  Humid tropical
air from the northern hemisphere frequently drifts southward in summer and joins the
trade current from the South Atlantic to produce the high rainfall and cloudiness of
the Amazon Basin and adjacent southern territories.  The anticyclonic curvature of
the flow lines is stronger in winter than in summer.  East of the Andes, the north-
erly current persists to 25°S and even farther south in summer, but in winter fresh
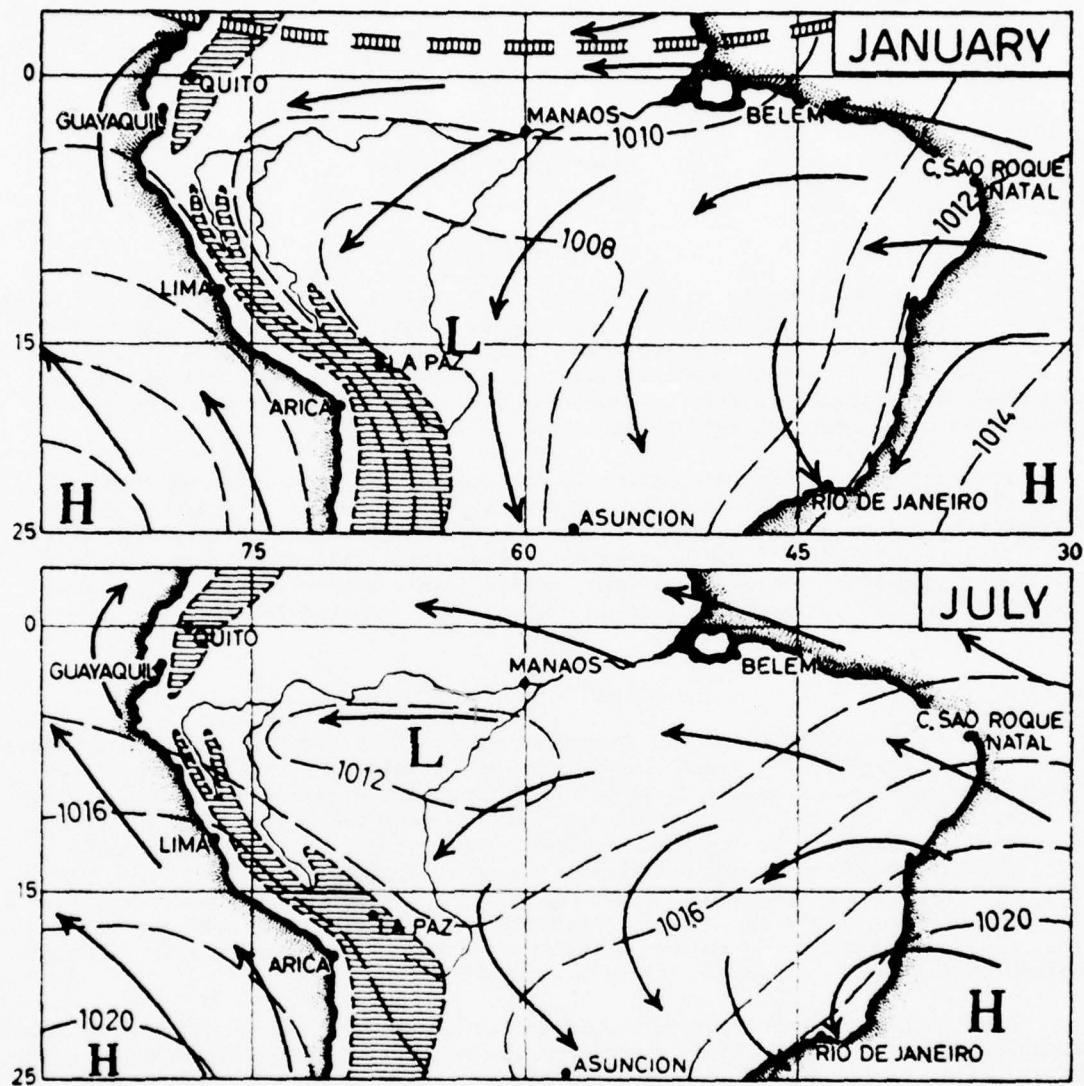
Figure 7. Mean sea-level pressure in January and July and average low-level (1-3 km) flow patterns over southern tropical South America in summer (top) and winter (bottom) (from Taljaard, 1972).

14

westerly winds are frequent at 20° and 25°S. In January the sea-level isobars are parallel to the east coast from Cape Sao Roque to Rio de Janeiro, but in July the pressure is 5 mb lower at Cape Sao Roque than at 20°S on the coast, and the onshore trade wind is consequently stronger.

Trewartha (1961) discussed the climatic controls and synoptic disturbances of tropical South America in some detail. Schematic representation of the disturbances that affect the region in summer and in winter are given in Figure 8. Little concrete knowledge exists about the systems between 0° and 15°S. It can be assumed that the humid air mass is potentially very unstable and that small perturbations lead to overturning and release of the potential energy whereby these systems are maintained for many hours. Thus, small convection elements may grow to extensive cumulonimbus clusters. Johnson (1970) showed a satellite cloud photograph over tropical South America that indicates a large number of rounded or slightly elongated cumulonimbus clusters. These clusters, said to be typical of the region, develop and decay diurnally and therefore represent convective elements rather than organized weather systems, which have life cycles of several days. However, it is unlikely that the abundant rainfall of the Amazon Basin consists solely, or even mainly, of diurnal convective showers. It must be assumed that propagating wave and line disturbances exist in the region. Trewartha suggested that westward-moving equatorial waves affect the zone close to the equator. Elsewhere, line disturbances similar to speed convergences in the low-level easterly and northerly currents are thought to contribute to the rainfall. The Andes form a barrier 4-5 km high that must necessarily terminate the horizontal westward movement of an almost equal depth of air north of 15°S. This can be achieved through speed convergence in gradual or steplike fashion, instead of through forced ascent along the eastern slopes of the cordillera.

The southern part of the tropical zone comes under the influence of disturbances of subtropical and middle latitudes in summer, though to a lesser extent than in winter. Heat lows are characteristic of Paraguay and the Gran Chaco. East of the Andes to 25°S, active cold fronts advance northward and in weakened form occasionally reach 20°S over the interior as well as over the east coast. The fronts are preceded by broad convergence zones and disturbed weather. When anticyclones pass eastward over the sea, rain belts of a warm frontal character occasionally develop on land along the leading edges of the returning tropical air. The surface systems are reflected in upper troughs and ridges (it may be argued that upper troughs and ridges in the westerlies induce the development of the surface system).

## Shear Velocity Measurements for Eolian Sand Transport Estimation

Sand transport by the wind is an important aspect of sedimentological studies of a given region, particularly in coastal areas (see, e.g., Svasek and Terwindt, 1974). On the basis of available laboratory and field measurements of the rate of eolian sand transport, Hsu (1971a) introduced a relatively simple method by which this rate can be scaled by a special Froude number. Recent measurements by Svasek and Terwindt (1974) confirm the validity of this method. The most important parameter in the formula is the atmospheric shear velocity. Extensive measurements of wind structures in various coastal environments indicate that the method can be extended and applied to these environments to compute the amount of sand transported by the wind. However, estimates of this rate in coastal sand dune areas are lacking. This section summarizes the development of the method and measurements of the shear velocity in a beach-dune-swale environment along the northeastern coast of

15
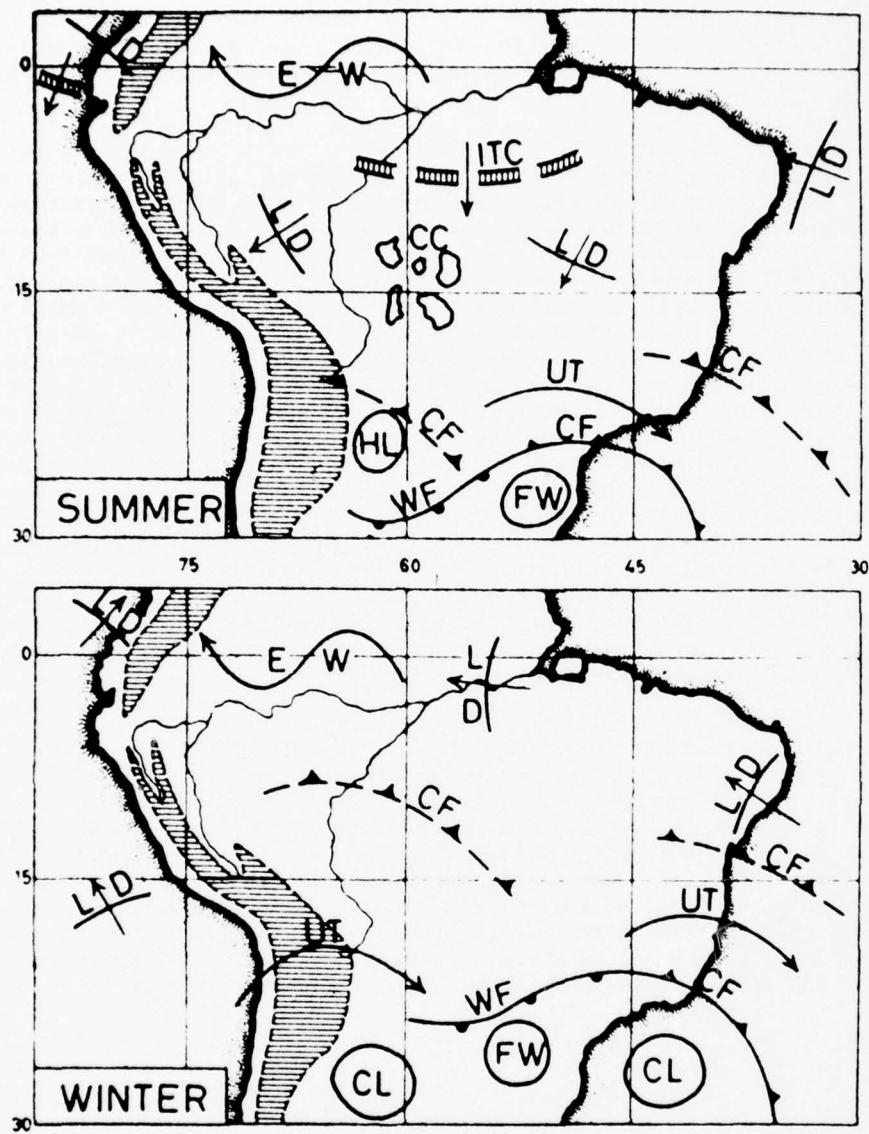
Figure 8. Schematic representation of weather disturbances that affect tropical South America south of the equator in summer (top) and winter (bottom): EW = equatorial wave; ITC = displaced intertropical convergence zone; LD = line disturbance; CC = diurnal cumulonimbus clusters; CF = cold front; WF = warm front; UT = upper trough; CL = cutoff low; HL = heat low; FW = frontal wave. Land above 3 km is marked by hatched pattern (from Taljaard, 1972).

16

Brazil. For comparison, similar measurements from other air-coast interfaces are also included.

The relationship formulated by Hsu (1971a, p. 8685) for computing the rate of sand transport by the wind is

$$q = K \cdot Fr^3 = K\left[\frac{U_*}{(gD)^{1/2}}\right]^3 \tag{2.1}$$

where q (gm/cm/sec) is the rate of sand transport by the wind and Fr is a special Froude number. Fr is a function of the atmospheric shear velocity $U_*$ (cm/sec) and the acceleration of gravity g (980 cm/sec$^2$). Note that, because the Froude number is dimensionless, the dimension of the mean grain size of the sand particles D is in centimeters. Note also that this Froude number is different from the conventional or normal Froude number because the velocity is replaced by $U_*$. K is defined as the dimensional eolian sand transport coefficient and has the same dimensions as q. The value of Fr is explicitly determined by the bracketed term in equation (2.1). The values of K are given by

$$K = 10^{-4} \, e^{(-0.42 + 49.1 \, D)} \tag{2.2}$$

where e is the base of natural logarithms and is approximately equal to 2.7183. Equation (2.2) was obtained by incorporating the data listed in Hsu (1971a) and recent measurements by Svasek and Terwindt (1974). The procedure was outlined in Hsu (1971a).

If the value of $U_*$ is known, the rate of eolian sand transport can then be computed. The procedures have been given in Hsu (1973). Briefly, $U_*$ can be obtained by the logarithmic wind profile law, which states that

$$U_z = \frac{U_*}{\kappa} \, \ell n \, \frac{Z}{Z_o} \tag{2.3}$$

where $U_z$ is the mean horizontal wind velocity at any given height Z, $\kappa$ is the von Karman constant ($\approx 0.4$), and $Z_o$ is the aerodynamic roughness length, defined under the boundary condition that $U_z = 0$ at $Z = Z_o$. The value of $Z_o$ depends upon the characteristics of the underlying surface.

The quantities $U_*$ and $Z_o$ can be obtained easily from the wind profiles inasmuch as $\kappa/U_*$ is the slope of the least-square linear fit of the profile on a semi-logarithmic scale and $Z_o$ is the intercept with the $\ell n$ Z axis (where $U_z = 0$). Some examples of the logarithmic wind profiles were given by Hsu (1972a) and Svasek and Terwindt (1974).

It is convenient to define the drag coefficient $C_z$ at height Z by (e.g., Priestley, 1959, p. 21)

$$C_z = (U_*/U_z)^2 \tag{2.4}$$

In other words, if we know $C_z$ for a given area, the shear velocity $U_*$ can be calculated from the wind velocity and then substituted into equation (2.1) to give the value of q. For brevity, two examples will serve to illustrate the method and

17

are given in a later section.

The experiment to measure the shear velocity at the air-beach-dune-swale inter-
face in Brazil was performed during June 1975 (Fig. 9). In order to compare the
results with those from other air-coast interfaces, measurements are included that
were made over beaches near Fort Walton, Florida, in May 1970 (Hsu, 1971b); on
northern Padre Island, Texas, in September 1972 (Hsu, 1973); on Point Lay Island,
Alaskan Arctic (Walters, 1973); near Playas, Gulf of Guayaquil, Ecuador (Hsu,
1971a); and near Bath, Barbados, West Indies. Similar experiments were performed on
a low dune field (average height 50 cm) on northern Padre Island, Texas, in Septem-
ber 1972 and on a tidal flat in Estero de Data (Guayas Estuary), Ecuador (Hsu,
1972a). These results are summarized in this report, along with pertinent measure-
ments made by others, such as those by Bagnold (1941), who reported data from
experiments in a Libyan desert.

The main instrument used for the experiments was a portable Thornthwaite Wind
Profile Register System (Model 106, C. W. Thornthwaite and Associates, Elmer, New
Jersey, U.S.A.) with six-unit, three-cup, fast-response anemometers mounted at 20,
40, 80, 160, 240, and 320 cm above the surface. Some examples are shown in Figure
9. The instrumentation and wind data reduction and analysis procedures have been
described by Hsu (1971b, 1972a).

As discussed in a previous section, a convenient way to express the shear
velocity is the value of $C_z$. For reference purposes $C_z$ at 2 meters above the
surface is usually employed (e.g., Priestley, 1959, p. 21). It should be noted that
$C_z$ is relatively insensitive to $Z_o$. An equivalent statement is that $C_z$ can be
determined without having to specify too closely the height to which it relates.

Table 3 summarizes the results from those areas investigated by the author and
his associates during the past few years. For reference purposes, some of the data
listed by Priestley (1959) and Bagnold (1941) for similar environments over coastal
and inland sites are also included in Table 3.

Figure 10 summarizes our shear velocity measurements in various coastal
environments. Because it is not always convenient for an anemometer to be located
2 meters above the surface, the following equation may be used (cf equation 2.3):

$$U_* = \frac{\kappa \, U_z}{\ln Z/Z_o} \tag{2.5}$$

where $Z_o$ may be approximated by applying pertinent values as shown in Figure 10.
Note that values of $Z_o$ were obtained from $C_z$ at 2 meters (Fig. 10 and equation
2.3). Fortunately, in the atmospheric surface boundary layer (say, Z does not
exceed 25 meters above the surface, according to Sutton, 1953, p. 79), the value of
$U_*$ may be treated as a constant. Almost all National Weather Service anemometers
are located within this layer, and it is safe to use equation (2.5) for general micro-
meteorological applications.

For a sand budget study of a given region, the rate of eolian sand transport is
required. The method developed is based on both field and laboratory experiments
(Hsu, 1971a, 1973) and should therefore be applicable to natural beaches and deserts
such as those discussed in Kadib (1965) and Svasek and Terwindt (1974). Estimates
of this rate in coastal sand dune areas are lacking. However, recent measurements
of shear velocity in a beach-dune-swale environment in Brazil (see Table 3 and

18
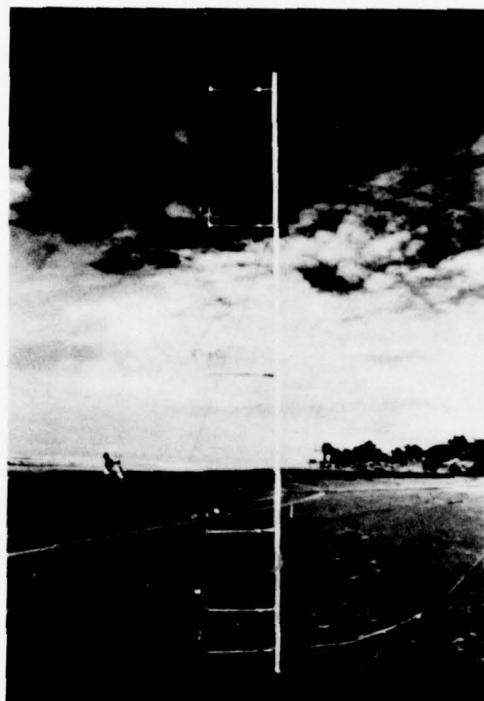
A



B

Figure 9. Wind profile measurements in a beach-dune-swale environment near Aracaju, on the northeastern coast of Brazil (cf. Fig. 5) where $\underline{A}$ shows the instrument array on the beach; $\underline{B}$ indicates an area near a dune scarp (average scarp height from beach $\simeq$ 1 meter); $\underline{C}$ is a region near the top of a dune (average dune height $\leq$ 2 meters); $\underline{D}$ shows a site near the lee side of the dune; $\underline{E}$ is the swale area; and $\underline{F}$ is an area from the swale region toward the sea.

C



D

20
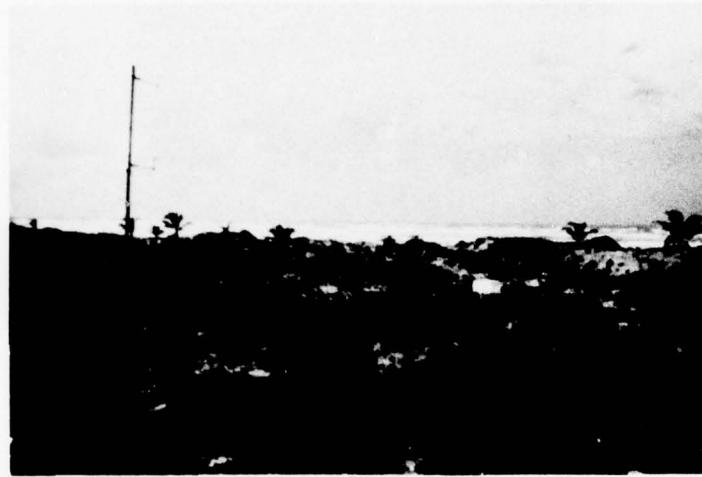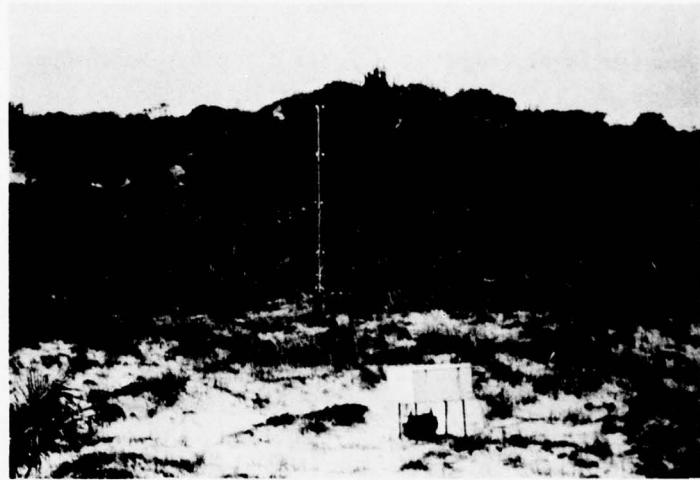
E



F

## Table 3

### Measurements of Drag Coefficients $C_z$ in Air-Beach-Dune-Swale Environment near Aracaju, Brazil

| Type of Surface | $C_z$ at 2 m ± Standard Deviation | |
|---|---|---|
| Upper swash zone on Bath Beach, Barbados, West Indies | 0.000872 | 0.0000748 |
| Smooth mud flats[a] | 0.0010 | |
| Tidal flat, Estero de Data (Guayas Estuary, Ecuador) | 0.00135 | 0.000082 |
| Beach near Playas, Gulf of Guayaquil, Ecuador | 0.00147 | 0.00108 |
| Beach on northern Padre Island, Texas | 0.00205 | 0.00068 |
| Desert (Pakistan)[a] | 0.0020 | |
| Beach near Aracaju, Brazil (Fig. 9A) | 0.00211 | 0.000602 |
| Beach near Fort Walton, Florida | 0.00222 | 0.00069 |
| Low dune field (average height 50 cm), northern Padre Island, Texas | 0.00232 | 0.00076 |
| Dune area scarp (average scarp height from beach ≈1 m) near Aracaju, Brazil (Fig. 9B) | 0.00248 | 0.00137 |
| Desert (Libya)[b] | 0.0027 | |
| Beach on Point Lay Island, Alaskan Arctic | 0.00291 | 0.00036 |
| Swale area near Aracaju, Brazil (Fig. 9E) | 0.00340 | 0.000638 |
| Dune area (near top) (average dune height ≤ 2 m) near Aracaju, Brazil (Fig. 9C) | 0.00495 | 0.00101 |
| Dune area (near lee side) (average dune height ≤ 2 m) near Aracaju, Brazil (Fig. 9D) | 0.00984 | 0.000756 |

[a]From Priestley (1959)
[b]From Bagnold (1941)

NOTE: For comparison, measurements from other coastal and inland surfaces are included (see text).
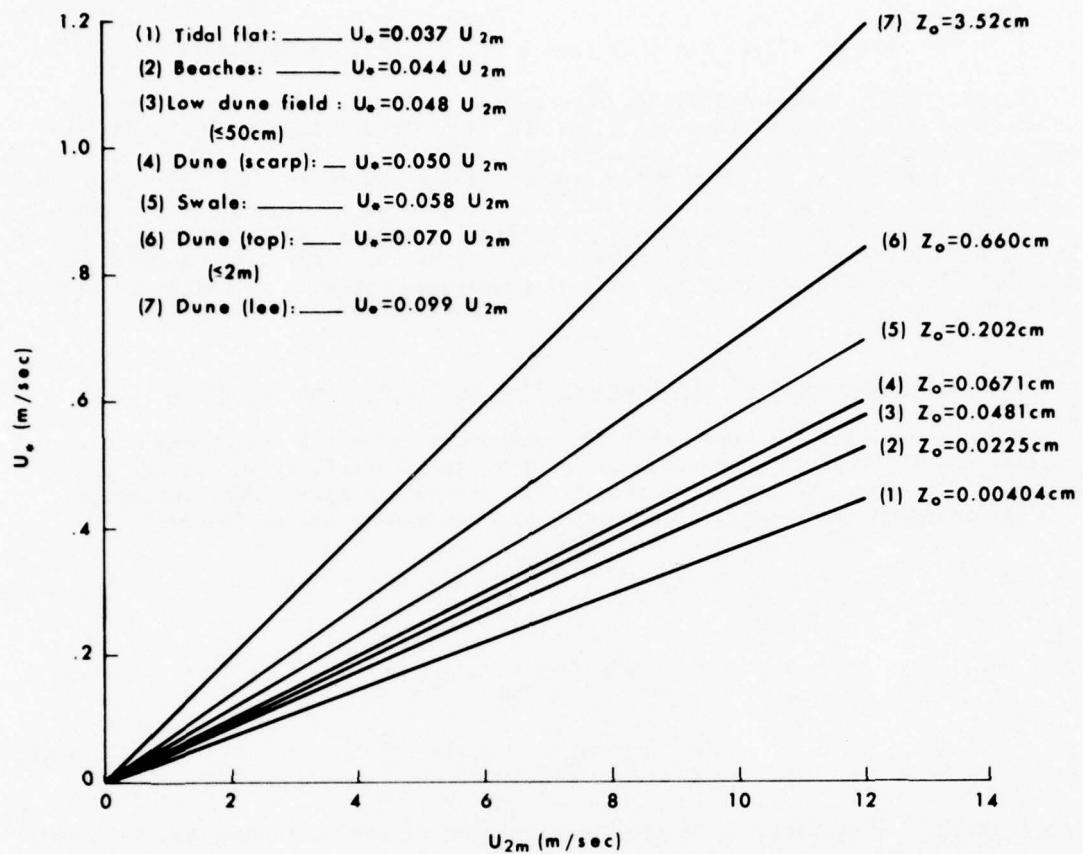
Figure 10. Summary of the aerodynamic roughness length, $Z_o$, and the relationship between the shear velocity, $U_*$, and the wind velocity at 2-meter height, $U_{2m}$, measured in various coastal environments for eolian sand transport estimation. All data are based on Table 3; (1) was obtained from Ecuador; (2) is a synthesis of six beaches, i.e., Barbados, Ecuador, Texas, Brazil, Florida, and the Alaskan Arctic; (3) is from Texas; and (4) through (7) are all from Brazil.

Fig. 10) indicate that the method may be extended to such regions. Two examples are given below.

Inman et al. (1966) have stated that $D = 0.015$ cm and $U_{2m} \simeq 4$ m/sec (approximate mean annual value) in coastal sand dunes in Baja California, Mexico. From equation (2.2) we find that $K = 1.37 \times 10^{-4}$ gm/cm/sec. The average relationship between $U_*$ and $U_{2m}$ from the scarp through the swale environment [i.e., average of (4), (5), (6), and (7) in Fig. 10] indicates that $U_* = 0.07 \ U_{2m}$; therefore, $U_* = 28$ cm/sec. Substituting g (= 980 cm/sec$^2$), D (= 0.015 cm), K, and $U_*$ into equation (2.1), we find that $q = 0.053$ gm/cm/sec. The annual average value for q measured by Inman et al. (1966) is 0.049, which is obtained by applying a mean annual velocity of dune travel (d) of 5 cm/day, bulk density of the dune sand ($\rho_b$) of 1.5 gm/cm$^3$, and average dune height (H) of 6 meters to the equation formulated by Bagnold (1941, p. 217):

$$q = \frac{d \ \rho_b \ H}{t} \tag{2.6}$$

23

where t is the time of travel (in this case $t$ = 1 day or 24 x 3600 sec).

Finkel (1959), Lettau (1967), and Lettau and Lettau (1969), among others, studied coastal barchans in southern Peru. Pertinent data used in this study are based on these publications: d = 30 m/yr (or 8.22 cm/day), D = 0.0314 cm, $U_*$ = 28 cm/sec, H = 3 m, $\rho_b$ = 1.3 gm/cm$^3$. Applying these values to equations (2.1) and (2.6) as before, we have $q_{predicted}$ = 0.039 gm/cm/sec and $q_{observed}$ = 0.037 gm/cm/sec. It is evident that the agreement is good. From these two examples we conclude that the method and procedure developed in this report are useful for estimating eolian sand transport, not only for natural beaches and deserts but also for coastal sand dunes.

## Measurement of the Momentum Flux at the Air-Sea Interface

The momentum flux ($\tau$), heat flux (H), and evaporation (E) across the air-sea interface can be computed approximately under variable stability conditions (Roll, 1965, p. 279). They are essential elements in energy and heat budget estimation for a given region (see, e.g., Kraus, 1972) and are summarized as follows:

$$\tau = \rho \; U_*^2 \qquad\qquad\qquad (2.7)$$

$$H = c_p \; \rho \; U_*^2 \; (\theta_{sea} - \theta_z)/U_z \qquad\qquad (2.8)$$

$$E = \rho \; U_*^2 \; (q_{sea} - q_z)/U_z \qquad\qquad (2.9)$$

where $\rho$ is the air density, $c_p$ is the specific heat at constant pressure, $\theta_{sea}$ and $q_{sea}$ are the potential temperature and specific humidity at the sea surface, respectively, and $\theta_z$ and $q_z$ are corresponding parameters at height z.

It can be seen from equations (2.7) through (2.9) that, if we know the value of $U_*$, these fluxes can be computed. Other parameters are easier to obtain from meteorological records. The problem now reduces to parameterizing $U_*$. A formula proposed by Hsu (1974a) accomplishes this task:

$$\frac{2\pi z}{H/C^2} = U_*^2 \; e^{\kappa U_z/U_*} \qquad\qquad (2.10)$$

where $\kappa$ is the von Karman constant and H and C are the average wave height and phase velocity (obtained from the wave period) of the dominant waves. An improved nomogram for equation (2.10) is shown in Figure 11 (see Hsu, 1976). Note that equation (2.10) has been further verified by simultaneous observations of wind, wave, and stability parameters from the North Atlantic Ocean, Lake Michigan, and the Beaufort Sea. For more detail see Hsu (1974b; 1976). However, verification of equation (2.10) in other regions such as the South Atlantic Ocean is lacking. The main purpose of the measurement program in the offshore region of the study area (cf. Fig. 5) was to fill this void. The following sections are devoted to this goal.

The field experiment to measure the wind stress on the sea surface in the coastal waters of Brazil was conducted in June 1975 on a Petrobras offshore platform, PG-3 (Fig. 12), located approximately 12 km offshore in water 28 meters deep (cf.

24
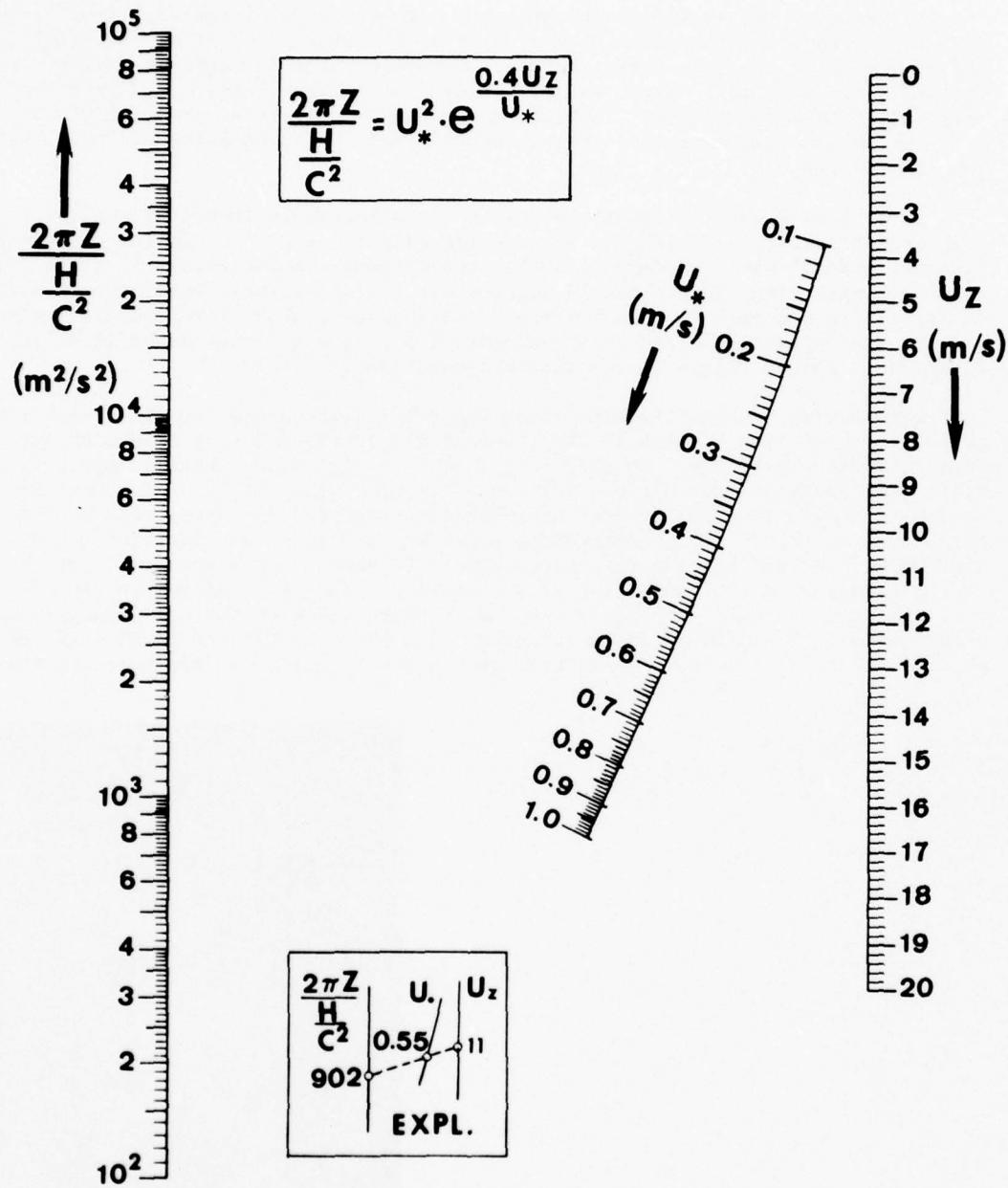
Figure 11. A nomograph representing equation (2.10). The figure gives an example of the use of commonly available wind ($U_Z$) and wave (H and C) parameters to obtain $U_*$ (from Hsu, 1976).

25

Fig. 5). The main instrument used for this study was a portable Thornthwaite Wind Profile Register System (C. W. Thornthwaite Associates Model 106). Six-unit, three-cup, fast-response anemometers were mounted approximately 170, 190, 230, 310, 390, and 470 cm above the mean water surface. Care was taken to minimize the effects of the platform (see, e.g., Hicks and Dyer, 1970; DeLeonibus, 1971). In particular, only those measurements that displayed a consistent logarithmic profile without the platform obstruction were used in this study. For instrumentation and data analysis, see Hsu (1972b).

Curve C in Figure 13 shows the result of measurements from this study. The drag coefficient $C_d$ [$= (u_*/U_z)^2$] is approximately $1.5 \times 10^{-3}$. Similar experiments in other coastal waters under different wind systems are included. It can be seen that no single drag coefficient is appropriate for all coastal environments because $U_*$ is related not only to $U_{10m}$ but also to atmospheric stability conditions (Hsu, 1974b), wave height (H), and phase velocity (C) of the dominant waves (Hsu, 1974a). Equation (2.10) or Figure 11 was thus proposed (Hsu, 1974a).

Information on synoptic meteorological conditions during our field measurement period, from 14 June through 17 June, was kindly provided by the Brazilian Air Force Weather Office in Recife. An example is shown in Figure 14. Logarithmic wind profiles were obtained from 3 p.m. on 15 June through 3 p.m. on 16 June. Weather map series indicated that the frontal system had passed over the study area at 3 p.m. on 15 June and moved to the northeast, as shown in Figure 14. Therefore, the on-shore wind had been blowing for approximately 20 hours. From the wind profile data during this period the wind speed at 10 meters was extrapolated and was found to be equal to about 9.3 m/sec. This value was in agreement with the ocean-going-ship observation (approximately 30 km southwest of PG-3, as indicated in Fig. 14) of about 11 m/sec. From the significant wave forecasting method (see Bretschneider,



Figure 12. A photograph of the Thornthwaite Wind Profile Register System on an offshore platform (PG-3, Petrobras). Note that the working catwalk is about 14 meters above the mean water surface.

26

1963) the significant wave height is found to be 1.9 meters (or $\bar{H}$ = 1.2 meters) and wave period is 7.5 sec (or C = 11.7 m/sec). Utilizing values of H, C, and $U_{10m}$, it is estimated from Figure 11 that $U_* = 34$ cm/sec. This value is in good agreement with the observed $U_*$ value of 36 cm/sec derived from curve C in Figure 13. The acoustic radar observation in the study area near Aracaju indicates that during this period very weak, unstable conditions prevailed in the atmosphere. These results are shown in Figure 15. In other words, Figure 11 or equation (2.10) has been further verified by our observations from the study area. Other verifications, shown in Figure 15, have been reported (Hsu, 1976).
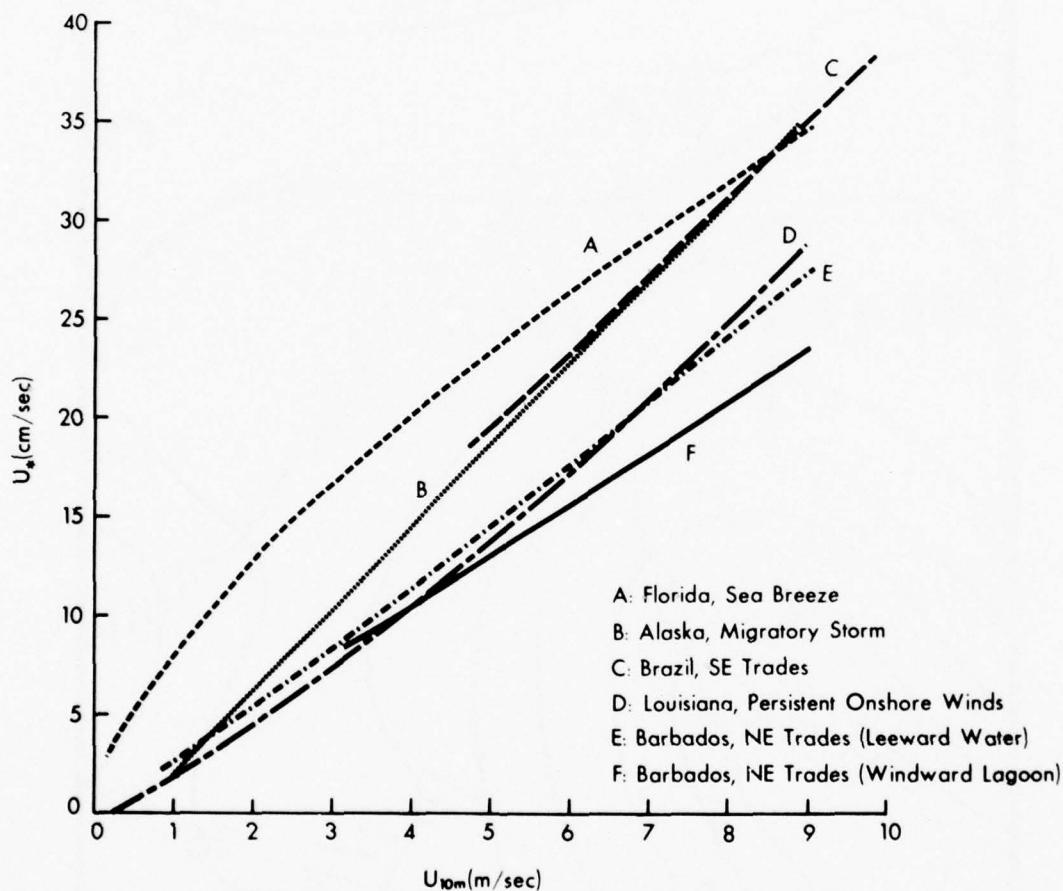


Figure 13. Measurements of $U_*$ as a function of $U_{10m}$ over the coastal water under southeastern trade wind effects in the shallow water near Aracaju, northeastern Brazil (curve C). For comparison, curve A was based on experiment performed under diurnal sea breeze conditions (limited duration and fetch) near Fort Walton, Florida (Hsu, 1972b); B, under migratory storm conditions (variable duration and fetch) near Point Lay, on the Alaskan Arctic coast (Walters, 1975); D, under relatively persistent onshore winds caused by the Bermuda high-pressure system in Caminada Bay, Louisiana (longer duration and shorter fetch) (Kjerfve, 1973); E, under northeastern trade wind effects (unlimited duration and somewhat limited fetch) in leeward coastal waters in Barbados, West Indies (Hsu, 1975); and F, under trade wind effects in a windward lagoonal environment (unlimited duration but limited fetch) in Barbados (Hsu, 1975). Note that the same type of instrument, (i.e., C. W. Thornthwaite Wind Profile Register System) and instrumentation setups were used in all experiments (see Hsu, 1972b).

27
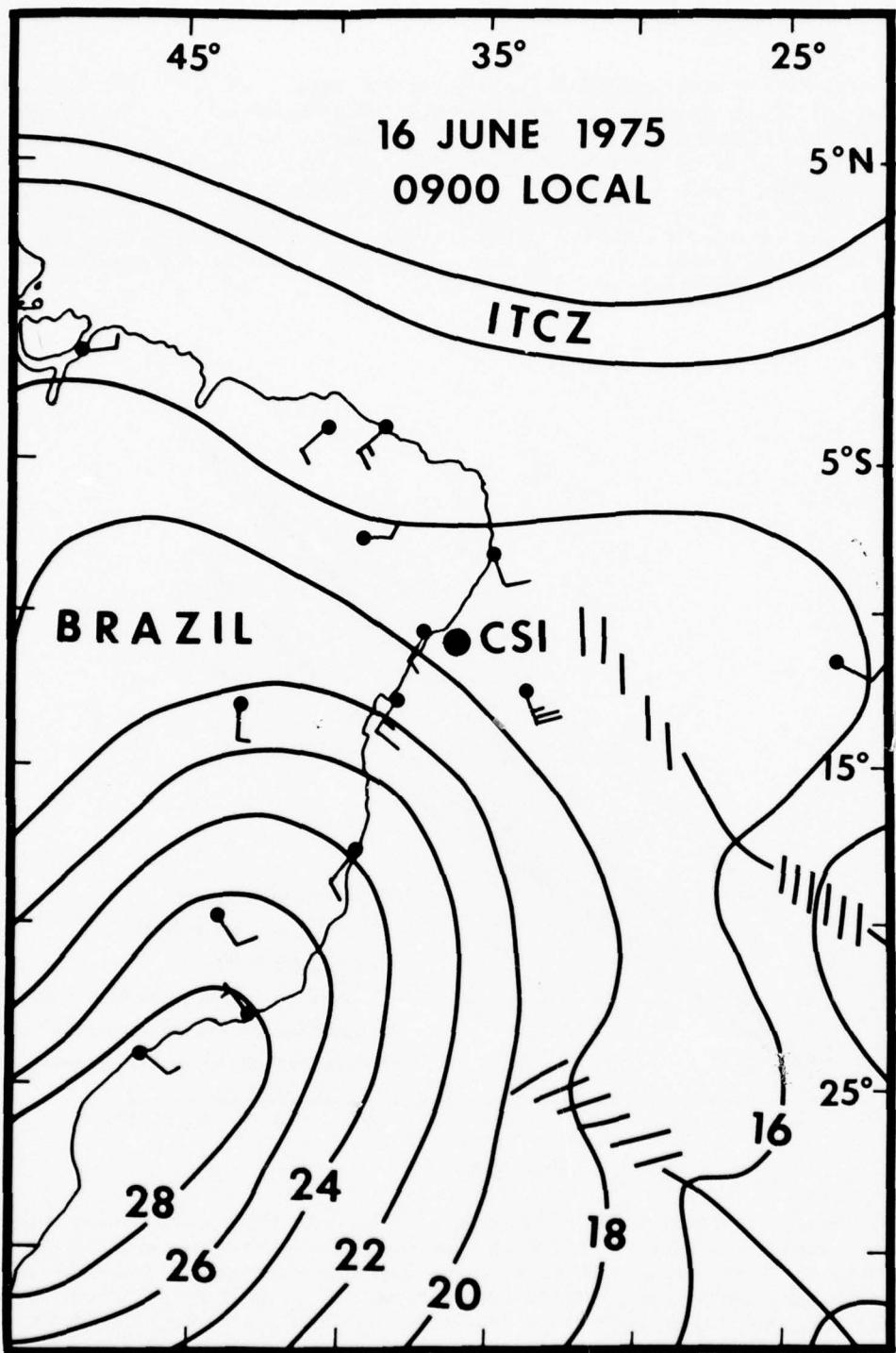
Figure 14. The synoptic meteorological condition during the offshore experiment. ITCZ represents the intertropical convergence zone. The initials CSI stand for the Coastal Studies Institute experimental location (cf. Fig. 5).
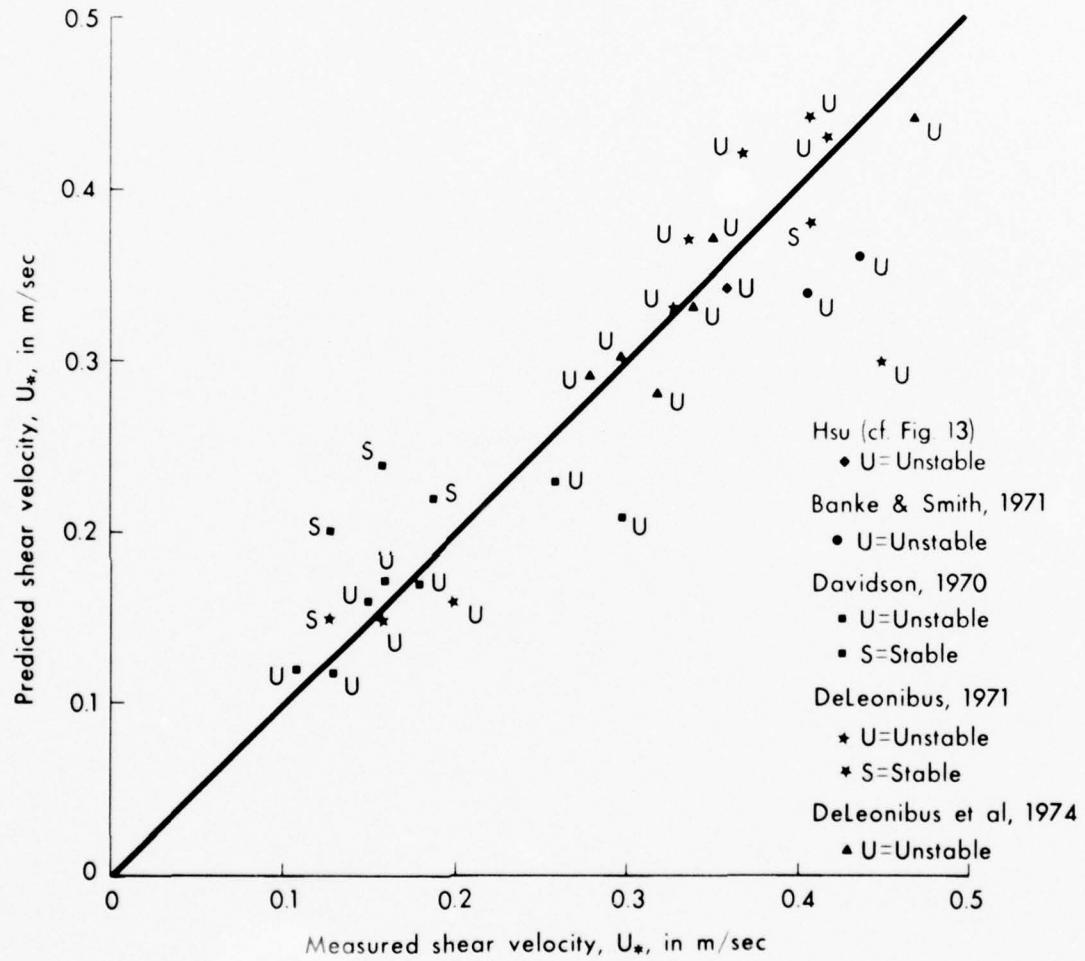
Figure 15. Verification of equation (2.10) or Figure 11 from available studies by Banke and Smith (1971) in the Beaufort Sea, by Davidson (1970) in Lake Michigan, by DeLeonibus (1971) and DeLeonibus et al. (1974) in the Atlantic Ocean, and by Hsu (cf. Fig. 13, curve C) in the shallow water near Aracaju, on the northeastern coast of Brazil.

III.   COASTAL OCEANOGRAPHY


Introduction

Coastal oceanography concerns those hydrodynamic processes occurring near the shoreline that are either input from the deep oceans, i.e., tides and waves, or have their origin in shallow water, i.e., breakers, surf zone currents, and lagoon circulation.   This section will describe the coastal oceanographic conditions of the study area.   Attention is focused upon three topics:   sea level, waves, and nearshore processes.


Sea Level

Sea level is an important datum for coastal processes because it determines the position on the shoreline of the surf zone processes and the final gradient of rivers and estuaries and because changes in sea level are correlated with current systems affecting the whole continental shelf.   In estuaries and lagoons these sea level changes can result in mixing and changes in water mass properties.

The sea level datum is controlled by several processes, ranging from tides and wind set-up to atmospheric and oceanographic pressure systems.   Of these processes, tides are usually the most significant factor.   However, wind stress can cause set-up and draw-down near shore, which can occasionally produce larger sea level variations than tides.   These wind effects are amplified on broad, flat, shallow shelves.

Sea level variations were observed at two points along the northeast coast during the study.   One gage was located at the entrance to the Suape Lagoon complex (see Fig. 6) and the other was located in 28 meters of water on platform PG-3A, offshore of Aracaju (see Fig. 5).   The data from Aracaju are shown in Figure 16. The sea level variation shows the overwhelming dominance of the semidiurnal astronomical tide.   Shown on the figure are the times of high and low water, taken from the tide tables for Aracaju (U.S. Department of Commerce, 1975).   The predictions are within 20 min of the observations; our time base was approximately the same. Tide levels showed good agreement with tide height tables, to within about 6 cm.   A front that moved into the area on 15 June produced winds of about 10 m/sec.   These conditions prevailed for several days, but no major wind effect was noted in the offshore tide record as a result of the storm.

The sea level data from Suape are shown in Figure 17.   Again, the dominance of the astronomical tides is obvious.   Winds were light during the measurement period. Comparison with tide table predictions shows good agreement.   For the period of the data the discrepancy in times of high and low water between observations and the tables averaged 18 min.   The discrepancy in heights averaged 8 cm.   These discrepancies were within our error in time and slightly greater than the error in height. At Suape, sea level variations controlled the flow of water into the lagoon complex and the amount of wave action reaching into the lagoon from the ocean.   These factors are considered in the section on nearshore processes.


31
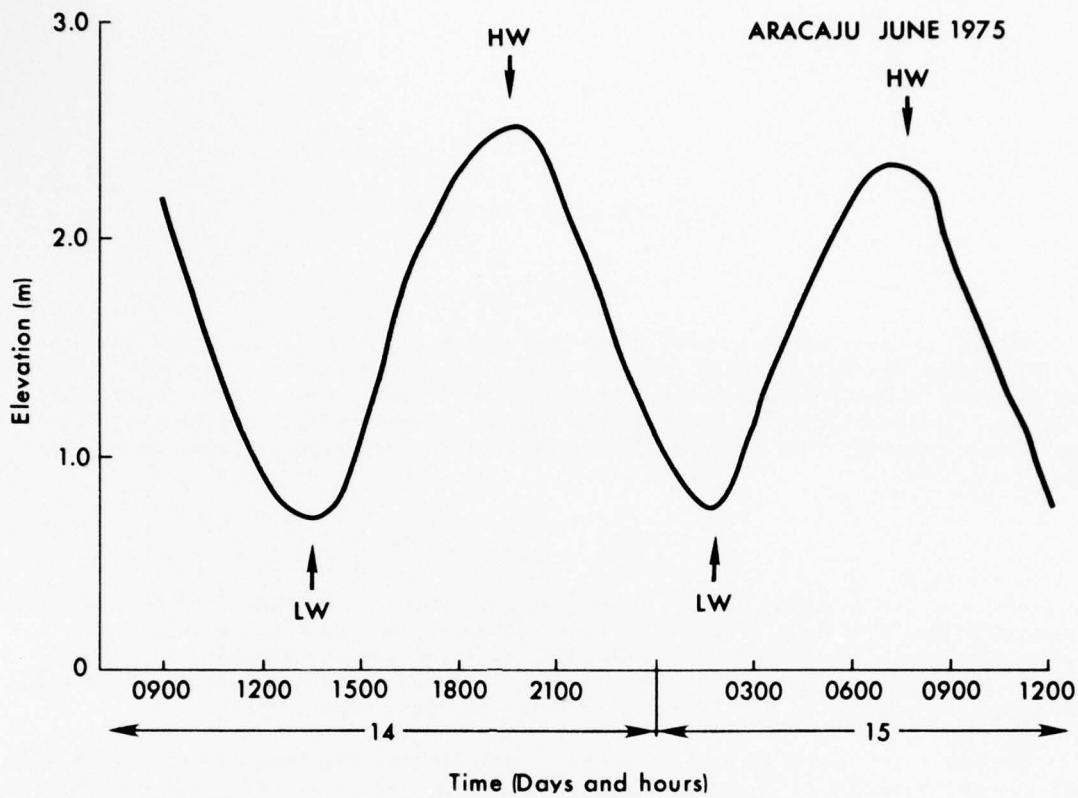
Figure 16. Segment of sea level record taken at Aracaju and times of predicted low tide (LW) and high tide (HW).

Since the tide tables have apparently predicted well the sea level variations at two widely separated points along the coast, they can be used to consider the regional variation in tides.

The time of high tide increases southward and northward from Recife. These time differences are given in Table 4. The table indicates that there is a general trend for points farther west of Recife to have a proportionally later time of high tide. The exception to this trend is Salvador, where high tide occurs 2 min earlier than the high tide at Recife. Tidal heights are slightly larger to the north of Recife and smaller to the south. The mean range at Recife is 1.62 meters, but to the north, at Tambau, the mean range is 1.83 meters. To the south the mean ranges are 1.55 meters at Maceio and 1.43 meters at Aracaju. Again Salvador, having a mean range of 1.68 meters, is an exception to this trend.

Recent research on ocean tides (Hendershott, 1973) indicates that tides in the South Atlantic are poorly understood. The existence of an amphidiomic point in the South Atlantic is still uncertain. The tide system throughout the South Atlantic, as determined from stations along South American and African coasts by Dietrich

32
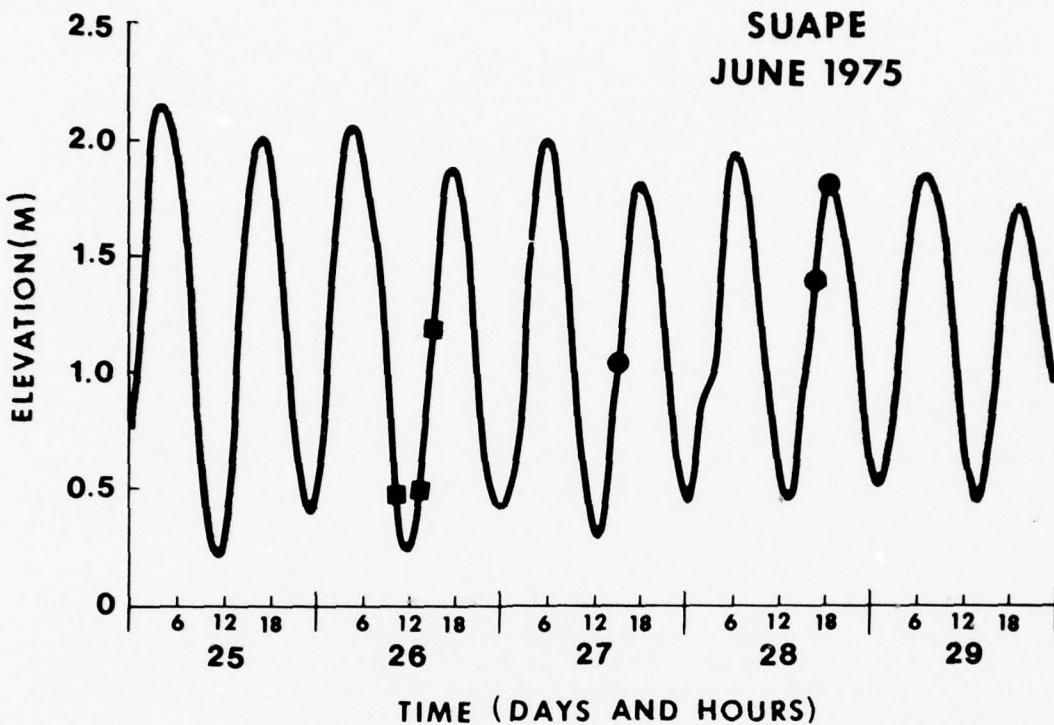
Figure 17. Segment of sea level record from Suape and times of current measurements (squares) and wave measurements (dots) in Suape lagoon.

(1944), indicates a northward-propagating $M_2$ tide having co-tidal lines roughly parallel to lines of latitude. In this system the times of high tide along the northeast coast of Brazil should increase everywhere to the north. There is an apparent reversal of this trend between Aracaju and Recife.

### Waves

The wave climate of the South Atlantic is poorly known because of the lack of direct observations of wave heights. Until such a time as more data are available, we must rely primarily upon hindcasting and visual observations for the information upon which to base conclusions about the offshore wave field, which must be tentative, especially regarding severe conditions, because these times are likely to be the least well represented in the data.

Annual wave statistics for the northeast coast of Brazil are shown in Figure 18. Three sets of data are shown. The lines indicate the probability of exceeding a wave of a given height. These data include the reports of visual observations (Hogben and Lumb, 1967), a 1-year record at Aracaju (Petrobras), and data presented by Russell (1969). The three sets of curves show that wave heights average between

33

Table 4

High Tide

| Location | Time Difference on Recife (minutes) | West Longitude |
|---|---|---|
| Macau, Acu River | +89 | 36°41' |
| Natal | +28 | 35°12' |
| Cabedelo | +36 | 34°50' |
| Tambau | - 4 | 34°50' |
| Recife | 0 | 34°52' |
| Maceio | +10 | 35°43' |
| Rio Sao Francisco | + 6 | 36°24' |
| Aracaju | +33 | 37°03' |
| Porto Du Salvador | - 2 | 38°31' |

0.75 and 1.25 meters. This value is slightly greater than that of Southern California or the Atlantic coast of the U.S. and higher than the average along the U.S. Gulf Coast. However, at lower probabilities the wave climate in Brazil has lower wave heights than either the East Coast of the United States or the Gulf of Mexico, as indicated in Table 5.

Thus, although the average wave height is large in Brazil, extreme wave heights are indicated to be relatively infrequent.

The concept of a high- and low-energy coastal environment has been employed for several decades to describe the general characteristics of coastal wave action. These data indicate that a quantitative definition of wave energy level along a coast might make distinction between extreme wave height (say, at the 1 percent level) and average wave height (50 percent). Because the wave climate probability curve is roughly exponential, these two points would determine the probability line so that other probabilities could be determined.

The variability of wave action over a short period of time (a few days or less) is also an important consideration in characterizing the coastal sea state. Measurements of wave spectra were made at the offshore station to determine these characteristics. In Figure 19 the wave spectra measured at 0800 on 14 June and 17 June show major effects of swell and wind waves on the wave characteristics.

The spectrum from 14 June (lower curve) shows two well-defined peaks, one at a radial frequency of 0.5 rad/sec (frequency of 0.0796 Hz) and another at a frequency of 0.8 rad/sec (frequency of 0.127 Hz). The low-frequency peak is produced by swell in the South Atlantic.

Swell climate for this coastal location is difficult to predict because the effective source area for the northeast coast is the whole South Atlantic. However, swell can be a major source of wave action for the northeast coast in the winter months. Swell waves are not easily identified through visual measurements, and correct resolution requires wave staff measurements.

34
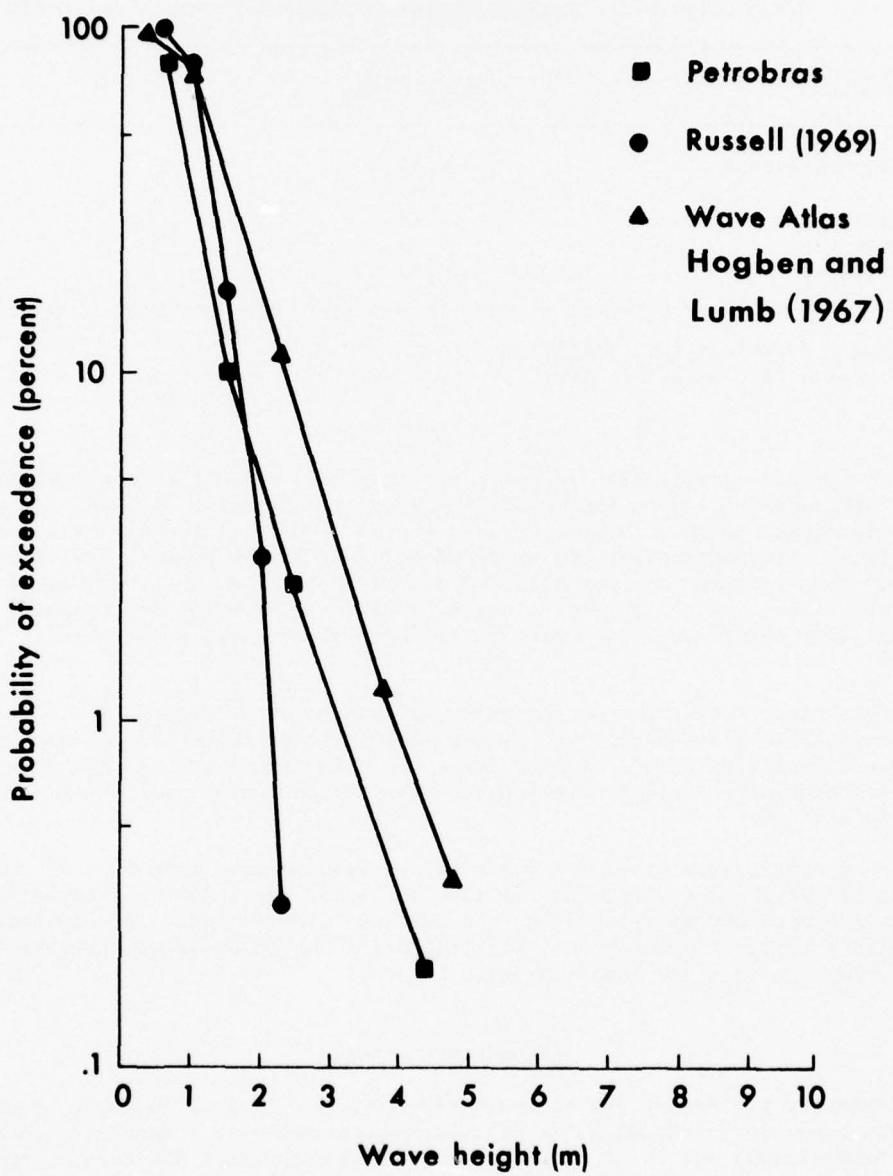
Figure 18. Annual probability of exceeding a wave of a given height for the Aracaju area.

35

Table 5

Wave Heights for Various Locations for Two Probability Levels

| Location | $H_{ave}$ (50%) | H (1%) |
|---|---|---|
| Southern California | 0.75 m | 3 m |
| Brazil | 1.0 m | 3 m |
| Washington | 1.75 m | 5 m |
| Louisiana | 0.75 m | 3.5 m |
| Cape Hatteras | 0.75 m | 4.5 m |

$H_{ave}$ = average wave height
H (1%) = wave height exceeded by 1% of waves

The spectrum for 17 June (upper curve, Fig. 19) shows the effect of high local winds. The wind wave peak increased in energy by a factor of 10, and the peak period increased to about 9 sec (frequency of 0.11 Hz). The swell is now almost obscured in the spectrum but can be discerned as a slight peak at low frequency. The wind wave spectrum was not well reproduced by the P.M. spectrum (Pierson and Moskowitz, 1964) for the appropriate wind speed (9.0 m/sec). The measured significant wave height was 1.41 meters, but the P.M. spectrum would predict 1.72 meters.

Statistical properties of the wave conditions during each of the times of measurement were also considered. For example, the distribution of wave heights during the measurement made on 17 June is shown in Figure 20. It shows the probability of exceeding a given wave height. The critical observed wave heights are given in Table 6.

Based upon the observed 243 waves and an average wave height of 95 cm, the theoretical Rayleigh distribution is also shown in Figure 20. The Rayleigh distribution is a good approximate fit to the observed distribution. At low values of probability (i.e., 1 percent) the Rayleigh distribution predicts a higher wave height than the observed data suggest.

## Nearshore Processes

Nearshore processes involve the action of waves in shallow water, surf zone processes, and wave-induced water circulation and sediment transport. Understanding of nearshore processes is of prime importance in describing the coastal processes of the region because it is in these processes that waves, currents, and sediment transport are most intense and interactions are strongest. Detailed studies are described in this section. These studies include the longshore variation of infragravity waves within the surf zone, the effect of offshore reefs on wave action, and the circulation behind a stone reef.

Infragravity waves are surface waves whose frequencies lie between 0.1 and 2 cycles per minute (cpm), i.e., they have periods between 10 min and 30 sec. The general characteristics of these waves in the nearshore zone appear to be, from the
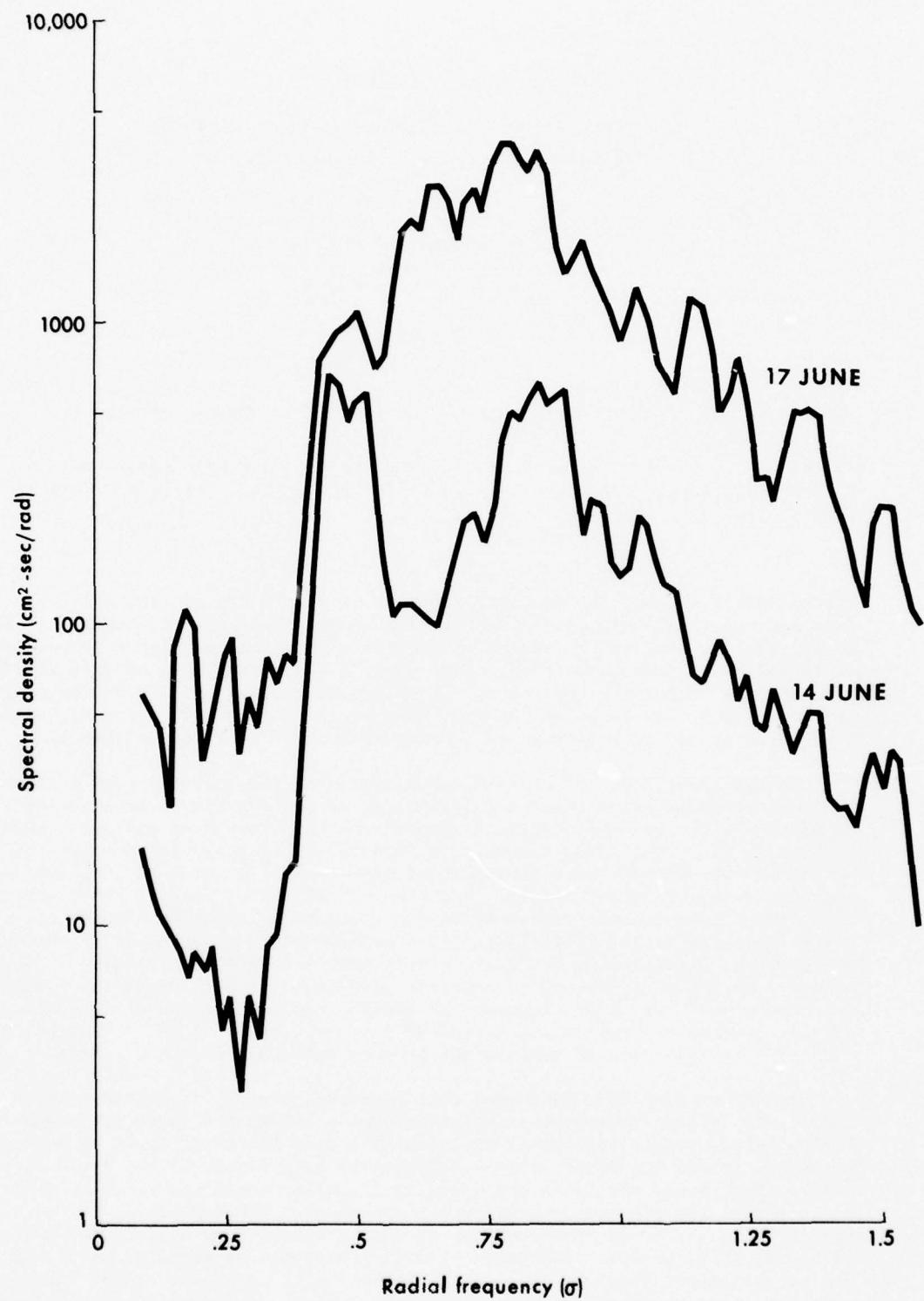
Figure 19. Spectrum of waves measured at platform PG-3, offshore of Aracaju, at 0800 on 14 June (lower curve) and on 17 June (upper curve).

37

Table 6

Observed Wave Conditions at 0800 on 17 June

$H_{ave}$ = 95 cm

$H_{rms}$ = 105 cm

$H_s$ = 141 cm

$H_{1/10}$ = 227 cm

$H_{max}$ = 238 cm

where $H_{ave}$ is the average wave height, $H_{rms}$ is the root mean square wave height, $H_s$ is the significant wave height, $H_{1/10}$ is the 10th highest wave, and $H_{max}$ is the highest wave.

little data available, fundamentally different from those of wind waves and swell. They are apparently highly reflective from natural beaches and, because of their relatively low amplitudes, occupy a spectral valley between higher frequency wind waves and lower frequency tides. These unique characteristics of infragravity waves require data collection, analysis, and interpretation techniques different from those used for wind waves and swell. This study reports both the results and the techniques of an investigation of infragravity waves on a natural beach.

Energy enters the infragravity wave region of the spectrum from a number of sources, including submarine earthquakes and volcanic action, storm systems, actions of wind on pack ice, and nonlinear interactions of wind waves and swell (Munk, 1951; Hunkins, 1962; Munk, 1962). Energy in this frequency range is generally quite low, having an average root mean square (rms) amplitude of about 1 cm, but may peak sharply during transient events. Surf beat (Munk, 1949; Tucker, 1950) and high-frequency tsunamis are examples of infragravity waves whose amplitudes are characteristically 10 to 100 times larger than mean conditions. Because of their long wavelengths, infragravity waves are highly interactive with bathymetry. A wave having a period of 2 min has a deepwater wavelength of 22.5 km and is a shallow-water wave over the entire continental shelf. The combination of long wavelengths and low amplitudes implies low steepnesses (on the order of $10^{-7}$) that ensure high reflectivity from natural beaches and produce standing waves near shore.

Recent studies have indicated that long-period waves (periods between 30 sec and 10 min) affect nearshore circulation (Sonu, 1972a) and swash processes (Waddell, 1973). Also, long-period standing waves have been indicated to be an important mechanism in forming beach cusps and longshore bars (Sonu, 1972b; Bowen and Inman, 1971). Surf beats are large-amplitude infragravity waves generated by shoaling waves (Munk, 1949; Tucker, 1950; Hasselmann et al., 1963; Suhayda, 1974a) and appear to be reflected from beaches, so that a standing wave is produced near shore (Suhayda, 1972, 1974b). However, two different types of standing waves can occur, and no systematic study of the spatial variation of surf beat or the induced velocity field has been made to resolve this point. The velocity field is an important consideration because it is the critical factor that controls sediment movement.

38
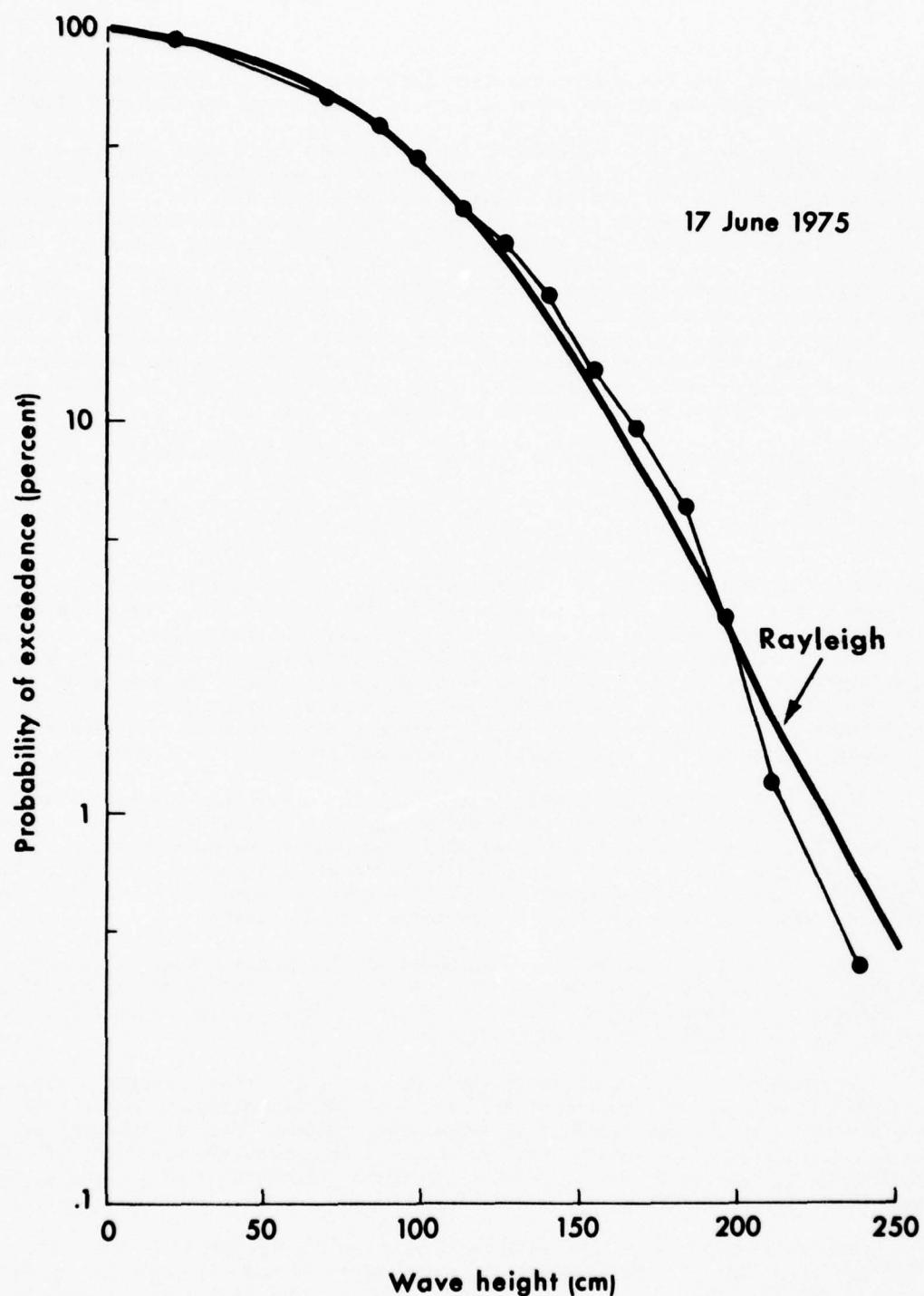
Figure 20.  Observed distribution of wave heights on 17 June (line with dots) compared with theoretical Rayleigh distribution (thick line) having the same average wave height.

Investigation of this phenomenon requires field measurements of nearshore wave heights and velocities in sufficient detail to resolve beat wave contributions.

Wave instruments were deployed at the Plantation beach site (Fig. 5). Repeated surveys revealed that on 20 June a bar was beginning to develop. Instruments were then deployed on 21 June in a line running offshore (see Fig. 40). The results of the data taken are shown in Figure 21; they indicate that well-developed standing surf beat waves occurred. The phase difference between sensors showed the rapid change from in phase (0°) to out of phase (−π) over a narrow frequency band, a characteristic of standing waves (Suhayda, 1974). On the following day, the instruments were deployed alongshore (see Fig. 41) at separations of 20 and 50 meters. The results are shown in Figure 22. The data show no rapid alongshore phase variation that would indicate edge wave modes. On the next day the instruments were again placed along shore at distances of 100 and 200 meters (see Fig. 41). Still no alongshore variation was observed, as shown in Figure 23.

Edge wave wavelengths (Le) on a plane beach are given for various modes N by (Ursell, 1952):

$$Le = \frac{2\pi g}{\sigma^2} \sin{(2N + 1)} B$$

where g is the acceleration of gravity, $\sigma$ (= $2\pi f$) is the radial frequency, f is the frequency in cycles/sec, and B is the slope of the beach. Using the slope of the Aracaju beach (B = 0.015), the spacing of the modes of standing edge waves is given in Table 7. The spacing of the modes of the standing wave is one half an edge wave wavelength, or Le/2. The spacing varies from 465 meters for the zero mode at a frequency of 0.005 to 12.8 meters for the zero mode at a frequency of 0.03 Hz. Thus measurements with a spacing of up to 200 meters would have shown the presence of standing edge waves over the range of frequencies from 0.007 to 0.030 Hz.

Close inspection of the phase difference between measurements made along shore indicates a slightly increasing phase difference with frequency. This increase is possibly due to long-crested, low-frequency surf-beat waves approaching the shoreline at a slight angle so that a phase difference between points along shore is produced. Assuming a phase speed of about 2 m/sec, the measured phase differences imply an incidence angle of about 10° to normal to the beach.

This test for the presence of edge waves was important because the assumed presence of these waves has been used to explain the generation of rip currents and crescentic bars along beaches. This test indicates that there may be other mechanisms that can generate these features.

The presence of the stone reefs along much of the northeast coast causes waves to break at a distance from the shoreline. This filtering action causes wave height and period to be greatly modified from deepwater values. Most of the data available in the scientific literature on this effect is from laboratory studies. One of the objectives of this study was to measure the waves inshore of a stone reef to quantify this filtering effect.

The measurements were made inshore of a break or depression in the stone reef at Suape (see Fig. 6). Measurements of waves near the shoreline are shown in Figures 24 and 25. The data indicate that waves within the lagoon were highly reflected by the steep lagoon beach and that longer period components formed standing components.

40
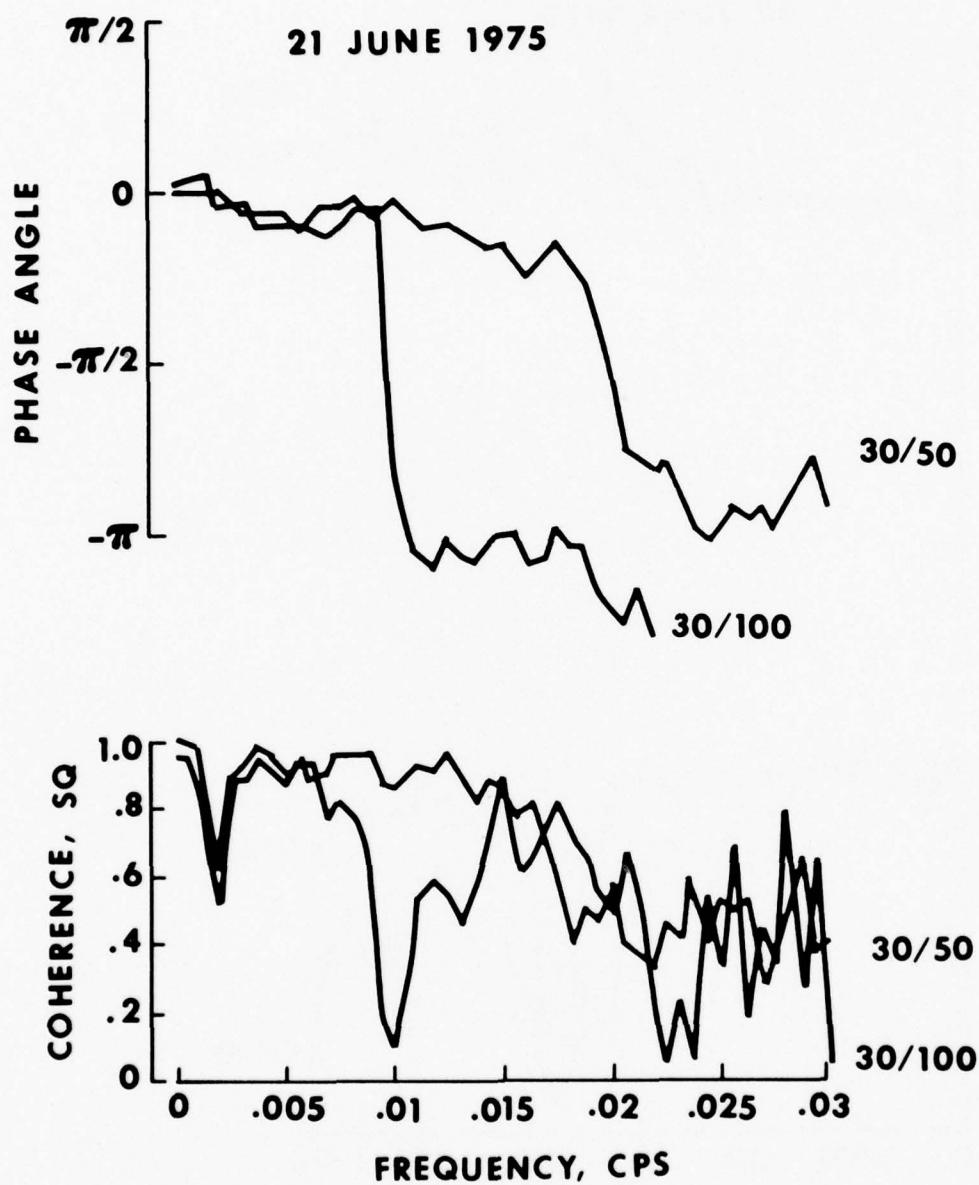
Figure 21. Coherence and phase difference between three infragravity wave records taken at Aracaju at separations of 20 meters and 70 meters offshore. Note rapid phase change from 0 to -π in both sets; standing waves are indicated.

41
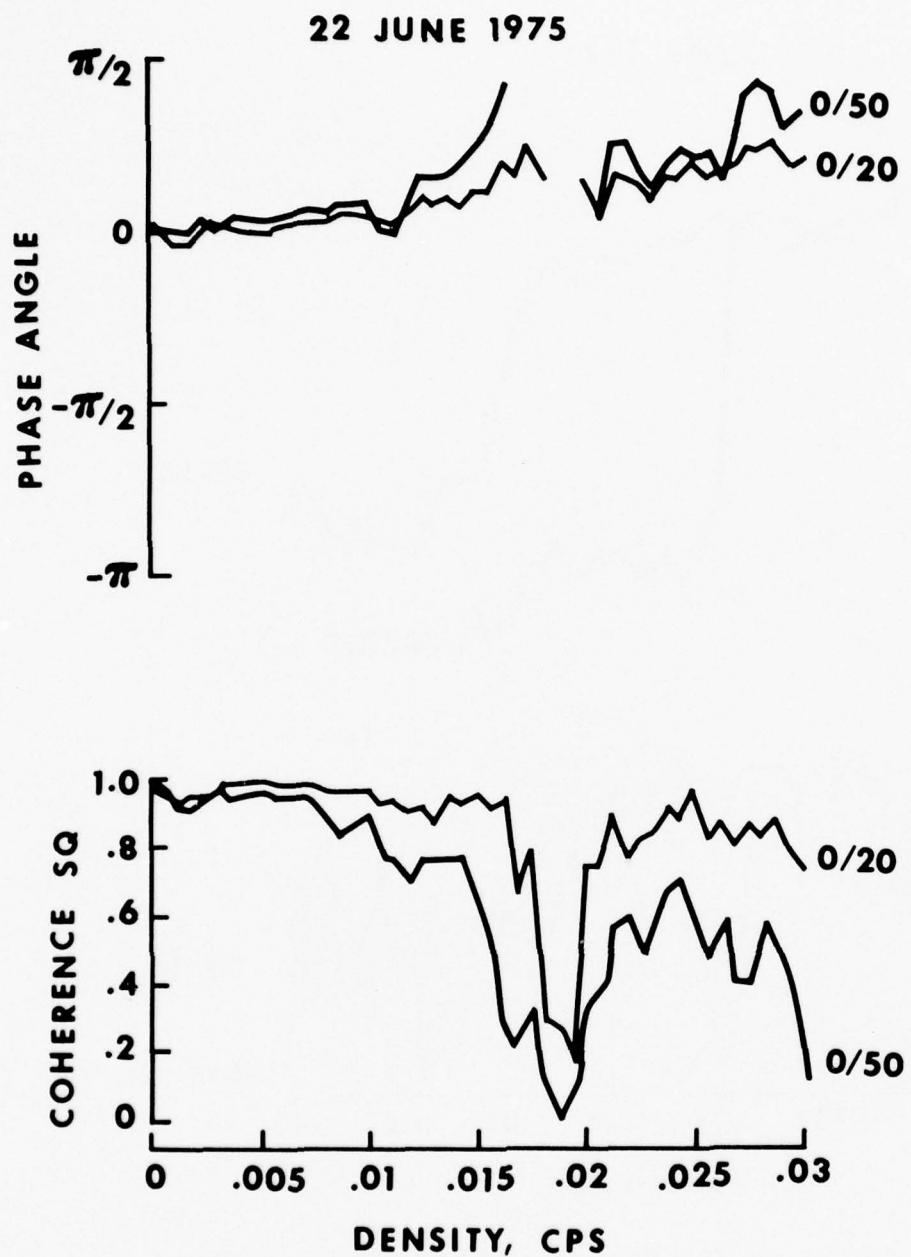
Figure 22. Coherence and phase differences between three infra-gravity wave records at Aracaju taken at separations of 20 meters and 50 meters alongshore.
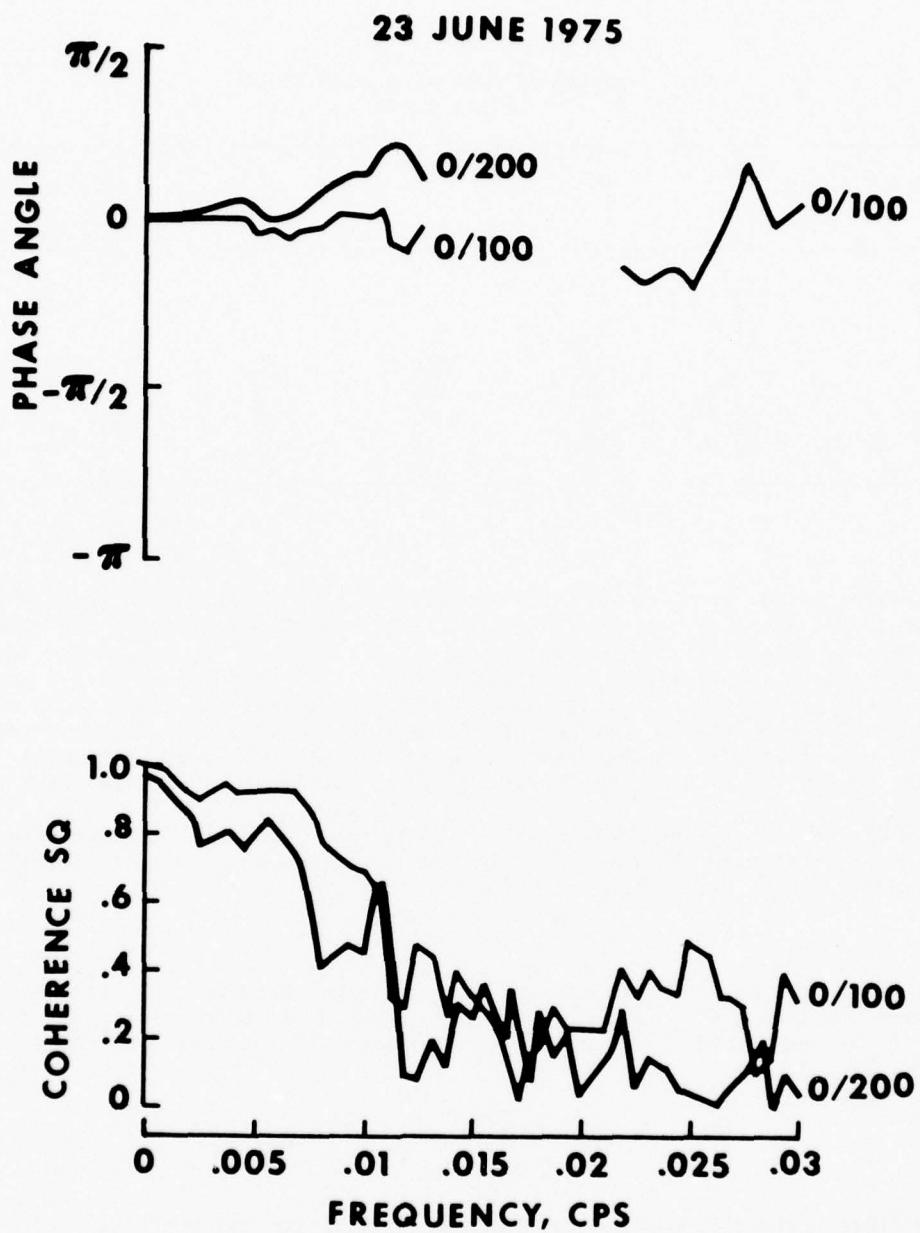
Figure 23. Coherence and phase difference between infragravity wave records taken at separations of 100 meters and 50 meters alongshore.

Table 7

Spacing of Nodes for Edge Waves
(meters)

| Frequency (Hz) | 0 | 1 | 2 | 3 | 4 | 5 |
|---|---|---|---|---|---|---|
| 0.005 | 465 | | | | | |
| 0.007 | 238 | | | | | |
| 0.01 | 117 | 351 | | | | |
| 0.015 | 52 | 156 | 260 | | | |
| 0.02 | 29.3 | 88 | 146 | 203 | | |
| 0.025 | 18.7 | 56 | 93 | 130 | 167 | |
| 0.030 | 12.8 | 38 | 64 | 88 | 116 | 142 |

The wave height at the beach as a function of tide level varied greatly (Fig. 25). At a tide datum of 1.1 meters (water level even with the top of the stone reef at the break), lagoon wave height was 7 cm. At a tide level of 1.4 meters (or 0.3 meter higher), wave height increased to 28 cm. At a tide level of 2.0 meters (or 0.9 meter higher than the first point), the wave height increased to 56 cm. For an offshore (near breaking) wave height of 1 meter, these results indicate good agreement with laboratory measurements of waves crossing a submerged barrier (Nakamura et al., 1966). The reef crest width to wavelength ratio was about 0.5.

The fairly abrupt seaward face of the stone reefs (see Fig. 50) presents a strong slope break from which wave reflection can take place. The transmission coefficient T can be defined as

$$T = 1 - R$$

where R is the reflection coefficient. For submerged reefs where $h_1$ is the water depth over the reef and $h_2$ is the water depth seaward of the reef (therefore the height of the reef is $h_2 - h_1$), the transmission coefficient can be estimated from (Kajiura, 1963):

$$T = \frac{2(h_1/h_2)^{\frac{1}{2}}}{1 + (h_1/h_2)^{\frac{1}{2}}}$$

In Table 8 the transmission coefficient is given for various ratios of $h_1$ to $h_2$.

Thus, for the offshore reefs having a ratio on the order of 0.25-0.5 ($h_1 = 1-2$ m, $h_2 = 4$ m), the reef could cause a reduction in wave height to about three-fourths of the offshore value owing to the reflection process. The actual filtering of waves by the reef would therefore be a combined effect of partial reflections and wave breaking on the reef crest. Both processes are dependent upon the depth of water over the reef crest.

FREQUENCY, HZ

SUAPE
27 JUNE 1975

SPECTRAL DENSITY, cm²sec/RAD

RADIAL FREQUENCY, RAD/SEC
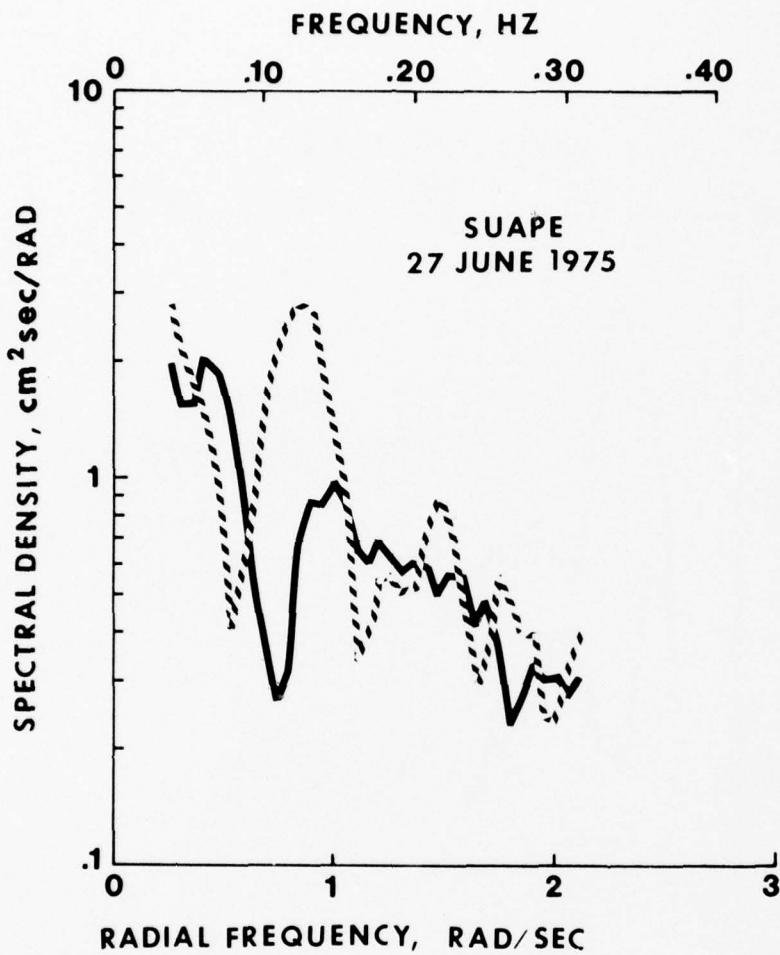
Figure 24. Measured wave spectra at two positions within the Suape lagoon.

The presence of an impermeable offshore barrier such as beach rock in the vicinity of Suape, south of Cabo de Santo Agostinho, has a dominant influence on back-barrier lagoonal circulation. The barrier-lagoon system at Suape terminates to the south as the linear beach-rock exposure intersects land in the vicinity of the small village of Cupe. At the northern end there is a channel approximately 400 meters wide between the beach rock and the granitic cliffs of Cabo de Santo Agostinho One other small break in the beach-rock exposure occurs, at about the midway point. Elevation of the barrier is such that it is submerged at high tide and is recognizable only by a line of breaking waves; shelf water is readily transported across the barrier into the lagoon by the process of wave breaking as well as by gravity-driven flow owing to the hydraulic head difference between the rising tide level outside the barrier and the lagging water level of the lagoon. This difference in
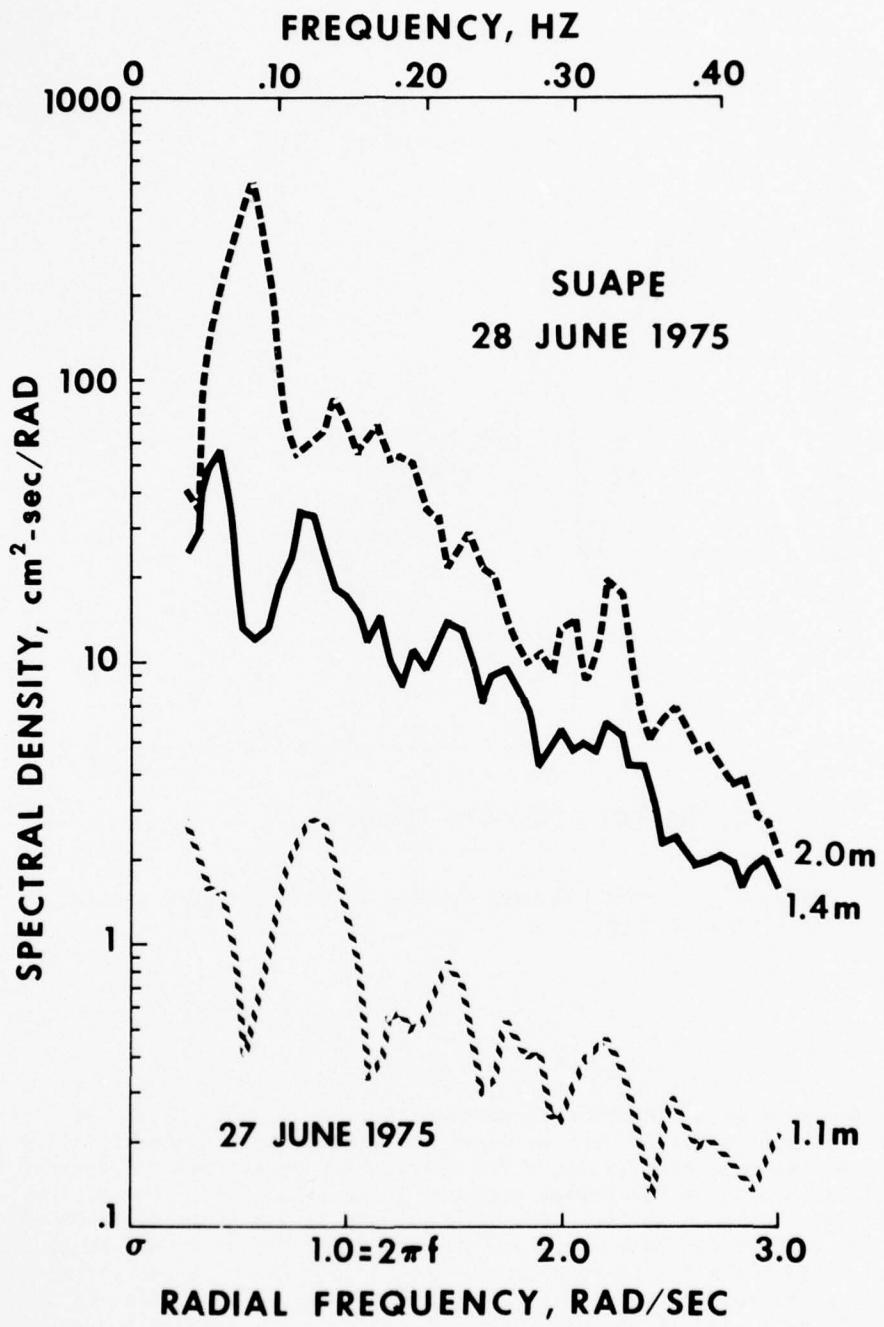
Figure 25. Measurements of wave spectra in Suape lagoon at three stages of the tide (1.1 meters, 1.4 meters, and 2.0 meters).

Table 8

Transmission Coefficient for Submerged Reef

| $h_1/h_2$ | T |
|-----------|------|
| 0.05 | 0.36 |
| 0.1 | 0.48 |
| 0.2 | 0.62 |
| 0.3 | 0.71 |
| 0.4 | 0.77 |
| 0.5 | 0.82 |
| 1.0 | 1.0 |

water level is intensified by an additional elevation of the water surface on the shelf side owing to set-up of waves against the impermeable barrier. Figure 26 illustrates the system under rising tide conditions. Note the foam lineations as they move away from the barrier and into the lagoon. The foam line on the lagoon side of the barrier denotes a density interface between brackish lagoon water and the intruding normal-salinity shelf water. Because the northeast coast of Brazil has a semidiurnal tide, the lagoonal water surface is elevated and depressed through about a 2.2-meter range twice daily. Therefore, the back-barrier lagoon is filled and drained over a 12-hour period twice each day.

As the water level outside the barrier drops below the point at which waves can transport significant amounts of water into the lagoon, the impounded lagoonal water flows northward toward the channel adjacent to Cabo de Santo Agostinho. In order to study this circulation system, the spatial or Lagrangian characteristics of the current field were monitored with the aid of drifting drogues, which were tracked from the shoreline by theodolites. The two shore-based theodolite stations, as well as the boat from which the drogues were deployed, were kept in constant radio contact to assure drogue identification and synchronization for position fixes.

Figure 17 shows the tide record for 25-29 June 1975, which spans the time period of drogue and other experiments run in the Suape area. Three drogue experiments were conducted on 26 June: one on falling tide near the low-tide part of the cycle and two on rising tide. Of the latter, one was run near the low-tide level and one was run near high tide. Figures 27 to 30 summarize results from the drogue studies. Drogues used in these experiments consisted of crossed PVC panels (0.3 m x 0.6 m). Because of the shallow nature of the lagoon, drogues were deployed at a depth of 1 meter.

In the falling tide experiment four drogues were deployed in the southeastern part of the largest lagoonal area near the beach-rock barrier (Fig. 27). They were placed in the channel that occurs in the lee of the barrier along its entire length and were tracked until they reached the channel at the northern end of the beach rock. Figure 27 illustrates the nearly unidirectional paths taken by all four drogues as they were transported northward along the beach-rock trend. The average speeds of the four trajectories range from 67 cm/sec to 55 cm/sec. A maximum velocity of 77 cm/sec was recorded for part of the trajectory of drogue B.

Figure 26.  Seawater intruding into the Suape back-
barrier lagoon through a small tidal channel in the
barrier trend during rising tide.  Also note wave
overwash, as indicated by the linear foam lines.
Foam line in the lagoon denotes a density interface
between normal saline shelf water and brackish lagoon
water.


The second drogue experiment was run during early flood tide as the water level
of the lagoon was starting to rise.  Only two drogues were tracked during this inves-
tigation.  Essentially, the same unidirectional trend of flow to the north along the
barrier existed at this time (Fig. 28).  Velocities for the two drogues, averaged
over the trajectories, were 54 cm/sec and 43 cm/sec.  The velocity variation in these
two drogues is apparently related to their slightly different positions in the ebb
channel behind the barrier.  Drogue B, the slower drogue, was temporarily slowed by
an unusual exposure of beach rock in the ebb flowing channel.  The maximum velocity
recorded by either drogue between consecutive position fixes was 62 cm/sec.  Both
average and maximum velocities in this rising-tide experiment were lower than those
recorded during falling tide.

Approximately 3 hours after the rising-tide experiment, the results of which are
shown in Figure 29, ebb flow had ceased and there was a very strong input of shelf
water to the lagoon through the channel at the northern end of the beach rock.  Three
drogues were placed in the back-barrier channel to determine whether it functioned as
a major conduit for incoming water during the flood portion of the tidal cycle.
Figure 29 shows the results of the late-flood-tide experiment.  All drogues moved
southward into the lagoon from the channel mouth.  Only drogue A followed the back-
barrier channel.  Approximately halfway through the experiment this drogue apparently
met an opposing flow that turned it toward the lagoon interior, possibly in response
to water moving across the beach rock as the tide continued to rise.  The other two
drogues followed an arcuate pattern from the channel mouth to the interior of the
lagoon.  Flow velocities were as high as 51 cm/sec at the beginning of these tra-
jectories.  However, the velocities dropped below 10 cm/sec at the end of trajectory

48
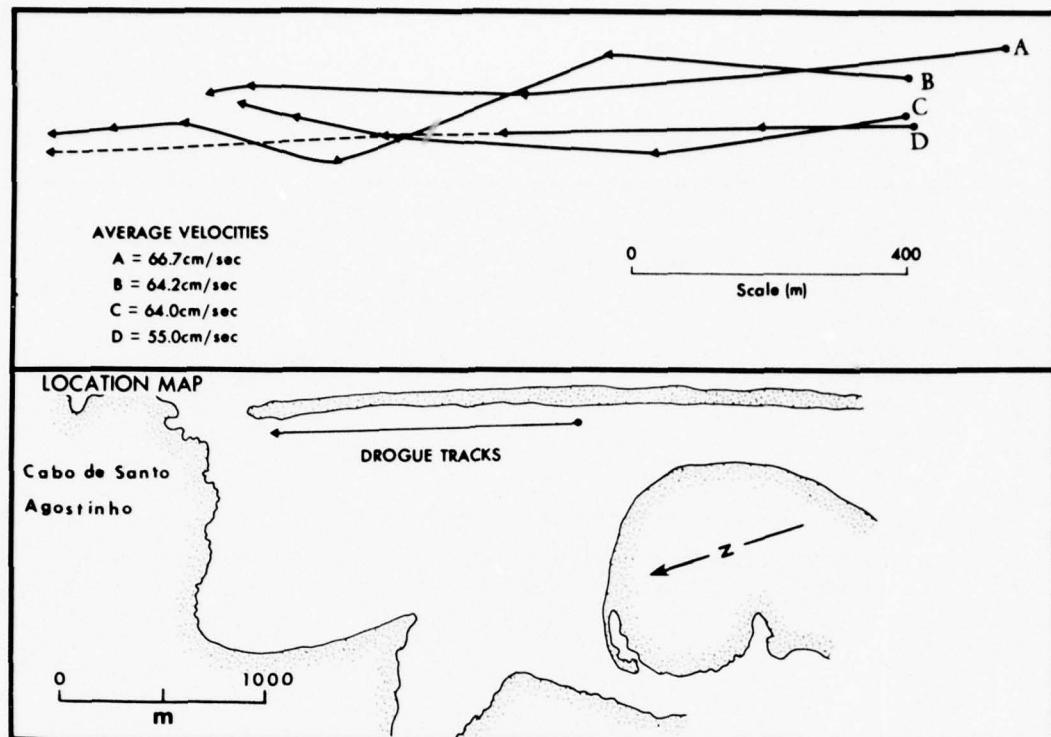
Figure 27. Falling-tide drogue experiment (see Fig. 17 for time of experiment with regard to the tidal cycle).
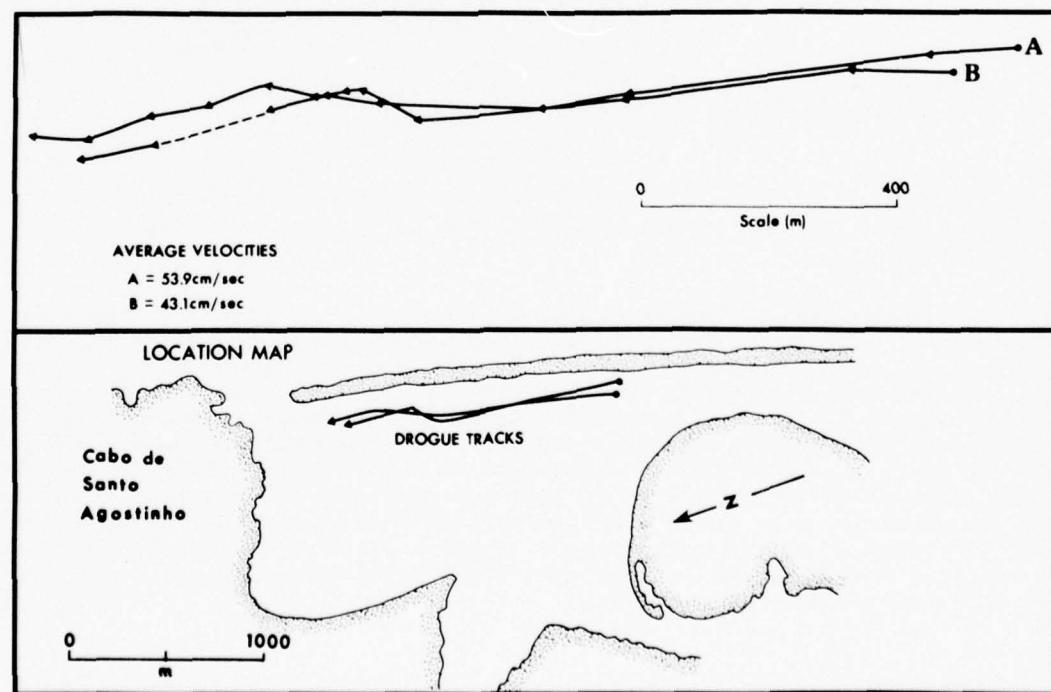


Figure 28. Early-flood-tide drogue experiment (see Fig. 17 for time of experiment with regard to the tidal cycle).

49
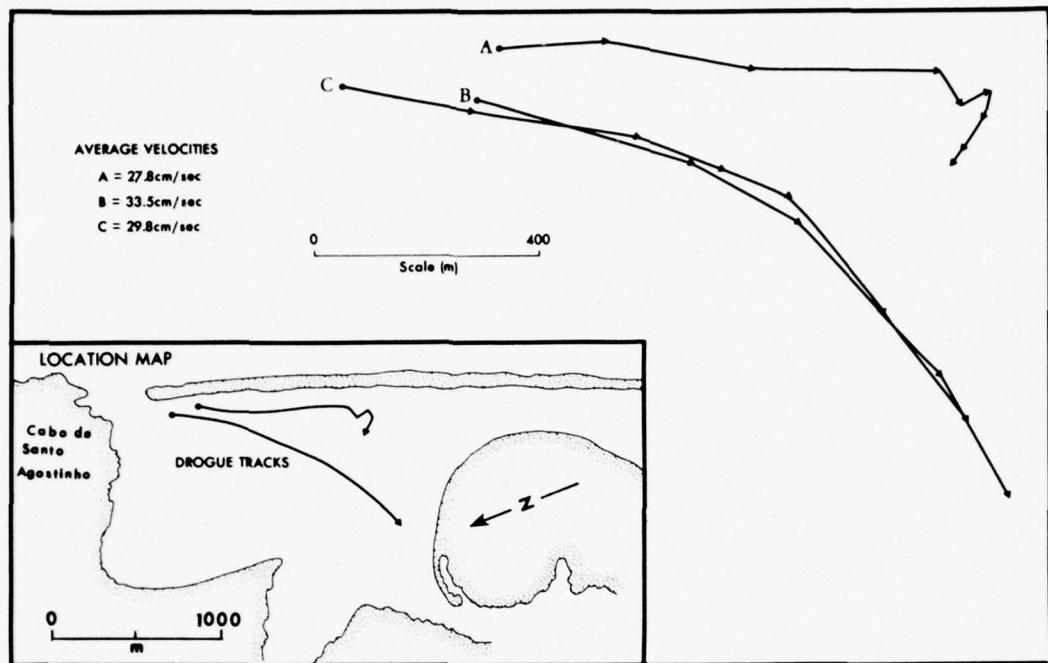
Figure 29. Late-flood-tide drogue experiment (see Fig. 17 for time of experiment with regard to the tidal cycle).

B, for example. Average velocities during this experiment ranged from 28 to 34 cm/sec, values that are considerably lower than those recorded during the other two experiments.

The ebb-dominated circulation system indicated by the preceding drogue experiments is verified on the scale of the entire lagoon by a representation of major bedform distribution. Figure 30 was compiled both from analysis of air photos and from selected fathometer profiles. Two types of bed forms are plotted: megaripples, which have a relief of <0.5 meter and a wavelength in the range of 1-6 meters, and sand waves, which have a relief of >0.5 meters and wavelengths >6 meters and usually in the range of tens of meters. Bed-form distribution illustrates the ebb-dominated flow (flow to north) in the system. Most sand waves are oriented toward the channel at the northern end of the barrier, the only effective exit point for impounded water as the tide level on the outside of the lagoon drops below the level of the beach rock. Bed forms directed up river are apparently in response to rapid saltwater tidal flooding during rising tide.

50
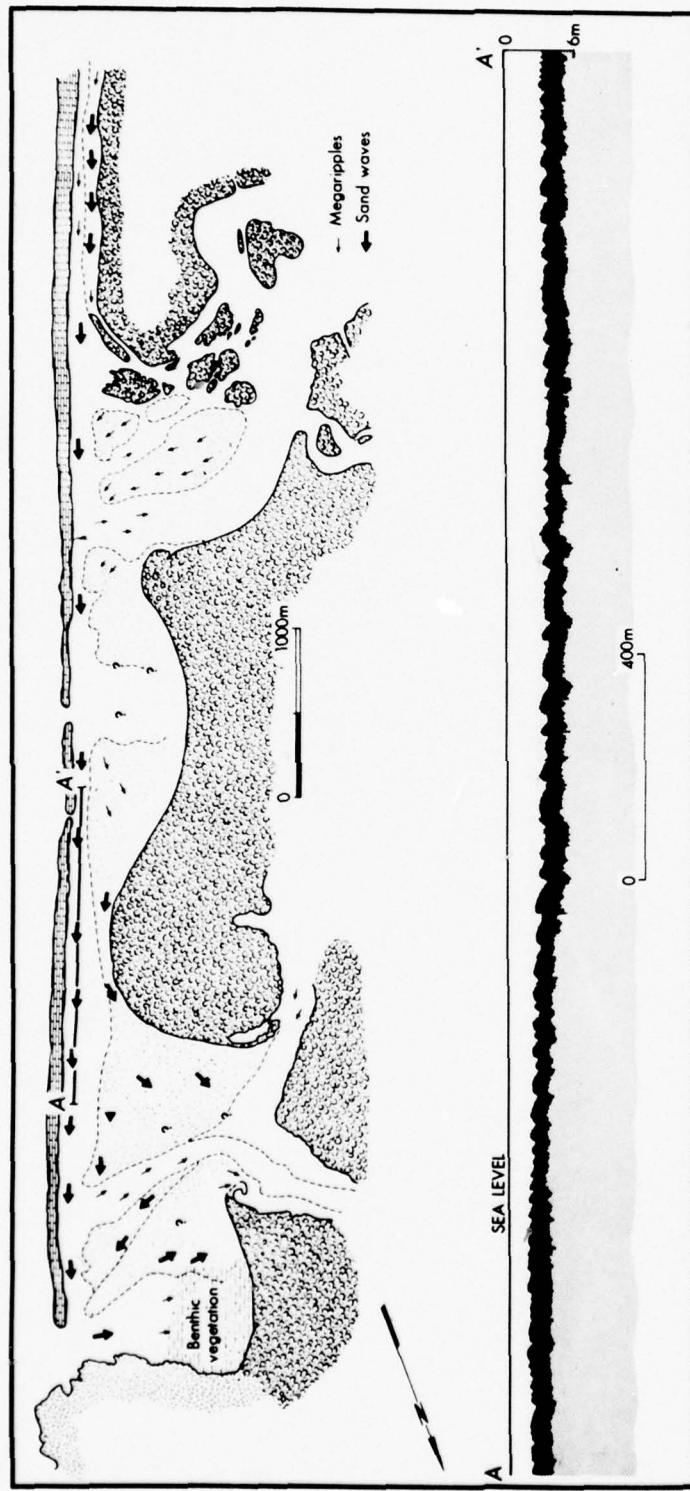
Figure 30. Major bed-form distribution in the back-barrier lagoon at Suape as interpreted from aerial photographs and selected fathometer profiles. Note the complete ebb flow domination of bed forms in the back-barrier channel, as indicated by the fathometer profile (line A-A').

51

## IV. GEOMORPHOLOGY

### Introduction

The coastal geomorphology of northeast Brazil is dominated to a great extent by the presence of lithified beaches and barriers now stranded at various distances offshore. Fortaleza (3°43'S) is the northern limit of occurrence for these features, which extend south to about Abrolhos (16°30'S) (Fig. 31). A major interruption in this trend occurs as a stretch of coastline extending from the Sao Francisco River south to near Salvador. In this central portion, between about 10° and 11°30'S, sediments from the Sao Francisco, Sergipe, Vasa Barris, and Itopicura Rivers have built a coastal beach-ridge plain averaging 10 km in width.

In general terms, the moderately dissected Tertiary plain along the coast has been drowned by the Recent Transgression (Fig. 32). The central portion of the coast has experienced a recent history of progradation, as evidenced by the successive beach-ridge accumulations that resulted in the wide accretional coastal plain. Elsewhere, an initial stage of progradation, followed by beach-rock development and retreat, is evident from the numerous beach-rock bands now stranded offshore. Although an abundant sediment supply and constant wave energy characterize this coast as a wave-built depositional feature, the numerous offshore beach-rock obstructions function as modifiers of coastal processes; as a result, coastal sediments have been redistributed and the modern shoreline has been readjusted. These lithified beaches and barriers occur intermittently and approximately parallel to the coast, and many protected ports and harbors have been created.

In response to persistent southeast winds and waves, the availability of sediment, and/or the occurrence of beach rock, either parallel beach ridges or a complex crenulated coast has developed. Transgressive dune fields commonly cap the beach-ridge plain, forming extensive sand sheets where sediment is abundant (e.g., the Rio Sao Francisco area). The morphological control and modification of physical processes by beach-rock barriers, in contrast, creates complicated barrier-lagoon systems.

This part of the Brazil study reports on the investigation of the morphodynamics of these two adjacent coastal systems. At Aracaju a beach-ridge/dune-plain complex and input wave and wind conditions were studied, and at Suape (near Recife) process-form relationships in a beach-rock/lagoon system, as well as beach-rock petrology and geochemistry, were investigated.

### Aracaju Field Site

The Aracaju field site (Fig. 5) is located on a relatively narrow beach-ridge plain lying between the Sergipe and Vasa Barris Rivers immediately south of the city of Aracaju. The site possesses both the morphological characteristics and process setting required for the study: it consists of a beach-ridge plain lying in the path of persistent southeast winds and waves. In addition, no beach rock is present. Aracaju is also a regional Petrobras center; it services oil rigs located in the offshore study area. These offshore facilities provided the investigators a platform

53
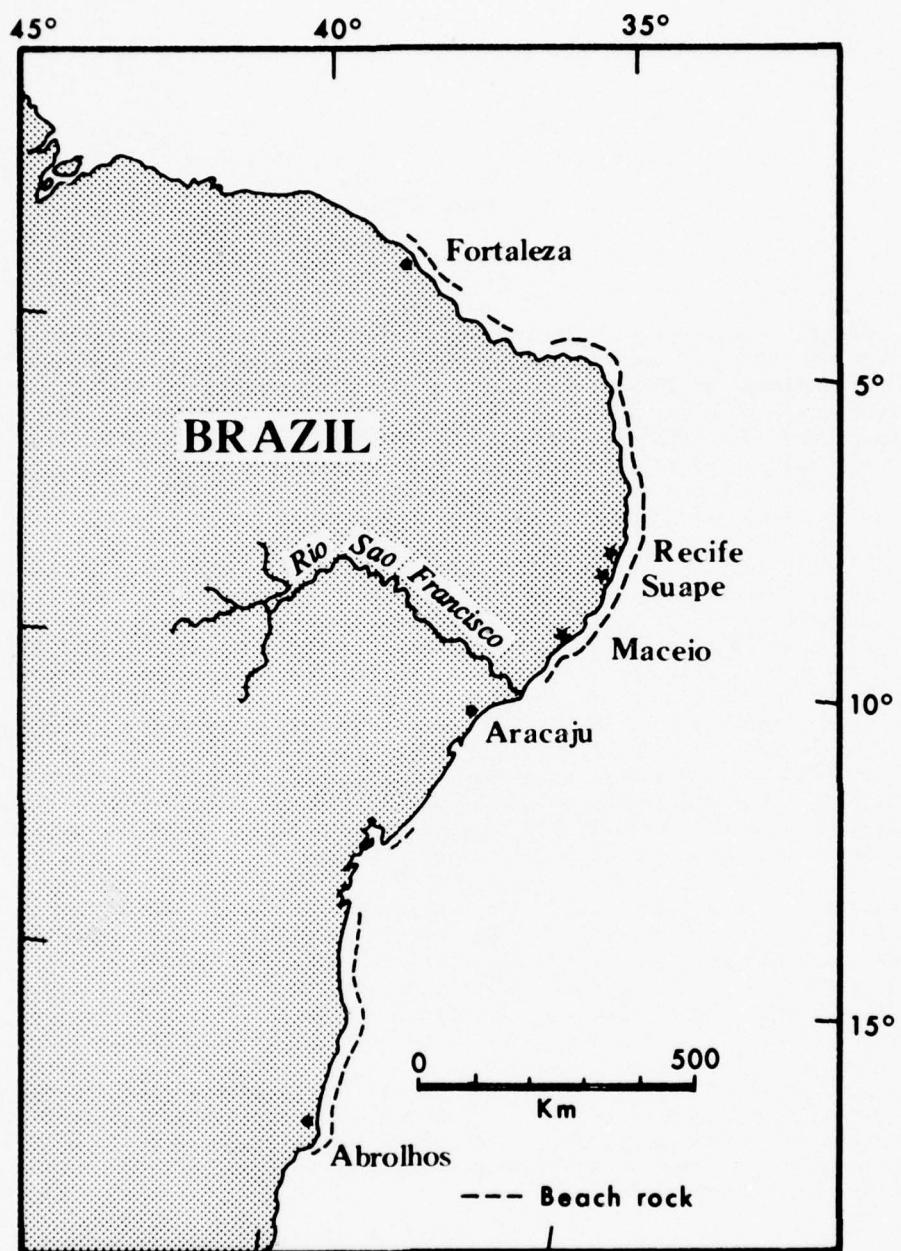
Figure 31. Location map showing the distribution of beach-rock barriers along the northeast coast of Brazil.
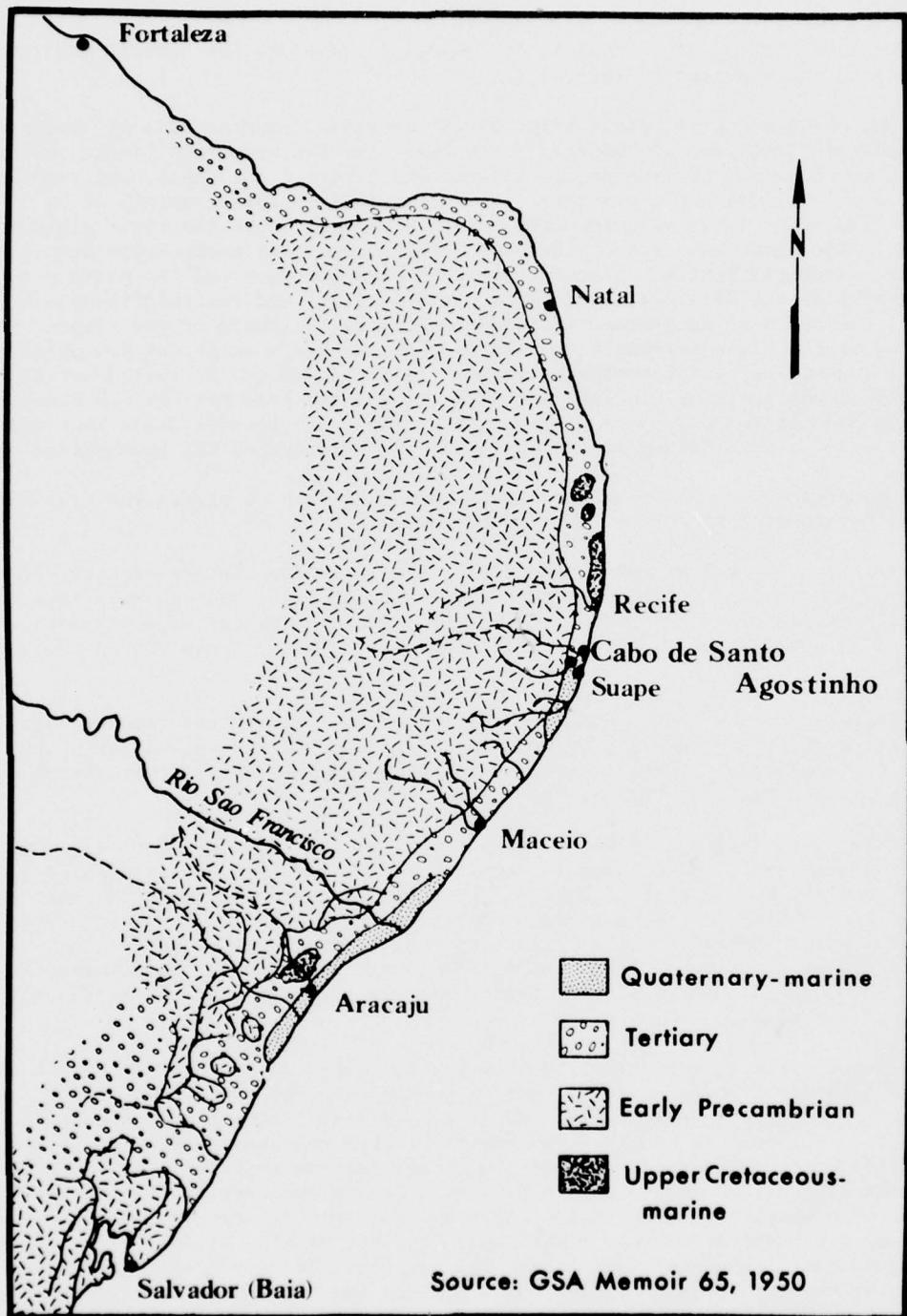
Figure 32. Surface geology of study area.

Map labels: Fortaleza, Natal, Recife, Cabo de Santo Agostinho, Suape, Maceio, Rio Sao Francisco, Aracaju, Salvador (Baia)

N

Legend:
Quaternary-marine
Tertiary
Early Precambrian
Upper Cretaceous-marine

Source: GSA Memoir 65, 1950

55

for mounting instruments.  Additional logistical support, such as air and sea trans-
portation, was provided by Petrobras.

The Aracaju coastal plain (Fig. 5) is composed of unconsolidated Quaternary
sediments derived from at least four sources:  the Sao Francisco River, to the
north, the Sergipe and Vasa Barris Rivers, which border the plain, and reworking of
local sediment during the transgression.  The plain is approximately 22 km in length
and 5-6 km wide, increasing in width toward each end, where the river plain extends
inland.  The inner boundary of the plain lies against the marine-truncated and
heavily dissected Tertiary plateau.  Between this boundary and the plain proper,
meandering of the Rios Poxim and Santa Maria have cut and reworked the plain, gener-
ating  two bands of mangrove-dominated tidal flats.  Seaward of the rivers, the major
portion of the plain extends 4 to 5 km to the coast as a series of low parallel beach
ridges and swales, which number between 20 in the south and 34 in the north.  Imme-
diately to the south of Rio Vasa Barris 47 ridges are present.  At the coast, recent
erosion has cut the outermost ridges, generating transgressive dunes that have
migrated up to 1 km inland (average 0.5 km) and have buried the beach-ridge plain.

The present morphology of the Aracaju coastal plain suggests the following
recent development since the last transgression.

First, there was a drowning of the coast, including the Sergipe and Vasa Barris
valleys, and initial infilling of the smaller tributaries and possibly some beaches
abutting the Tertiary (Fig. 33A).  Sediment moving shoreward during the transgres-
sion would permit the initial infilling to coincide with attainment of the sea level
maximum.

Second, there was a continued infilling of the larger tributaries (Fig. 33B),
drowned valleys, and the Sergipe and Vasa Barris.  Little progradation at the coast
would be expected until the large sediment traps in the form of the Sergipe and Vasa
Barris valleys had been filled.

Third, completion of filling of the large embayments took place and sediment
could be utilized in prograding the coast.  This filling resulted in the rapid and
fairly uniform development of a 4-6-km beach-ridge plain and reached a maximum per-
haps a little seaward of the present shoreline (Fig. 33C).  The ridges are parallel
to the present shoreline and normal to the southeast winds and waves.  During this
period the attainment of tidal equilibrium in the Rios Piaui, Santa Maria, Real,
and Pamonga would have permitted them to meander and thus rework the adjacent por-
tions of the plain.

Finally, the present situation was reached (Fig. 34).  Following cessation of
beach-ridge development, initial erosion of the outermost ridges occurred.  The
blowouts that were generated have now developed into transgressive dunes that extend
up to 1 km inland.  In addition, sediment has been released to move northward, par-
ticularly during the winter season; two large recurved spits that extend into the
southern side of the mouths of the Rios Vasa Barris and Sergipe (Fig. 5) have been
generated.  Whether this situation represents a periodic mechanism for movement of
sediment northward across the river mouths by spit growth, truncation of the spit
at its southern extremity, and subsequent amalgamation of the spit with the northern
shore, or whether it is occurring for the first time is unknown.  No doubt, however,
the present situation is a stage in the development of this type of pulsative sedi-
ment movement.

An estimate of contemporary shoreline retreat can be obtained by comparing the
original and present sites of a freshwater well drilled at the Petrobras tank farm
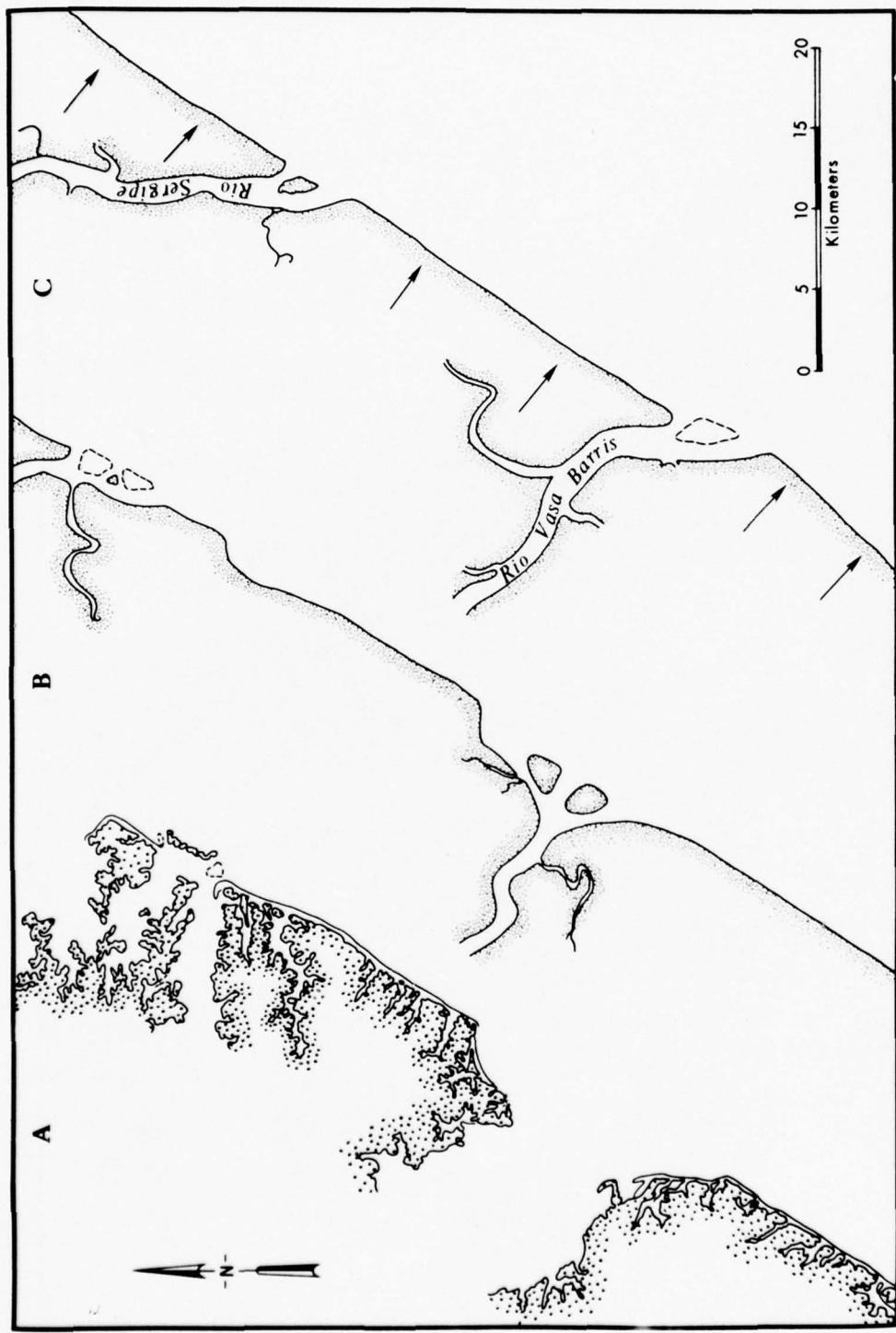
Figure 33. Recent development of the Aracaju coastal beach-ridge plain. A. Initial drowning of Tertiary hinterland and infilling of minor embayments. B. Infilling of major embayments, Sergipe and Vasa Barris river valleys. C. Rapid progradation of beach-ridge plain to maximum seaward position.
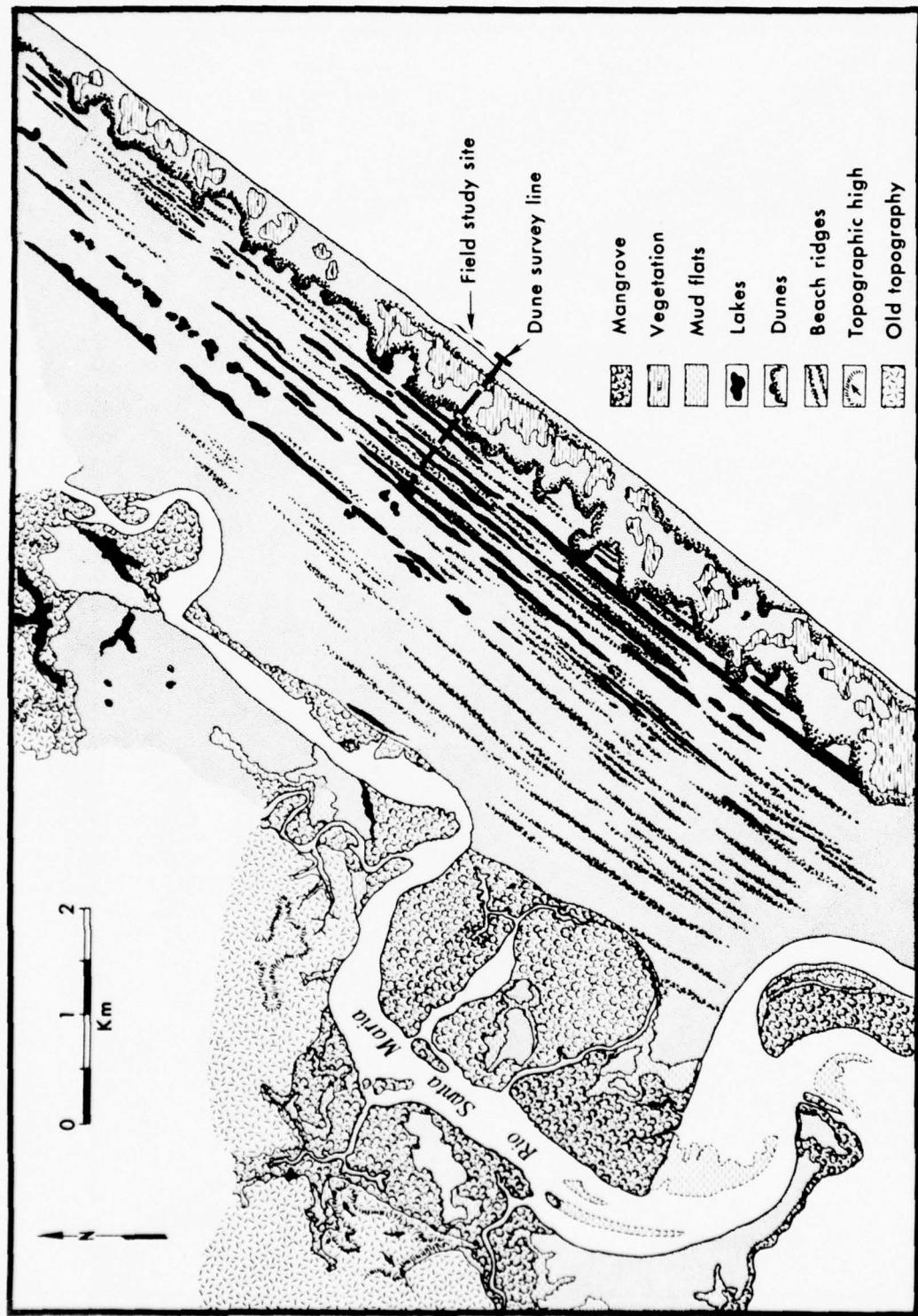
Figure 34. Present morphology of the coastal plain in the vicinity of the study site south of Aracaju. Partial erosion of the outer beach ridges and development of transgressive dunes are apparent.

site near Aracaju. The well was drilled in 1950 on dry land, possibly on the fore-
dune. In July 1975 the well was situated on the beach face, 100 meters seaward of
the dune escarpment, and was awash at high tide. Therefore, since 1950 retreat of
the dune escarpment has occurred at a rate averaging 7 meters per year.

The contemporary erosion of the dune escarpment is also evidenced along the
entire Aracaju coast by the undermining of trees along the seaward portions of coco-
nut plantations (Fig. 35).

A survey was made across the dune and beach-ridge field along a 1,500-meter line
(position of line shown on Fig. 34). The survey profiled seven low beach ridges,
eight intervening swales, and the dune field which is gradually encroaching land-
ward. The dune field has extended 700 meters inland; it covers and is possibly
reworking the underlying ridges and swales (Fig. 36).

The beach ridges and swales surveyed have an average wavelength of 110 meters
(standard deviation $\sigma$ = 10 m); the average for the entire plain is between 90 and
120 meters (Figs. 34 and 37). Their present amplitude is 1.5 meters ($\sigma$ = 0.4 m);
however, considerable infilling of the swampy swales has occurred since the ridges
were generated. Their height above sea level averages 7 meters for the ridges and
5.5 meters in the swales.

The dune field that is presently migrating westward over the outer beach-ridge
plain consists of series of large transgressive dunes in various stages of advance-
ment and stabilization (Fig. 38). Dunes in the survey reached a maximum elevation
of 15 meters above mean sea level, and the largest was 400 meters long.

Twenty-seven surface sand samples were collected from the dune field and the
crests and troughs of the beach ridges and swales, respectively (Fig. 36). Grain
size analysis was performed at $1/4$ $\phi$ intervals. The results shown in Table 9 indi-
cate an extremely uniform sediment pattern. All samples are characteristically fine
grained (mean grain diameter = 2.97 $\phi$, $\sigma$ = 0.03 $\phi$) and very well sorted (sorting
coefficient = 0.35, $\sigma$ = 0.03). No discernible variation in sediment size or sorting
characteristics exists between the ridges and swales, seaward or landward beach
ridges, or the ridge plain and the dunes. A common sediment source for all the
features is suggested.

The beach sands between the low-water mark and the upper beach are slightly
coarser than in other environments. They have a mean grain diameter of 2.61 $\phi$ ($\sigma$ =
0.48 $\phi$), and are well sorted (sorting coefficient = 0.50, $\sigma$ = 0.1). This trend indi-
cates that there is a slight winnowing of the finer grain sizes and transportation
of these particles by eolian processes to the ridges and dunes and secondary
infilling of the swales. Basically, however, the beach, dune, and ridge-plain sur-
face sediments have similar textural characteristics.


## Beach Dynamics

Fronting the dune/beach-ridge plain is an active straight beach that extends
22 km from Rio Vasa Barris to Rio Sergipe (Fig. 5). The morphological response of
this beach to winter wave conditions was monitored throughout the field project
(22 days). Two beach surveys were established on grid patterns. One was located
in front of the Petrobras tank farm (Tank Farm site) and was surveyed on five occa-
sions between 10 June and 3 July 1975. The main grid was established midway along
the beach on the Fazenda Sao Jose coconut plantation (Plantation site, Figs. 5 and
35). This locality was surveyed on 13 occasions between 10 June and 1 July 1975.

Figure 35. Photograph of the beach in the vicinity of
the Plantation site showing the transgressive dune field
and the erosion scarp undermining the coconut trees.
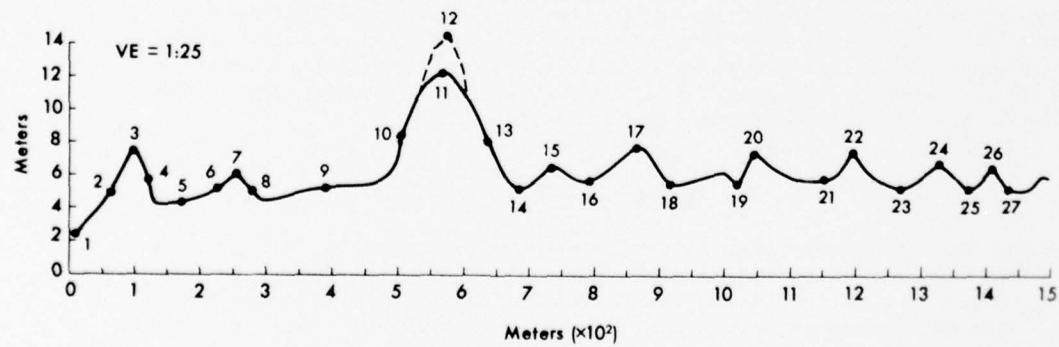


Figure 36. Aracaju dune/beach-ridge survey. Numbers indicate sand sample loca-
tion. See Figure 5 for location of survey.

60

Figure 37. Photograph showing beach-ridge plain between
Rio Santa Maria and coast. Note water lying in many of the
swales. Coconut trees line the ridges. Viewed to north.



Figure 38. Photograph of transgressive dune field viewed
to the north. Mouth of Rio Sergipe at top.

Table 9

Dune and Beach-Ridge Plain Sediment Analysis

| Sample No. | M$\phi$ | $\delta\phi$ | Sample No. | M$\phi$ | $\delta\phi$ | Sample No. | M$\phi$ | $\delta\phi$ |
|---|---|---|---|---|---|---|---|---|
| 1 | 2.81 | 0.34 | 10 | 2.88 | 0.37 | 19 | 3.90 | 0.35 |
| 2 | 2.63 | 0.41 | 11 | 2.98 | 0.31 | 20 | 2.83 | 0.37 |
| 3 | 2.73 | 0.39 | 12 | 3.29 | 0.27 | 21 | 2.91 | 0.36 |
| 4 | 2.80 | 0.35 | 13 | 2.78 | 0.44 | 22 | 3.04 | 0.36 |
| 5 | 3.10 | 0.36 | 14 | 2.92 | 0.37 | 23 | 3.12 | 0.39 |
| 6 | 3.01 | 0.34 | 15 | 2.94 | 0.34 | 24 | 2.99 | 0.37 |
| 7 | 2.89 | 0.38 | 16 | 3.01 | 0.28 | 25 | 2.97 | 0.39 |
| 8 | 2.85 | 0.37 | 17 | 2.89 | 0.34 | 26 | 3.00 | 0.34 |
| 9 | 2.88 | 0.37 | 18 | 2.99 | 0.39 | 27 | 3.13 | 0.32 |

NOTE:  See Figure 36 for location.

The grid extended from the base of the foredune to the seaward limit of wading during low tide (approximately 160 meters).  Seaward extension of the survey by echo sounding was prevented by the continuous 1.5- to 2-meter-high waves breaking across the 400-meter-wide surf zone.

The beach in the vicinity of both grids and along its entire length is extremely straight and uniform.  Large winter waves had removed any depositional forms, and a gently sloping concave beach extended from the base of the foredune to the edge of the inner bar within the study area.  No berm was present, and only occasionally very subdued cuspate features were observed within a wavelength of approximately 300 meters.

Beach sediments were sampled at the Plantation grid along three lines extending from the 0-meter baseline to the bar crest at 160-180 meters.  Twenty-eight samples were collected and sieved at $\frac{1}{4}\phi$ intervals (Table 10).

The entire beach is covered by fine-grained (mean grain diameter = 2.61$\phi$, $\sigma = 0.1$), well-sorted (sorting coefficient = 0.5, $\sigma = 0.1$) sand.  The sands tend to be trimodal, with modes at 2.5-2.75$\phi$, 3.25$\phi$, and 3.75$\phi$.  Although no longshore variation was apparent, there was an increase in grain size on the inner bar; the coarsest sand occurred at 160 meters (average mean grain size of 2.18$\phi$).  The coarsening resulted from the absence of the 3.25$\phi$ mode.  The trimodality of the sediments was also found in the dune, beach-ridge, and swale sands.

Surveying of the Plantation grid began on 10 June 1975.  The beach was essentially concave in slope and sloped gently to the low-water mark (Fig. 39).  Only very subtle longshore variation was apparent as the lower beach elevation increased to the south.  Conditions on 11 June permitted the beach to be surveyed to the 160-meter line.  The beach was essentially unchanged, though the faint outline of a slightly cuspate feature could be observed.  Evidently the relatively low wave conditions existing from 10 to 11 June moved little or no sediment onto the beach.

62
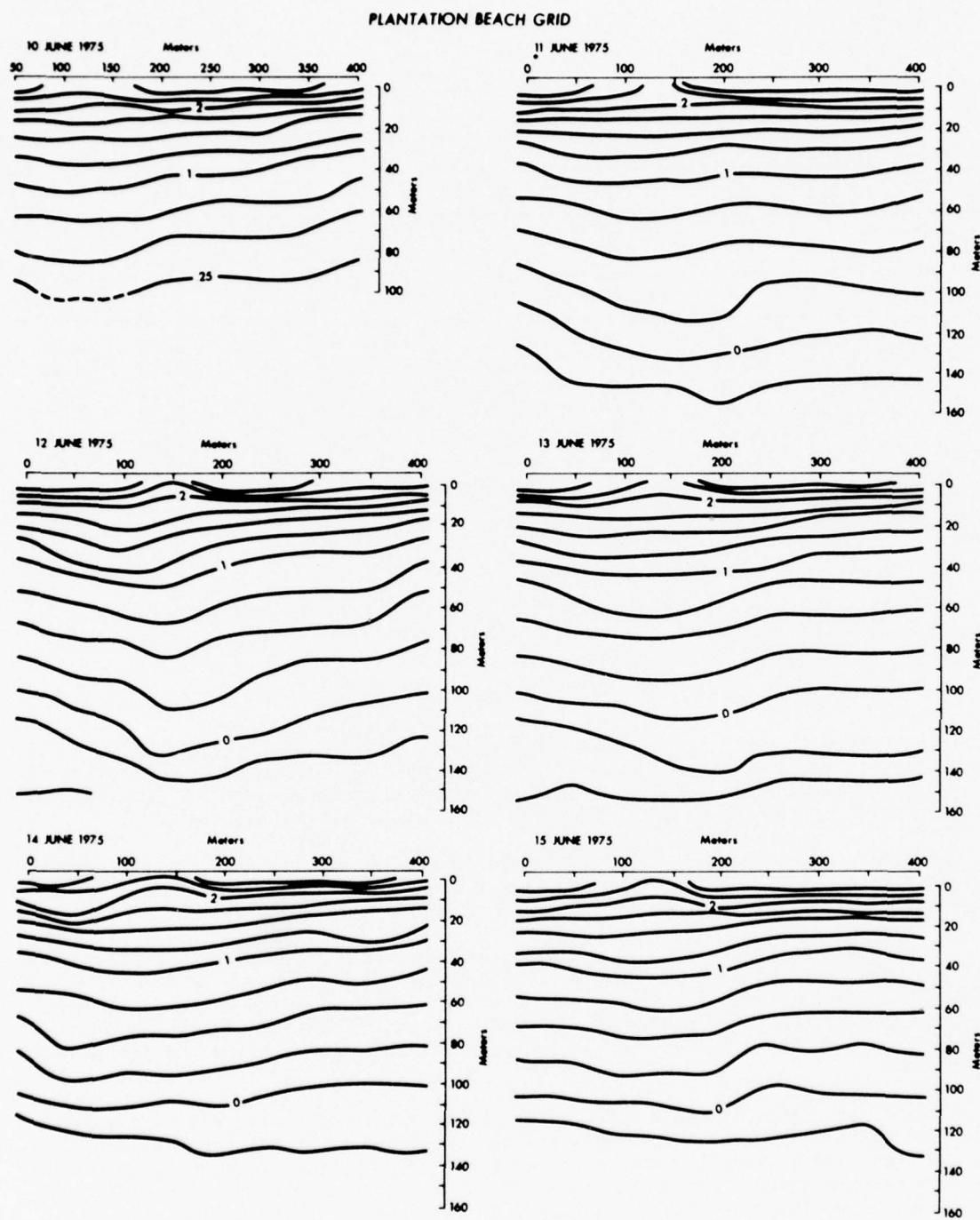
Figure 39. Plantation beach grid. Changes in beach morphology from 10 June to 15 June 1975.

Table 10

Plantation Beach Grid Sediment Analysis

| 4S | | | 0 | | | 4N | | |
|---|---|---|---|---|---|---|---|---|
| Distance from Baseline (meters) | M$\phi$ | $\delta\phi$ | Distance from Baseline (meters) | M$\phi$ | $\delta\phi$ | Distance from Baseline (meters) | M$\phi$ | $\delta\phi$ |
| 0 | 2.67 | 0.30 | 0 | 2.81 | 0.33 | 0 | 2.74 | 0.28 |
| 20 | 2.95 | 0.40 | 20 | 2.90 | 0.34 | 20 | 2.82 | 0.35 |
| 40 | 2.97 | 0.50 | 40 | 2.97 | 0.47 | 40 | 2.76 | 0.45 |
| 60 | 2.43 | 0.68 | 60 | 2.63 | 0.60 | 60 | 2.38 | 0.59 |
| 80 | 2.78 | 0.48 | 80 | 2.54 | 0.66 | 80 | 2.33 | 0.57 |
| 100 | 2.88 | 0.56 | 100 | 2.70 | 0.50 | 100 | 2.64 | 0.55 |
| 120 | 2.40 | 0.62 | 120 | 2.24 | 0.49 | 120 | 2.73 | 0.52 |
| 140 | 2.47 | 0.56 | 140 | 1.90 | 0.55 | 140 | 2.18 | 0.55 |
| 160 | 2.39 | 0.68 | 160 | 2.53 | 0.55 | 160 | 2.28 | 0.60 |
| 180 | | | 180 | | | 180 | 3.07 | 0.51 |

NOTE: Samples are located by their profile line, 4S, 0, or 4N, and their distance from the back beach baseline, 0, 20...180 meters.

Wave height began to increase on 11 June with the arrival of strong north to northeast winds and northeast waves 1.5 to 2 meters high. The survey on 12 June, however, indicated little morphological change in the upper beach. The lower beach seaward of 80 meters was slightly lowered but retained the cuspate feature.

On 13 June wave height peaked at 2 meters, causing slight lowering of the beach below 50 meters. Wave height subsided to 1.2 meters on 14 June. The entire beach face was essentially uniform and remained in this state through 15 June.

A strong southwesterly storm arriving on 16 June generated waves up to 3 meters. Although the central beach was lowered slightly and a channel began to form at the northern end between 100 and 130 meters, the high waves prevented surveying of the inner bar. The channel was observed, however, to extend the full length of the survey grid. A strong northward current existed both in the channel and across the surf zone.

On 17 June (Fig. 40) wave height subsided slightly and conditions on the beach remained unchanged. However, southerly waves continued to attack the beach on 18 and 19 June, and surveying was again restricted. The upper beach maintained its uniform concave slope. The beach was surveyed to the inner breaker line on 21 June (Fig. 40). The longshore trough developed in response to the high wave conditions, and the inner bar was apparent. The bar was rather subdued, particularly to the north, where a return flow from the channel moved seaward.

On 21 June wave height began to decrease and shoreward movement of sediment was generated. Rip cell development along the beach intensified. The central portion of the bar became more prominent, increasing in height by an average of 30 cm,
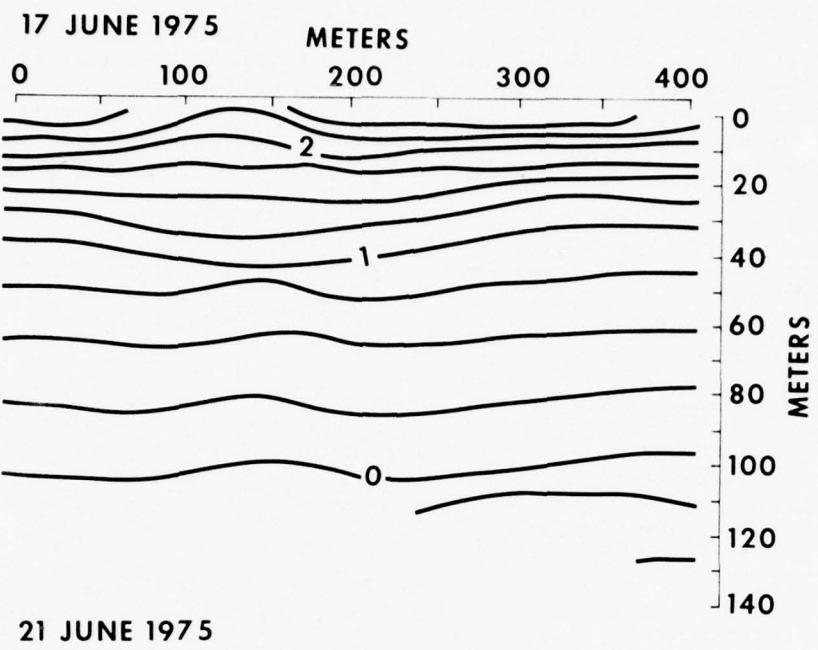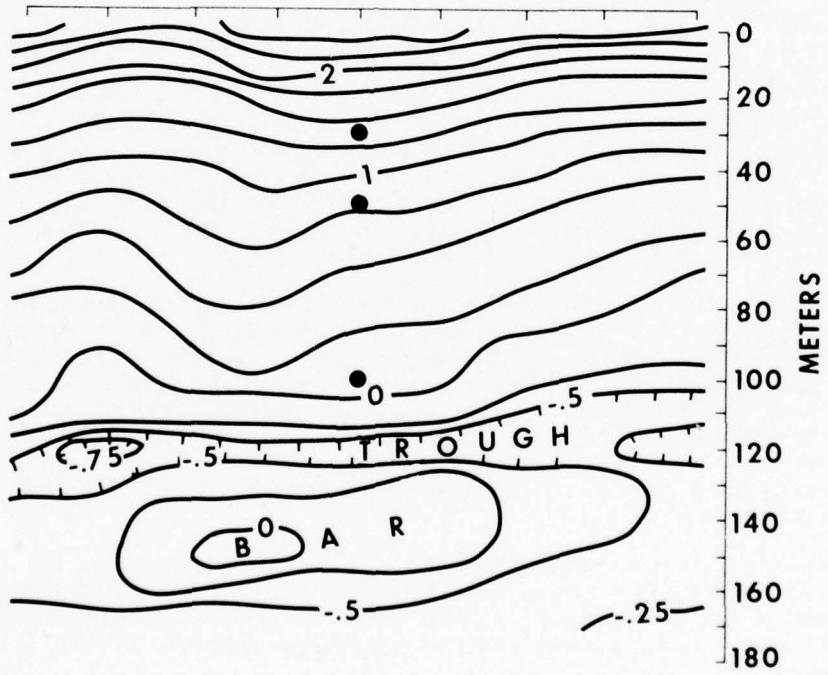
Figure 40. Plantation beach grid on 17 June and 21 June 1975.

and migrated shoreward approximately 10 meters along its landward edge. The shoreward migration removed the longshore channel in the central portion and intensified and excavated two rip channels on the other side of the bar. Water was therefore flowing in over the bar, moving into the longshore channel, and returning seaward through the rip channels. Well-developed sand waves 30-50 cm high were prominent in the rip channels. The upper beach face responded to the bar-channel morphology by accreting behind the bar and undergoing slight erosion behind the rip channels.

Wave height stabilized on 22 June (Fig. 41), and more sediment moved onto the beach. The bar continued to increase in height and move shoreward along its crest. The longshore channel remained stationary but narrowed slightly. The rip channel at the south end broke through the bar. A distinct channel was formed normal to the beach. The northern rip deteriorated, and partial filling of both the channel and adjacent bar section resulted.

On 23 June wave height decreased to 1 meter, and the entire bar began to move up onto the lower beach face. The central portion of the bar moved approximately 20 meters shoreward and almost filled the longshore channel. The southern rip continued to exert significant influence, maintaining a channel across the bar. The northern rip maintained a deep longshore channel and deepened its channel across the bar. The upper beach face remained unchanged.

A change in field locations on 23 June prevented continued observations of the shoreward migration of the bar. If low wave conditions had continued, the bar probably would have welded itself to the central-lower beach face as a series of cusps and/or a berm.

On 1 July 1975 a final survey was made of the Plantation grid. While the intervening process conditions between 21 and 29 June were expected to generate moderate to low wave conditions and beach accretion, a strong southerly storm arrived on 30 June, and on 1 July high waves attacked the coast. The survey therefore illustrates the beach in a state of erosion following the above-mentioned accretion (Fig. 42). The lower beach face, between 110 and 160 meters, had filled considerably: as much as 60 cm over the longshore channel, 20 cm over the bar, and approximately 80 and 90 cm over the southern and northern rip channels, respectively. This body of sediment was now being removed. The beach in its partially denuded state consisted of two erosional cuspate features and intervening erosion swales.

The subaerial section of the beach and adjacent inner bar responded to varying wave conditions generated by the periodic winter southerly storms and persistent strong onshore winds. Basically, the beach had been denuded by the first of these storms on and following 25 May, prior to the field period. The beach attempted to recover during the intervening periods of low to moderate waves; however, complete recovery was prevented by the persistent storms. The basic winter beach morphology is therefore a concave, gently sloping beach face that terminates at the inner bar, which during periods of high waves is separated from the beach by a longshore channel and/or rip channels.

The beach grid survey extended to a maximum of 180 meters from the dune scarp. The beach and surf zone, however, extended up to 500 meters seaward. High waves breaking across two bars and a wide shoal surf zone prevented echo sounding of the surf zone. Thus, even a generalized analysis of the response of this area cannot be verified.

The results of three aerial reconnaissance flights above the Aracaju beach area can, however, be used to define on a very broad scale the morphological response
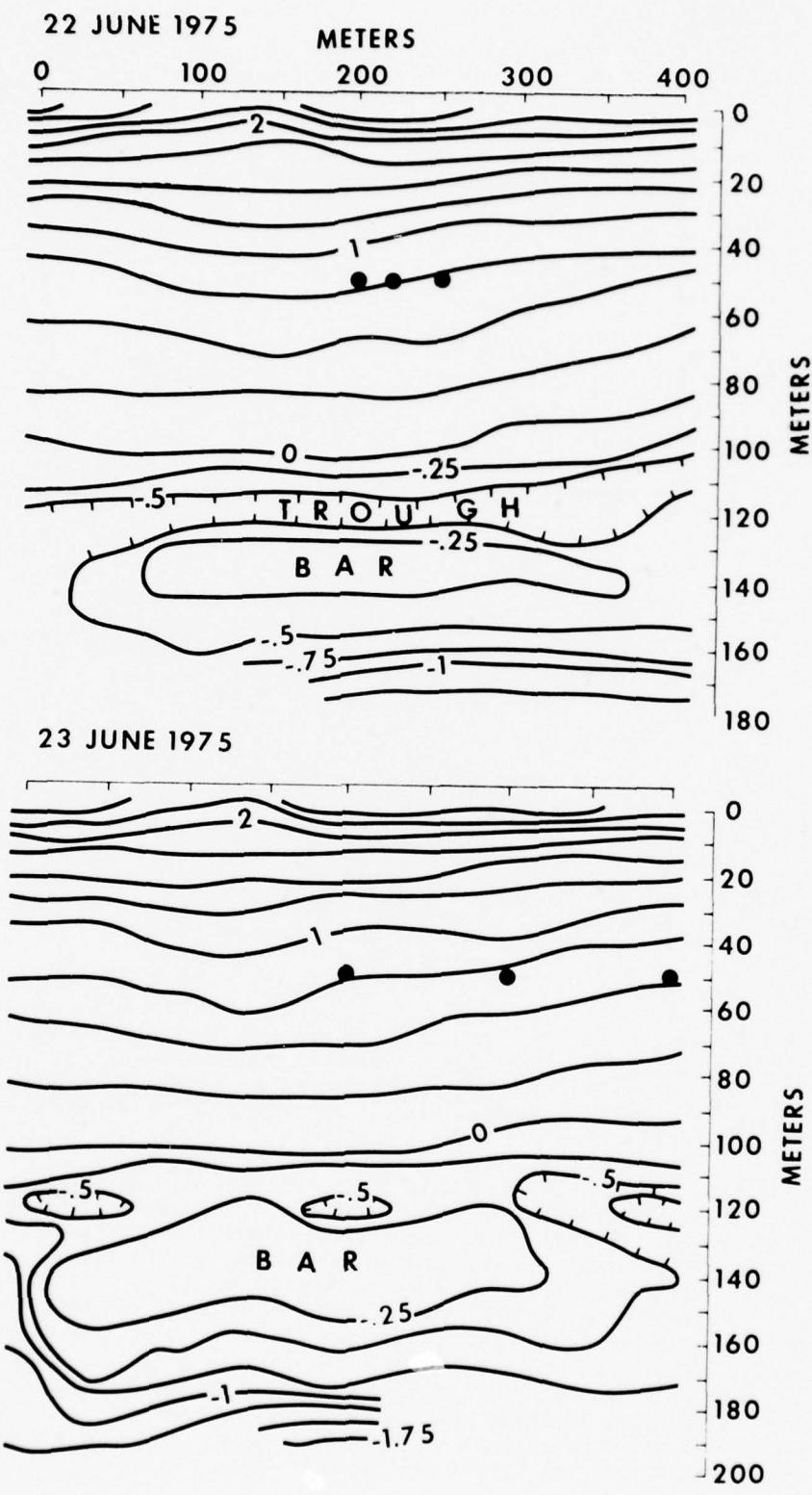
Figure 41.  Plantation beach grid on 22 and 23 June 1975.
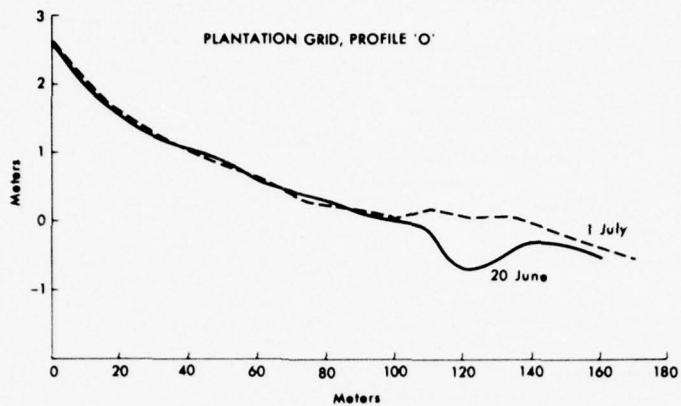
Figure 42.   Profile across Plantation beach
grid on 20 June and 1 July 1975, showing
maximum change in beach elevation during the
study period.

of the surf zone to winter storm conditions.

The first survey was made during a field reconnaissance trip in January 1974,
the latter two flights on 6 and 19 June 1975. The January survey (Fig. 43A) shows
the beach during the low to moderate summer southeasterly wind and wave conditions.
The foredune extended gently to the beach, no erosional scarp being present, and
the surf-zone slope was uniform, with no distinct bars apparent.

The winter morphology evidence in Figure 43B and C presents the eroded dune
escarpment and two distinct bars in the surf zone. On 6 June the inner bar is
attached to the lower beach; however, its outer edge is indicated by a fairly sharp
breaker line. Seaward of this edge a channel approximately 100 meters wide sepa-
rates it from the inner edge of the outer bar. This outer bar was apparently
generated by large waves associated with a severe southerly storm that occurred
around 25 May 1975.

Figure 43C illustrates the conditions on 19 June 1975 during a period of
moderate to high wave conditions. The inner bar is separated from the beach by a
longshore channel. Seaward of the inner bar a distinct trough approximately 5 meters
deep and 100 meters wide parallels the entire beach. At the seaward edge of this
trough is the sharp boundary with the outer bar at a depth of approximately 3 to
4 meters. The outer bar likewise continues along the entire length of this 22-km
section of coast. The crest of the outer bar has a width of approximately 70 meters.
The bottom slopes gently seaward from the crest of the outer bar (Fig. 44). Higher
waves break on this gentle slope, at times breaking up to 200 meters seaward of the
outer bar. Therefore, the effective surf zone during high wave conditions may extend
over 600 meters; waves break first on the outer slope, second on the outer bar,
third on the inner bar, and finally on the beach face.

68

Figure 43A.  View north along Aracaju
coast, January 1974.  Note the low, short
waves arriving parallel to the coast and
the broad, continuous surf zone.



Figure 43B.  View north along Aracaju coast, 6 June 1975.
Note the moderate waves arriving at an angle to the coast,
the broad inner surf zone, and waves breaking on the outer
bar.

Figure 43C. View north along Aracaju coast, 19 June 1975. Note the large waves breaking well seaward of the outer bar, the distinct outer and inner bars, and the swash zone--a total of four wave-breaking zones.
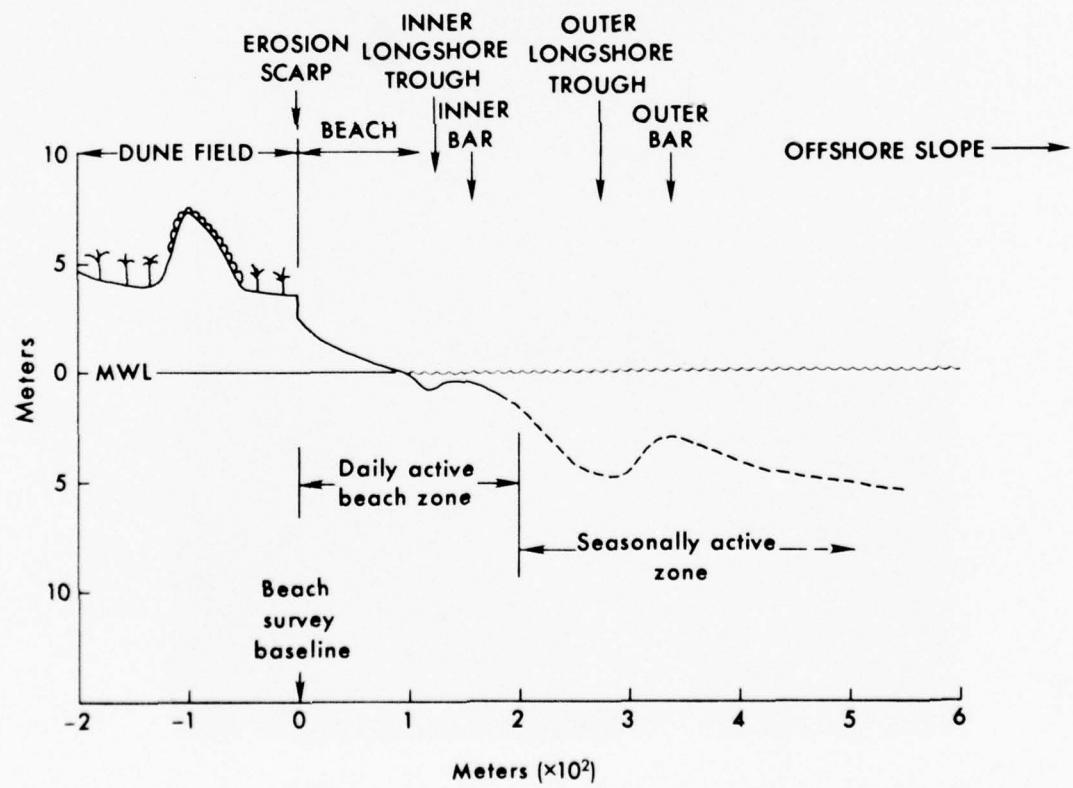


Figure 44. Schematic diagram of the beach morphology at Aracaju.

70

## Beach-Rock Barriers

Branner (1904) was the first person to describe in detail the lithified beaches and barriers of Brazil, which he referred to as "stone reefs." He recognized that these features had not been constructed by reef-building corals and calcareous algae but consisted mostly of quartz sand, shells, and terrigenous pebbles, all of which were bound together by a calcareous cement. This observation was not entirely original, however; Darwin (1841), a half century before, had recognized that the offshore obstructions at Pernambuco were composed of sandstone and were not organically constructed reefs. Since these early studies the "stone reefs" of Brazil have been the subject of several scientific investigations, most of which have been geomorphically and geologically oriented (Andrade, 1955; Tricart, 1959; most recently, Mabesoone, 1964, 1971; Mabesoone and Continho, 1970).

One of the most remarkable characteristics of these lithified beaches and barriers is the straightness of most well-developed examples. A single outcrop may extend for several kilometers parallel to the coast without interruption. In most localities more than one beach-rock band can be identified. Mabesoone (1964) reported that generally two or three ridges are exposed near the beach at low tide, and ten or more additional submerged ridges may occur offshore. Analysis of air photos suggests that this situation may be typical of many areas along the northeast coast of Brazil. The beach-rock bands that are exposed at low tide have a maximum height that commonly corresponds to the high-tide level. Those bands that are farther offshore are presumably older and are now permanently submerged owing to the Holocene sea level rise. The width of individual beach-rock bands is extremely variable. In general terms, they appear to fit into a range between about 5 and 150 meters, and thickness to underlying unconsolidated material is a maximum of about 4 meters for barriers whose tops are exposed at low tide. Consistent with the geomorphic descriptions of beach rock by Russell (1957) and many others, these recently cemented sandstones exhibit accretion units that dip at a very low angle (generally <5°) seaward and have an overall trend that is much the same as that of their modern beach counterparts. In addition to the similarity in gross structure and, in some places, small-scale cross bedding, the constituent particles that compose the beach rock are similar in most cases to those found on nearby active beaches. In terms of texture, however, it was our observation that many beach-rock exposures contained coarser material than was apparent along the adjacent modern shoreline. Mabesoone (1964) also reported coarser material in the beach rock near Recife.

The cemented sandstones are composed of from about 35 to 98 percent quartz. The remaining components are primarily carbonates, mollusc fragments, and coralline and calcareous green algae. Essentially these same proportions were reported by Mabesonne (1964) in his study of the Pernambuco sandstone reefs. However, most of our samples contained less than 10 percent carbonate allochems. Generally, a low percentage of heavy minerals (<3 percent) is also found.

Submerged exposures of beach rock have provided firm substrates for sedentary organisms. Along this sediment-rich depositional coast, corals and similar organisms would otherwise find very few bottom-fast objects on which to attach and grow. Although true coral reefs are virtually nonexistent along Brazil's northeast coast, many small patch reefs, composed mostly of encrusting forms of coralline algae in conjunction with a few corals, can be identified. Mabesoone and Coutinho (1970) reported that all reefs in the coastal waters of Brazil in which corals grow or grew have a substrate of cemented sandstone or another rock type that is cropping out on the sea floor. Two islands, Rocas and Fernando de Noronha, approxi-

71

mately 230 km off the north coast, have true coral reefs and appear to be rather exceptional with regard to the rest of the Brazilian coast.

Like true coral reefs, Brazil's beach-rock exposures significantly modify the incident wave energy to the coast. Not only is there a substantial loss of energy through the breaking process as waves encounter a beach-rock barrier, but the spectrum of those resulting modified waves is shifted significantly from input wave field characteristics, generally to lower frequencies. These observations were made by Roberts et al. (1975) in a Caribbean fringing reef system that is very similar in basic geometry to the beach-rock lagoon complexes along the northeast Brazilian coast. In the Caribbean setting it was estimated that approximately a 75 percent energy loss, calculated from the change in wave height, occurred during the breaking process as waves intersected the fringing reef, reformed, and entered the back-reef lagoon. A more detailed discussion of these interactions was given in an earlier section of this report.

In addition to simply transforming and attenuating wave energy through the process of wave breaking, offshore obstructions such as the beach-rock barriers tend to refocus wave energy along the back-barrier depositional coast by processes of wave refraction and diffraction. Figure 45 schematically illustrates the effects of isolated beach-rock bands and openings in long, linear bands on configuration of the adjacent shoreline. Although the combined effects of wave refraction and diffraction operate to produce the illustrated shoreline response features, diffraction is most noticeable where an otherwise regular train of waves is interrupted by an offshore barrier such as the beach-rock exposures. Through the diffraction of waves, energy is transferred laterally along the wave crest. If this transfer did not occur, straight, long-crested waves passing the end of a barrier would leave a region in the barrier lee devoid of any wave activity, whereas beyond the end of the barrier, waves would pass essentially unchanged in form and height except for refraction effects. This situation is obviously not the case, and in appropriate coastal settings the influence of offshore obstructions on configuration of the modern coastline can be striking. The overall effect is to produce a coastline that is highly crenulated. Figure 46 is an oblique aerial photograph of the Brazilian coast near Rio Serinhaem that shows the distinct formation of alternating cuspate features and crescentic bays. Nearly the entire northeast coast of Brazil has offshore beach-rock barriers (Fig. 31) and is characterized by a highly crenulated coastline geometry. Kaye (1959) illustrated a similar shoreline configuration along the northeastern coast of Puerto Rico that developed in response to small, discontinuous fringing coral reefs and offshore exposures of Pleistocene eolianite. Occasionally the tendency to build cuspate shoreline forms toward an offshore obstruction overrides local effects, and the cusps may build across barrier trends nearer to shore. This situation is illustrated by Figure 47, which shows a distinct accretional form building across a presumably older and nearshore beach-rock exposure at Ponta de Serrambi, just north of Rio Serinhaem. Branner (1904) discussed a similar example from the mouth of Rio Formoso.

Many cases may be cited along the northeast coast, where the modern shoreline has accreted toward and joined an offshore lithified barrier. This process of classical tombolo formation, if allowed to continue, under the present sea level stand will in time act to straighten the now crenulated coastline. Johnson (1919), in discussing tombolo formation, agreed that these depositional features are composed of sand that has been deposited primarily by waves on the sheltered sides of islands (or any offshore obstruction). Although waves generally approach a coast somewhat obliquely, refraction causes wave crests to become more parallel to the shore. Each part of a tombolo assumes an orientation at nearly right angles to the

72
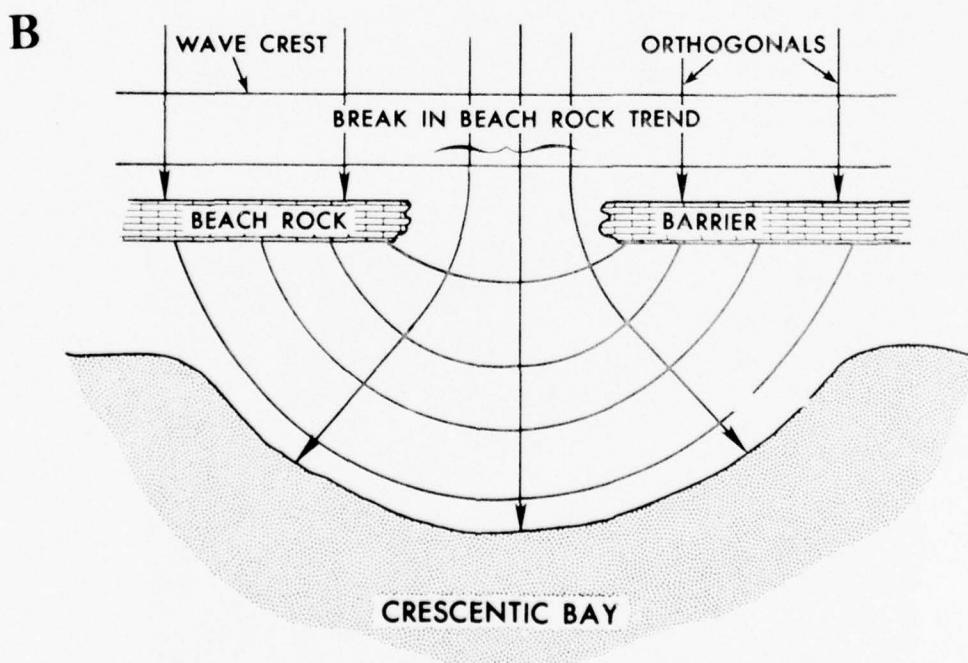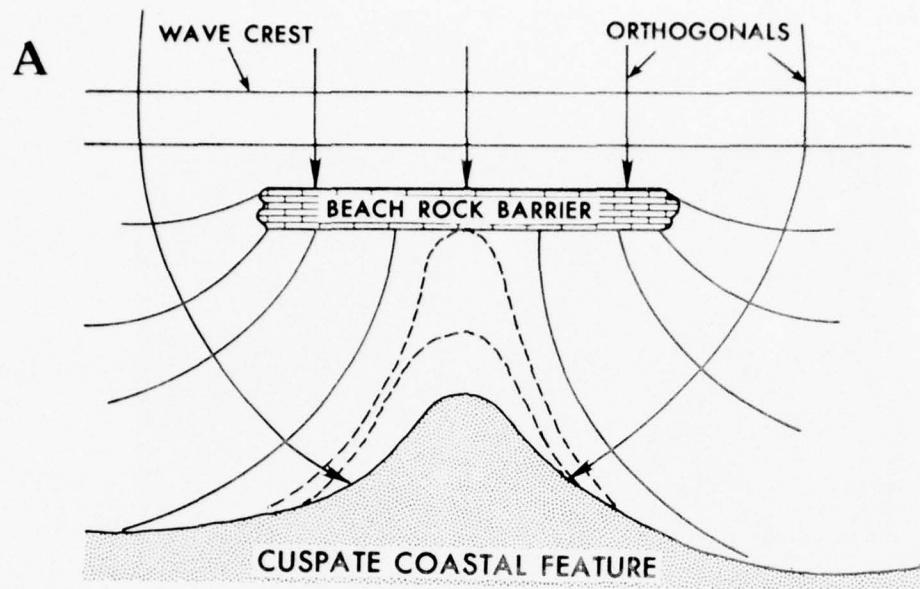
Figure 45. Schematic representation of the influence of offshore beach-rock barriers on a modern sandy shoreline. Changes are caused by the combined effects of wave diffraction and refraction. The shoreline generally accretes toward an isolated offshore barrier (A), eventually linking with the beach rock by means of a tombolo. Breaks in a long, linear offshore beach-rock barrier promote formation of back-barrier crescent-shaped shorelines (B).

Figure 46. Modern crenulated shoreline near Rio Serinhaem.
Crescentic bays have formed in response to the breaks in the
offshore beach-rock barriers. Note the same shoreline geome-
try forming on a smaller scale in response to the nearshore
beach-rock band.



Figure 47. Cuspate shoreline feature building across a
nearshore beach-rock band at Ponta de Serrambi, just
north of Rio Serinhaem.

direction from which the dominant waves approach, and it is maintained by continuous exposure to such waves. Figure 48 illustrates the cuspate accretion along the coast near Rio Serinhaem, where a tombolo-like feature has developed that links a beach-rock barrier to the adjacent shoreline.

Branner (1904) described the lithified barrier south of Cabo de Santo Agostinho, near the little town of Suape, as "the finest stone reef on the coast of Brazil" (Fig. 31). Figure 49 illustrates the remarkable straightness of this barrier, which extends some 12.5 km south from the cape to a point at which it merges with the shoreline near the small village of Cupe. The exposed barrier width varies between 60 meters and 160 meters in the transverse profiles given in Figure 50. Barrier width increases to the south and is widest where beach rock joins the shore near Cupe. The profiles show that the total width of this beach-rock exposure, submerged plus emergent portions, may be as much as 400 meters. A small part of the long beach-rock barrier is welded to the igneous rocks of Cabo de Santo Agostinho. Between this small segment and the main trend is the larger of two major breaks in the barrier system.

The only other break in the barrier occurs opposite the well-developed lunate bay midway between Cabo de Santo Agostinho and the southern extremity of the exposure (Fig. 51). This break is ineffective at low tide as an entry point for incident waves from the shelf. At high tide, however, waves pass through the narrow channel and play a dominant role in determining the configuration of the back-barrier shoreline. Similar processes are active in conjunction with the shallow main channel (approximately 400 meters wide) at the northern end of the barrier adjacent to Cabo de Santo Agostinho. The shapes of the wave fronts seen in Figure 51 conform well to the general configuration of the beach that has developed behind the beach-rock barrier.

The Suape lithified barrier has characteristics common to most beach-rock exposures. Accretion units that slope seaward at a gentle angle are readily apparent at low tide. The most elevated surfaces of the barrier are slightly higher but are very close to being coincident with the high-tide level. Coarse and fine units may be identified in the exposure, but in general the texture is that of a medium-grained sandstone composed primarily of quartz but including minor amounts of mollusc debris and coralline algae fragments. Figure 52 illustrates the internal structure of the beach-rock exposure, including accretion units and small-scale cross bedding. The surface over the entire length of the exposure exhibits long tide pools oriented along the trend of the barrier. Algal rims have developed around many of the tide pools, which generally form between the truncated updip ends of accretion units (Fig. 53).

Three sluggish little rivers, Rio Ipojuca, Rio Tatuoca, and Rio Massangana, enter the back-barrier lagoon and drain to the tidal channel at the northern end of the barrier at falling tide. Many shoals have developed in the lagoon in response to river sedimentation as well as lagoonal circulation. However, a channel is maintained directly in the lee of the barrier to accommodate tidal exchange; the geometry of this structure is very similar to that of a fringing coral reef and its accompanying back-reef moat channel.

Sediment thickness and facies relationships on both the seaward and the landward sides of the lithified barrier at Suape are shown in Figures 54 and 55. These figures were compiled from hydrographical and geophysical sounding data. Near the position of the barrier on the continental shelf, sediments have accumulated to a thickness of approximately 65 meters over bedrock. The entire sedimentary column is composed of sand-sized material; erratic blocks of the lithified barrier up to 8

Figure 48. Along the coast near Rio Serinhaem tombolo-like features now link the modern shoreline to once-offshore beach-rock barriers.



Figure 49. The long (12.5 km) and extremely straight beach-rock barrier south of Cabo de Santo Agostinho is one of the best examples of beach rock along the Brazilian coast. The village of Suape is pictured in the foreground.
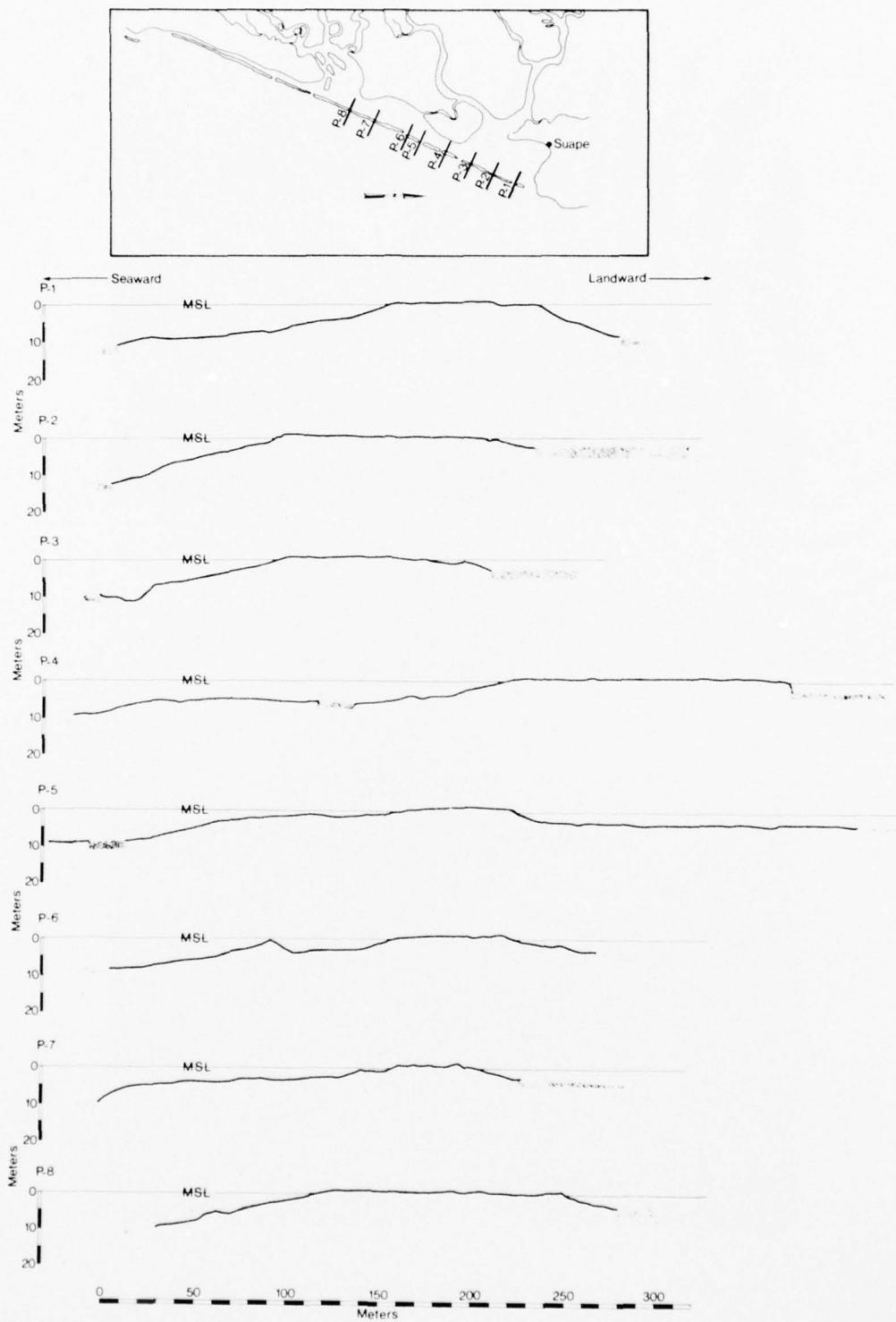
Figure 50. Elevation and width of beach-rock barrier near Suape as measured at eight localities along the beach-rock trend.

Figure 51. Waves entering the back-barrier lagoon during
rising tide at a position midway between Cabo de Santo
Agostinho (in the upper left) and the southern extremity
of the beach-rock exposure. Note the crescent-shaped beach
that has formed in response to the break in the beach-rock
barrier.



Figure 52. Internal structure of the beach-rock exposed
near Suape as viewed from the lagoon side. Note the
large accretion units and their small-scale internal
structure. Long tidal pools also occur along the length
of the barrier.

Figure 53. Algal rims around tidal pools on the beach-rock
barrier near Suape, shown here at low tide.

meters thick occur at the surface (Fig. 54, profile C-C'). Between these beach-rock
remnants occurs a thin facies (<5 meters) of sand containing a higher proportion of
carbonate components than the thick section of underlying sediments. Figure 54,
profile B-B', illustrates thinning of the sedimentary column in the vicinity of Cabo
de Santo Agostinho. The two prominent shelf sedimentary facies, a relatively thick
terrigenous sand overlain by a thin (2-3-meter) calcareous sand, fill irregularities
in the near-surface granitic basement rocks, which are highly faulted in this vicin-
ity. Profiles A-A', B-B', and C-C' of Figure 54 clearly show the multiple beach-rock
bands that occur seaward of the barrier that is so prominently displayed at low tide.
Profile C-C', Figure 54, which is oriented seaward of the small town of Cupe, illus-
trates three major beach-rock bands, each approximately 6-8 meters thick, that are
separated by thinner lithified and slumped material. Bedrock in this area is
approximately 30 meters beneath the base of the beach rock. Profile E-E' (Fig. 54)
was run parallel to the lithified barrier trend some 4-5 km offshore in water depths
of approximately 18 meters. At this distance seaward on the shelf, the thickness of
unconsolidated sediments over the basement is approximately 10 meters; both calca-
reous and terrigenous sand facies are identifiable, however.

The profiles presented in Figure 55 are representative of the facies relation-
ships found in the back-barrier lagoon and adjacent river mouth areas. Profile A-A'
parallels the barrier trend and is located between the tidal channel adjacent to
Cabo de Santo Agostinho and the break in the barrier near the mouth of Rio Ipojuca.
Along this trend unconsolidated sediments average about 60 meters thick above the
igneous basement rocks. Three facies are present: two terrigenous sand units aver-
aging about 20 meters thick, which are separated by a clay sequence whose thickness
varies from about 10 to 30 meters. Profiles oriented perpendicular to the barrier
trend (B-B', C-C', D-D' of Fig. 55) show basically the same three stratigraphic
units. However, thicknesses vary considerably from that shown in profile A-A'. In
general, the tendency is toward an overall thinning of the Holocene sedimentary
sequence in a landward direction. Profile C-C', which trends from the lithified
barrier up the Rio Massangana, shows an overall decrease in thickness of the sedi-
mentary section from about 60 meters at the seaward end of the profile to about
30 meters slightly landward of the river mouth.
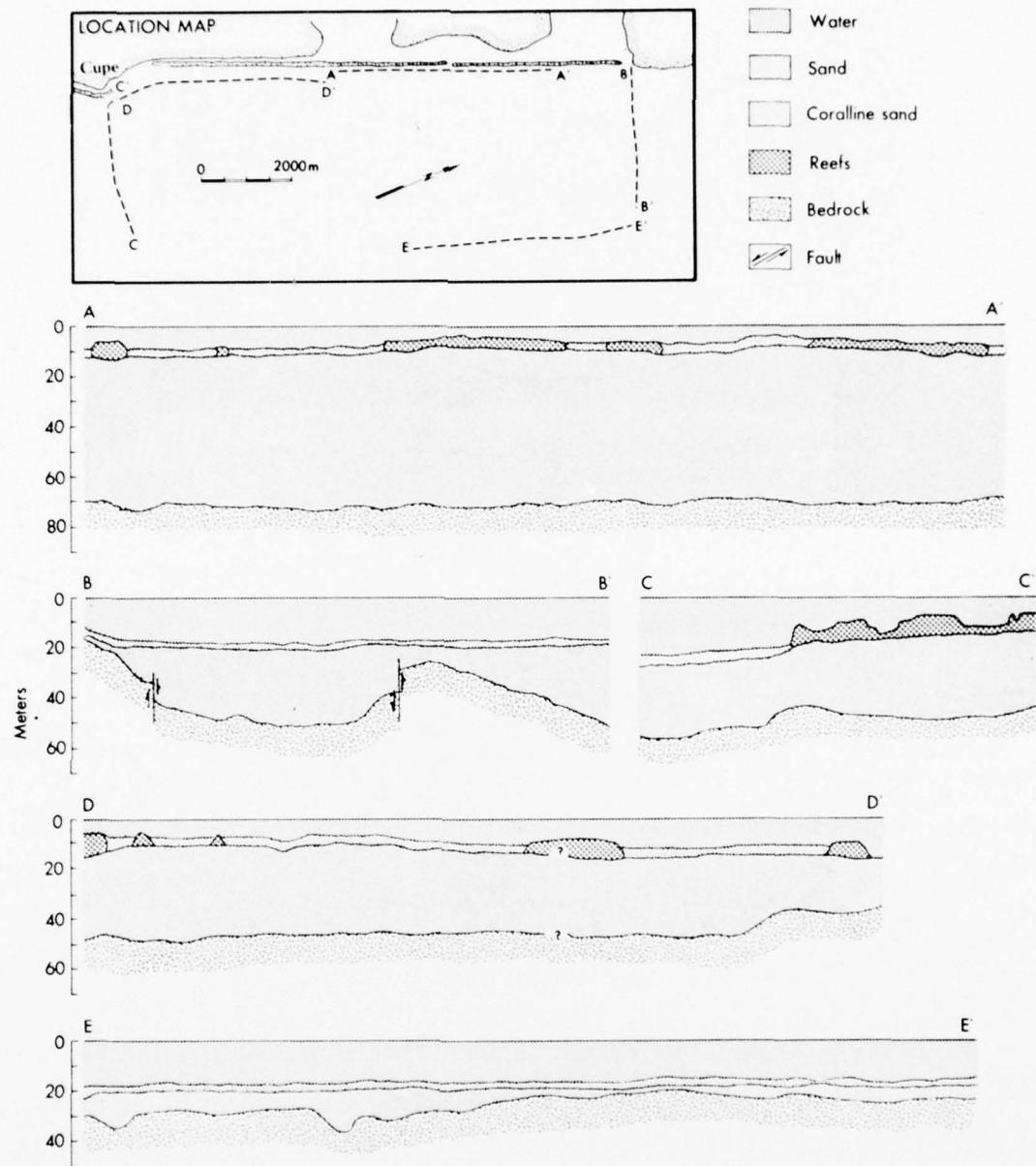
Figure 54. Sediment thickness on the shelf seaward of the beach-rock barrier near Suape as interpreted from shallow seismic subbottom profiles.

80
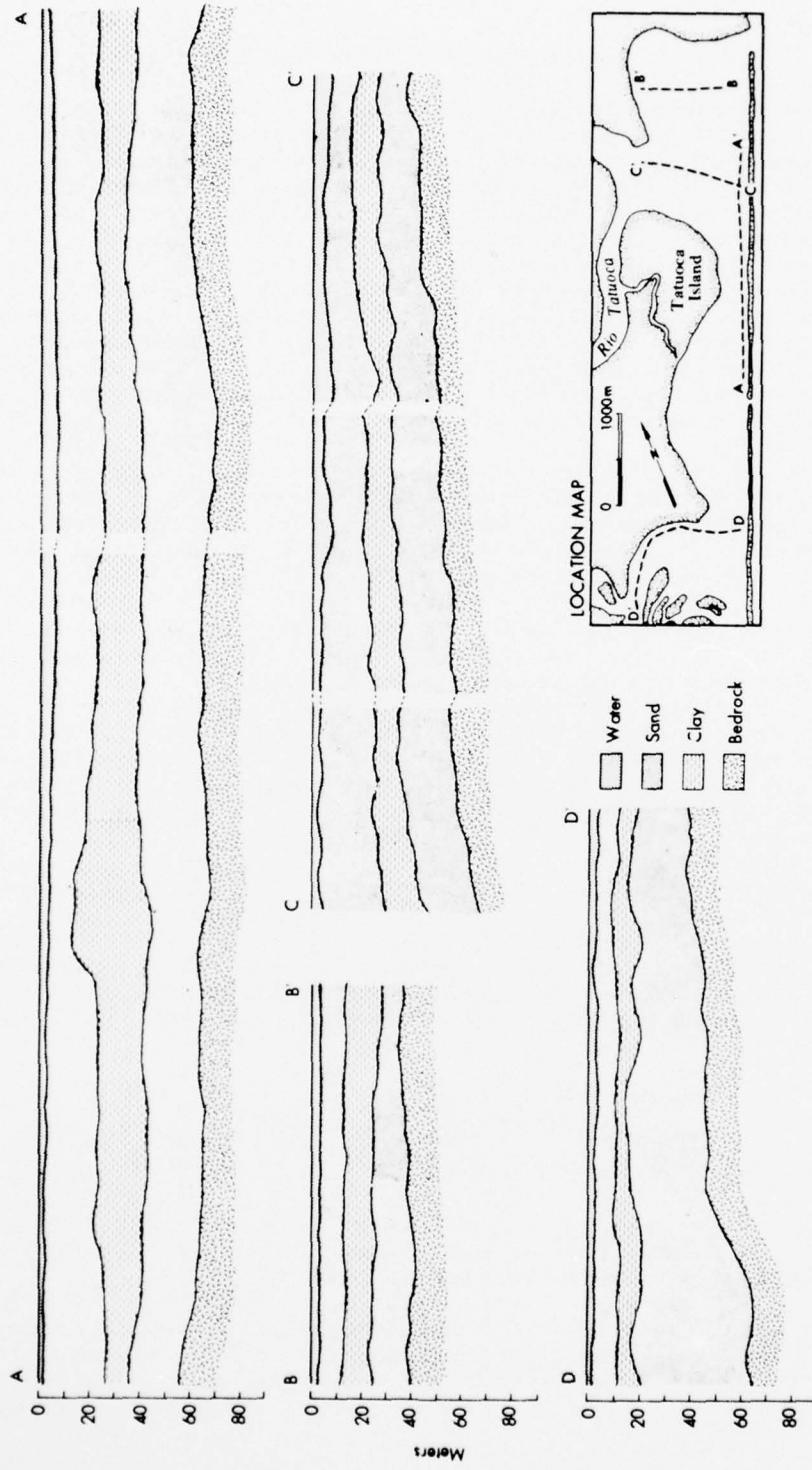
Figure 55. Sediment thickness in the lagoon behind the beach-rock barrier near Suape as interpreted from shallow seismic subbottom profiles.

81

## Sedimentology and Geochemistry

One of the most detailed sedimentological studies of Brazil's beach rock was published by Mabesoone (1964) and concerned the "sandstone reefs of Pernambuco." The purpose of his study was to determine the origin and age of the sandstone reefs in the general vicinity of the city of Recife. The approach used was both mega-scopic (geomorphic approach) and microscopic (granulometric approach). It was deter-mined that the macroscopic character of the sandstone reefs is typically that of beach rock, but the grain size characteristics indicate an offshore origin for the constituent sands. The age of the beach-rock bands was judged as Recent, and their occurrence is partially a consequence of the Holocene sea level rise. Every major band represents a temporary stillstand. Although this study contributed much to the understanding of beach rock along Brazil's northeast coast in the vicinity of Recife, many basic questions concerning the cementation characteristics and geochemical properties were left unanswered.

Samples were collected from a wide variety of beach-rock localities in order to answer some of the remaining questions relating to the petrologic and geochemical variability of Brazilian beach rock. Three widely spaced sample locations were selected: Ponta do Prego, near Maceio; Boa Viagem, south of Recife; and the Suape beach rock adjacent to Cabo de Santo Agostinho (Fig. 31).

Carbonate mineralogy was obtained on all samples by X-ray diffraction analysis (Matthews, 1966; Ebanks, 1967). Powder slide mounts of samples ground to pass a 200-mesh sieve were used on a Norelco diffractometer with Cu-K X-radiation. The scanning rate was set at $1/4°$ per minute over a two-theta interval from 25.5 to 32°. $MgCO_3$ content of the calcites was estimated by the peak displacement method utilizing silicon metal as an internal standard (Goldsmith et al., 1958, 1961). Thin sections and scanning electron microscopy provided a means of assessing cement morphology and grain-cement relationships. Carbon isotope analysis was performed to provide insight into the geochemical environment of cement deposition. Preparation of sam-ples for this analysis included acid washing with dilute HCl to remove surface con-tamination, rinsing with distilled water, and oven drying at 100°C. Cleaned samples were hand ground to pass a 200-mesh sieve. Separation of cement from grains was unnecessary in most samples because of the extremely low carbonate constituent grain content of most samples. Carbon dioxide was generated under vacuum by reaction with phosphoric acid and subsequently extracted and purified (Craig, 1953; McCrea, 1950). Carbon isotope ratios were determined with a 6-inch, 60° sector mass spectrometer. Delta $^{13}C$ values,

$$\delta^{13}C = (\frac{^{13}C/^{12}C \text{ sample}}{^{13}C/^{12}C \text{ standard}} -1) \times 10^3$$

are reported with respect to the PDB standard.

Table 11 summarizes data derived from beach-rock samples collected at these localities. Four basic cement fabrics were apparent from thin-section and scanning electron microscope analysis of the selected samples:

1) Acicular crusts, which consist of thin, needle-like crystals that completely cover grain surfaces and cavities. The crystals are about 15-40 microns in length and up to 5 microns wide. Cements of this nature have been shown by Shinn (1969), Moore (1973), and others, using staining and microprobe techniques, to be composed most commonly of aragonite.

82

Table 11

Summary of Beach Rock Petrographic and Geochemical Data

| Location | Sample No. | $\delta^{13}C$ | Mol % McCO$_3$ | Acicular Crust | Elongate Bladed Crust | Equant Bladed Crust | Micritic Crust | Micritic Void Filling | Degree of Cementation* | Carbonate Mineralogy** |
|---|---|---|---|---|---|---|---|---|---|---|
| Maceio | M-1-1 | 3.39 | 14.7 | X | X | | | | P | HMC, A(TR) |
| | M-2-1 | 3.66 | 16.0 | X | X | X | | | M | HMC, A(TR) |
| | M-2-3 | 3.68 | 16.0 | X | X | X | | | M | HMC, A(TR) |
| | M-3-1 | 3.16 | 15.1 | | | X | | | M | HMC |
| | M-3-3 | 3.06 | 15.9 | | X | X | | | M | HMC |
| Boa | R-1-1 | 3.36 | 15.9 | | X | X | | | M | HMC |
| | R-2-1 | 3.35 | 16.0 | | X | X | X | X | W | HMC |
| Viagem | R-2-2 | 3.01 | 15.6 | | X | X | | | W | HMC |
| | RB-1 | 3.60 | 15.6 | | | X | | | M | HMC |
| | RB-2 | 3.62 | 15.8 | | X | | X | | W | HMC |
| Suape | SA-1 | 3.62 | 14.7 | | | X | | | M | HMC |
| | SA-3 | 3.56 | 14.8 | | | X | | X | M | HMC |
| | SA-7 | -- | 15.8 | | | X | | | M | HMC |
| | SA-8 | 3.87 | 16.8 | | X | | | | W | HMC |

*Degree of cementation:

P = Poorly cemented; grain contacts and intermittent to thin crusts

M = Moderately cemented; well-developed crusts but abundant pore space

W = Well cemented; thick crusts, variable cement morphologies, limited pore space

**Carbonate mineralogy:  HMC = High Mg-calcite; A = aragonite  (TR = Trace amount)

2) Bladed crusts are composed of crystals that have a greater width to length ratio than acicular crystals. Two distinct varieties were encountered: crusts composed of elongate bladed crystals and those composed of more equant bladed crystals (Figs. 56 and 57). The individual crystals are up to 50 microns in length; however, the crusts average about 40 microns thick. These types of cements, especially the equant bladed varieties, have been described by Land (1971) from lithified Jamaican reefs as high Mg-calcite as well as by Alexandersson (1972) from the Mediterranean.

3) Micritic crusts are fine-grained carbonate rims that encrust grains and fill intergranular spaces. This type of cement is usually dark brown to gray and usually contains indistinct to distinct pelletoid structures. Occasionally small shell fragments and other forms of "debris" can be seen floating in this matrix material. It is common on carbonate grains to see the classical micrite rims described by Bathurst (1966) which are caused by the boring activity of micro-organisms (primarily algae and fungi). These types of crusts, as reported from beach-rock samples from Grand Cayman Island (Moore, 1973) and many other localities, are most commonly high Mg-calcite. Friedman and Gavish (1971) reported cements having similar morphology and mineralogy.

4) Micritic void fillings constitute the same type of cement as the micritic crust, but is a second generation cement formed after intergranular pore spaces were initially lined with acicular or bladed crusts.

The most striking trend with regard to cement fabric is the nearly universal occurrence of bladed crusts among the samples from all three geographic localities (Table 11). Only sample M-1-1, from Ponta do Prego, north of Maceio, exhibited no equant bladed crust fabric. This sample was taken from an incipient beach-rock band at the seaward margin of the modern beach. Both field inspection of this exposure and thin-section analysis suggest that cementation is in a very early stage of development. The cement most commonly encountered has an elongate bladed habit but occasionally appears acicular (Fig. 58). Cements are concentrated at grain contacts rather than having formed well-developed crusts. Incipient crusts are visible, but most primary void space is still intact.

Samples from the Boa Viagem localities exhibited the most variability with regard to cement fabric. All of the aforementioned fabrics were represented in these samples. Equant bladed crusts, however, were the most common cement morphology.

Samples selected from the long beach-rock barrier south of Cabo de Santo Agostinho showed the most similarity in cement fabric. All of the samples from this locality can be characterized by bladed crusts.

The fact that both elongate and equant bladed crystal habits with occasional acicular forms are well developed and form crusts suggests that these two types of cement were formed by precipitation directly from solution. Although it is tempting to suggest that this process is purely physical-chemical, one cannot rule out the possibility that biological activity in microenvironments may induce the carbonate precipitation. It is also significant to note that in all but one sample (M-1-1, the incipient beach rock) cements were deposited in crusts that completely covered grain surfaces and lined intergranular void spaces. In order for these cement fabrics to be generated, the pore spaces must be filled with the carbonate-rich solution, as in a phreatic environment.

As previously stated, the content of carbonate allochems in these samples is generally less than 5 percent. Therefore, a determination of carbonate mineralogy
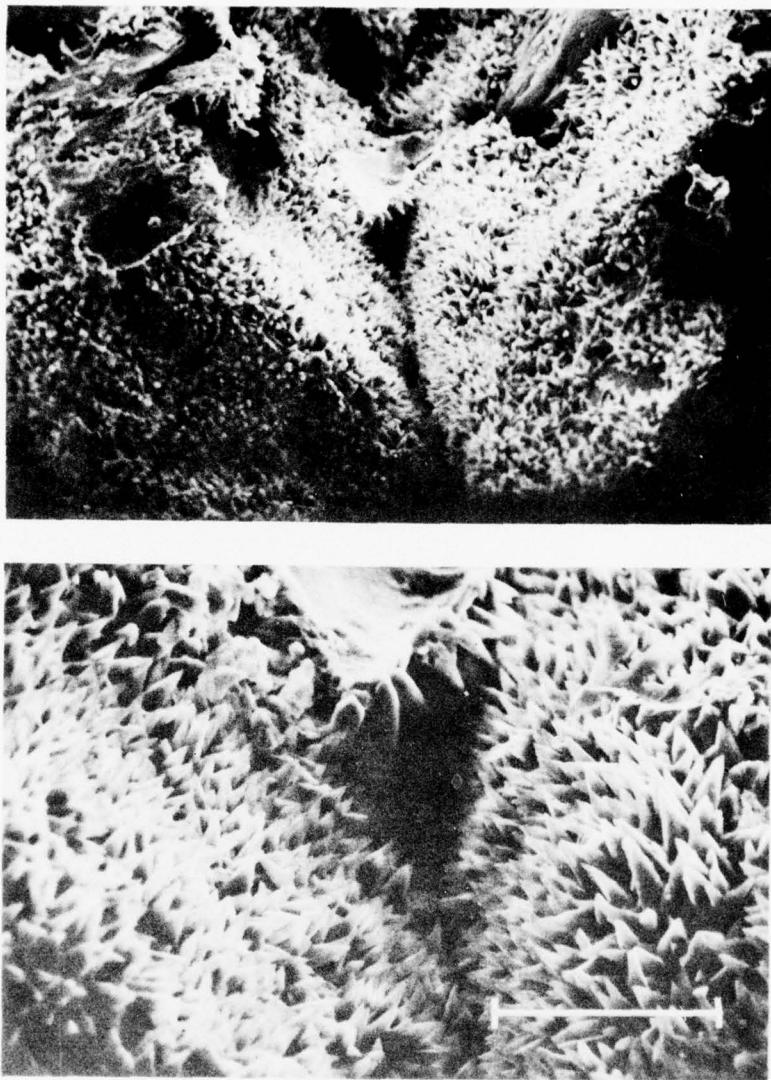
Figure 56. Elongate bladed crusts from sample M-2-2, col-
lected near Maceío. A. Note the nearly complete coverage
of grain surfaces and void spaces. B. Individual crys-
tals are well formed and have about a 2:1 length to width
ratio. Scale bar in these SEM photographs equals 0.2 mm.
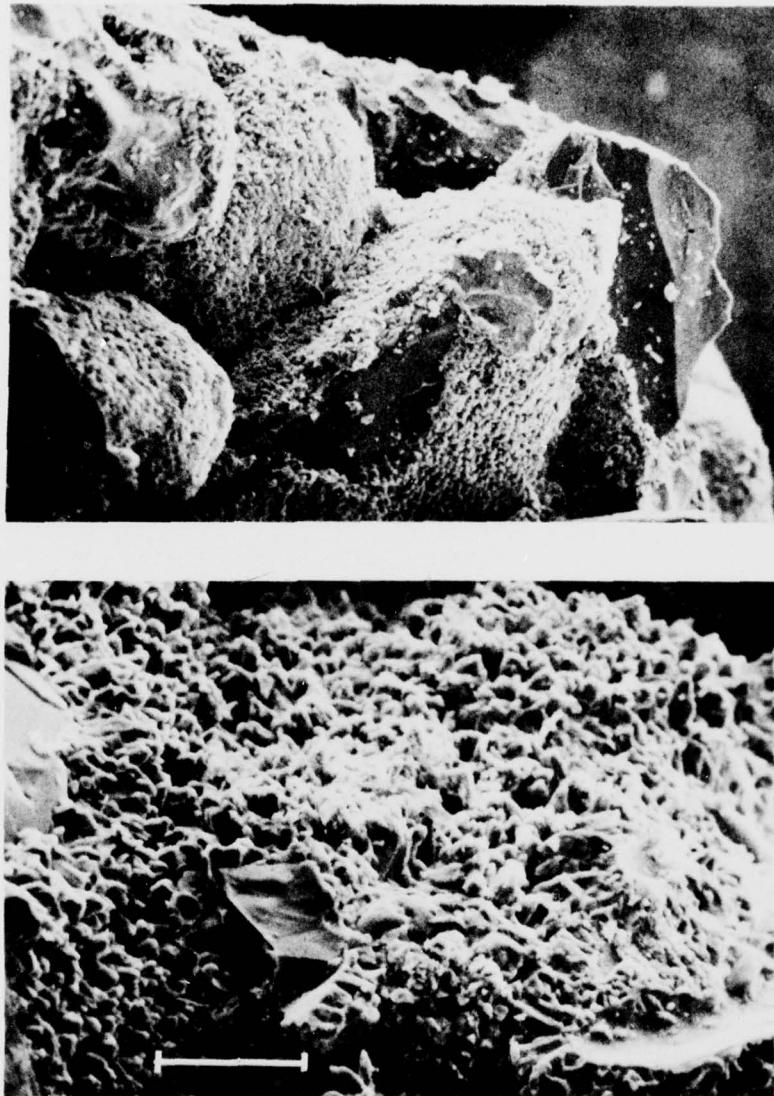
Figure 57. Equant bladed crusts from (A) sample M-3-3, collected near Maceio, and (B) sample SA-1, collected from the Suape beach-rock barrier. Length to width ratios of these crystals is close to 1:1. Scale bar in these SEM photographs equals 0.2 mm.

86
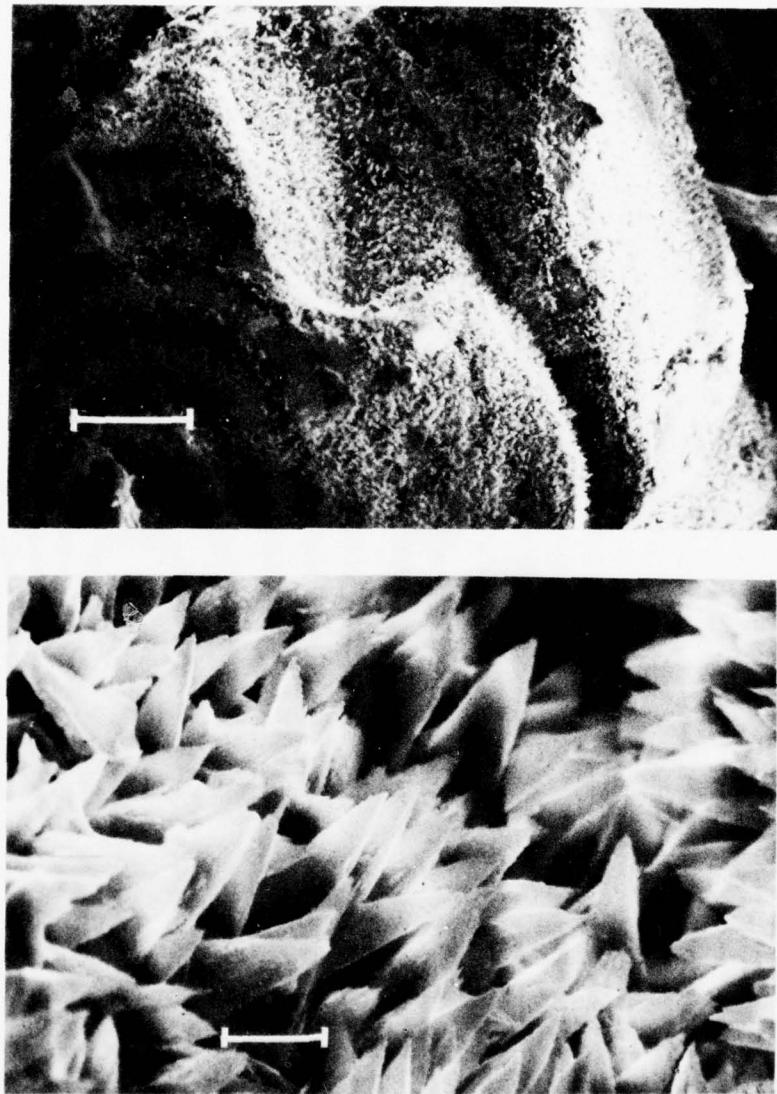
Figure 58. Incipient crust of elongate bladed crystals from
sample M-1-1, collected near Maceio. A. Note the incomplete
coverage of the grain surface. Scale bar equals 0.4 mm. B.
Closeup of elongate bladed crystals. Scale bar equals
0.04 mm.

utilizing the entire sample is primarily indicative of the cement composition. Table 11 shows that without exception the dominant carbonate phase in all samples is high Mg-calcite. Only samples M-3-1, M-2-1, and M-1-1, from Maceio, showed evidence of the presence of aragonite above the background level on the X-ray diffractogram (Fig. 59). In both of these cases the amount of aragonite was so small that an estimate of percentage using a peak area method would be unreliable. Therefore, only a trace of aragonite is indicated in Table 11.

It is interesting to note that the mode mol percent $MgCO_3$ in the high Mg-calcite cements is confined within a small range, 14.7 to 16.8 mol % $MgCO_3$ (Table 11). This is within the range of values so often reported in sedimentological literature for carbonate cements that have been precipitated under marine phreatic conditions.

Results of a carbon isotope analysis ($\delta^{13}C$ values of Table 11) of each sample show remarkable uniformity between these samples, which were collected over such a broad geographic area. An average $\delta^{13}C$ value of 3.46 was obtained; values ranged from 3.01 to 3.87. This range of values is consistent with results reported by Lowenstam and Epstein (1957) for Bahama ooliths, Shinn (1969) for Persian Gulf aragonitic submarine cement, Land (1971) for Jamaican magnesium calcite submarine cement, and Moore (1973) for beach-rock cements from Grand Cayman Island.

Carbon isotope ratios of sedimentary carbonate materials have been valuable to the understanding of geochemical processes operating in various environments. Sedimentary carbonate deposited from ocean bicarbonate in isotopic equilibrium with atmospheric $CO_2$ yields $\delta^{13}C$ values near zero. Freshwater carbonates are enriched in $^{12}C$ with respect to marine carbonates (Clayton and Degens, 1959; Weber et al., 1964) and thus result in negative $\delta^{13}C$ values. All of the $\delta^{13}C$ values derived from analysis of the Brazilian beach-rock samples exhibited a positive value near zero. These values suggest that the carbonate cements were precipitated under marine conditions. Comparisons of $\delta^{13}C$ values calculated from other carbonates precipitated in the realm of marine waters have already been presented. Carbon isotope values for the Brazilian beach-rock samples are consistent with values given in other studies of marine carbonates.

In summary, the occurrence of high Mg-calcite and trace amounts of aragonite as cements in the beach-rock samples collected from widely spaced sample sites along the Brazilian coast suggest a strong influence of marine waters at the site of precipitation. The fact that the common cement fabric is that of thick high Mg-calcite crusts of bladed crystals indicates a saturated or phreatic condition under which precipitation initially took place and probably is still continuing. In addition to the mineralogy and cement fabric, results of carbon isotope studies show a consistent trend toward values that must be interpreted as a product from carbonates precipitated under marine conditions. Therefore, the environment of deposition for these beach-rock samples, from the above lines of evidence, is marine phreatic. These results are in disagreement with the conclusion of Mabesoone (1964) from samples collected near the city of Recife. He stated that "beach rock formation in the investigated area is caused by evaporation of fresh calcium carbonate-rich water near the beach face." It must be pointed out, however, that beach-rock mineralogy can be extremely variable and that geomorphically similar exposures can have quite different diagenetic histories. Samples collected for this study, however, show a remarkable continuity in both petrographic and geochemical properties, even though they were selected from widely spaced geographic regions of the coast.
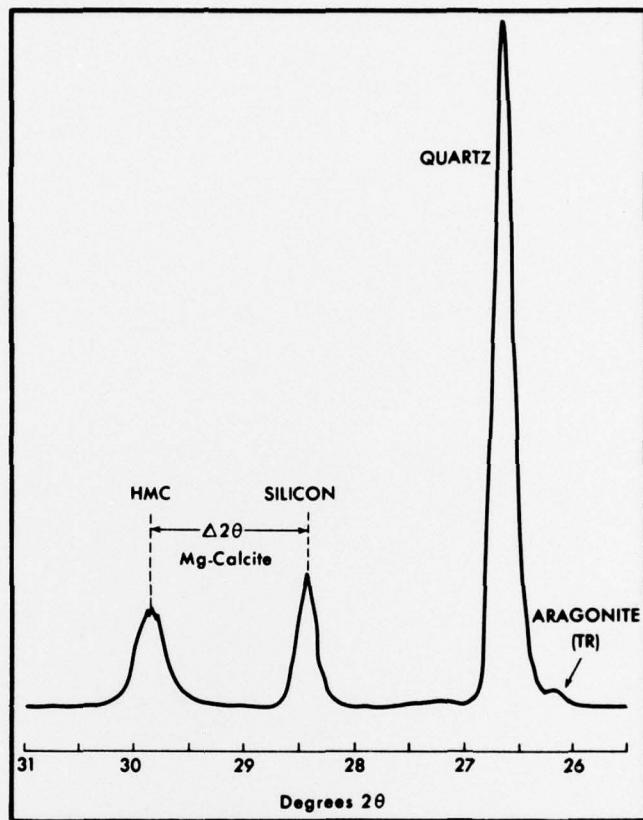
Figure 59.  X-ray diffractogram from sample
M-2-2 showing the small aragonite peak in
comparison to the well-formed high Mg-calcite
peak.  Diffractograms such as this one were
characteristic of most beach-rock samples
analyzed in this study.

## V.  SUMMARY OF RESULTS

### Atmospheric Studies

The mean circulation and the synoptic perturbations over the southern tropical
zone of South America are poorly known.  The low-level circulation pattern is simi-
lar in summer and winter.  Winds are generally from the southeast during winter but
change more to east in the summer.  Humid air masses from the northern hemisphere
that enter the study area are potentially very unstable, and small perturbations
lead to overturning.  Shear velocity measurements on land indicate a variation in
the aerodynamic drag coefficient at Aracaju.  The beach face had a value of 0.00211;
near the beach scarp the value was 0.00248; and in the swale area the value
increased to 0.00340.  Much larger values were observed in the dune area, where on
the top of a dune the value was 0.00495 and behind (leeward of) a dune the value
was 0.00984.

Over the ocean the shear velocity measurements indicate an average drag coef-
ficient of 0.0015; however, the drag coefficient varied with atmospheric stability.
The observed variation of shear velocity was found to be predicted by the theoreti-
cal formula proposed by Hsu (1974a).

### Coastal Oceanography

Sea level variations in the study area are dominated by a semidiurnal tide
whose height varies along the coast.  The largest heights are observed on the north-
ern part of the coast (i.e., Recife), and the lowest heights are in the south
(Aracaju).  These tides propagate along the coast from north to south, in opposi-
tion to the general trend of tides in the South Atlantic.

Wave studies indicate that the study area is subject to high levels of average
wave energy, but is not subject to extremely high levels.  Average wave height is
about 1 meter; 1 percent of the time waves will exceed 3 meters in height.  Near-
shore wave fields are affected by swell from the southern Atlantic during June;
however, the dominant source of wave energy is local wind waves.

Observations of long-period waves in the surf zone indicate standing waves are
formed which apparently are not in edge wave modes.  Edge waves may not be neces-
sary to produce bars having alongshore variation.

Measurements of wave action and currents in the Suape lagoon indicate that
tidal action is coupled with the input of water across the reef crest in determining
circulation in the lagoon.  In general, at higher tide levels waves transport water
across the reef crest and reach the back-reef lagoon.  The resulting currents tend
to drain the lagoon.  Variations in wave height from low tide to high tide amount
to about 800 percent (or from 7 cm to 56 cm).  Ebb-tidal currents dominate within
the lagoon.  Maximum velocities of approximately 77 cm/sec were recorded by a
drogue experiment conducted during falling tide.  The spatial distribution of sedi-
ments and bedforms reflect this ebb-tidal current domination of the beach-rock
barrier-lagoon system.

91

## Geomorphology

The coastal geomorphology of northeast Brazil is dominated in the north by lithified beaches and barriers and in the south by coastal beach-ridge plains. Since the Recent transgression of sea level the coast has prograded at Aracaju some 4-6 km. More recently, an erosional phase has been initiated and the shoreline has retreated, since 1950, at about 6 m/year.

Sediment samples indicate that sediments are generally quite uniform. Beach material is generally coarser than dune sediments; the coarsest sands occur on the inner bar. The average size of the beach sands is 2.61φ, and the dune sands are approximately 2.88φ.

Beach morphology was fairly static under average wave conditions and slowly changed during the initial increase in wave height during storms. However, during periods of decrease in wave height a longshore bar became prominent; it increased in height by 30 cm during 1 day and migrated shoreward 10 meters. As wave height decreased and stabilized, the bar continued to grow in height and migrate shoreward. During times of high waves the longshore bar causes wave breaking and therefore may extend the surf zone to more than 600 meters in width.

Beach-rock barriers control the movement of sand inshore from the barrier and therefore strongly influence shoreline morphology. The tendency is for the lithified offshore obstructions to modify and refocus incident wave energy along the back-barrier deposition coast by processes of wave refraction and diffraction. A highly crenulated coast results from these process-form interactions. Cases occur where the modern shoreline has accreted toward and joined an offshore barrier. Also, a break in a barrier may produce an arcuate embayment shoreward of the break, for example in the Suape lagoon. The beach-rock barriers are generally several meters thick (up to 8 meters) and have a width of about 250-300 meters. The barriers are underlain by unconsolidated sediments. Samples of beach rock from Maceio, Recife, and Suape were analyzed. The samples all appeared to be high Mg-calcite carbonate-cemented beach sediments, and the cementation occurred under marine phreatic conditions.

# REFERENCES

Andrade, G. O. De, 1955, Itamaraca. Contribucao para o estudo morfologico da costa Pernambucana. Recife (Tese de Concurso), 84 pp.

Alexandersson, T., 1972, Intragranular growth of marine aragonite and Mg-calcite: evidence of precipitation from supersaturated seawater. J. Sediment. Petrol., 42:441-460.

Bagnold, R. A., 1941, The physics of blown sand and desert dunes. First ed. London (Methuen) and New York (Morrow), 265 pp.

Banke, E. G., and S. D. Smith, 1971, Wind stress over ice and over water in the Beaufort Sea. J. Geophys. Res., 76:7368-7374.

Bathurst, R. G. C., 1966, Boring algae, micrite envelopes and lithification of molluscan biosparites. J. Geol., 5:15-31.

Bowen, A. J., and D. L. Inman, 1971, Edge waves and crescentic bars. J. Geophys. Res., 76(36):8662-8671.

Branner, J. C., 1904, The stone reefs of Brazil, their geological and geographical relations, with a chapter on the coral reefs. Museum of Comparative Zoology Bull., Geol. Ser. 7, v. 44, 285 pp. Cambridge, Mass. (Harvard College).

Bretschneider, C. L., 1963, Wave generation by wind, deep and shallow water. In (A. T. Ippen, ed.) Estuary and coastline hydrodynamics. Cambridge (Mass. Inst. Tech. Press), pp. 1-87.

Campos, C. W. M., F. C. Ponte, and K. Miura, 1974, Geology of the Brazilian continental margin. In (C. A. Burk and C. L. Drake, eds.) The geology of continental margins, pp. 447-461. New York (Springer-Verlag).

Clayton, R. N., and E. T. Degans, 1959, Use of carbon isotope analyses of carbonates for differentiating fresh-water and marine sediments. Bull. Am. Assoc. Petrol. Geologists, 43:890-897.

Craig, H., 1953, The geochemistry of the stable carbon isotopes. Geochem. Cosmochim. Acta, 3:53-92.

Darwin, C., 1841, On a remarkable bar of sandstone of Pernambuco on the coast of Brazil. London, Edinbutgh, Dublin Philos. Mag. and J. Sci., 19:257-261.

Davidson, K. L., 1970, An investigation of the influence of water waves on the adjacent airflow. Unpublished Ph.D. thesis, Univ. of Michigan, Ann Arbor.

DeLeonibus, P. S., 1971, Momentum flux and wave spectra observations from an ocean tower. J. Geophys. Res., 6:6506-6527.

DeLeonibus, P. S., L. S. Simpson, and M. G. Mattie, 1974, Equilibrium range in wave spectra observed at an open-ocean tower. J. Geophys. Res. 79:3041-3053.

Dietrich, G., 1944, Die Schwingungssysteme der halb - und eintagigeu Tiden in den Ozeanen. Veroffentl. Inst. Meereskunde Univ. Berlin, A41, 7-68.

Ebanks, W. J., Jr., 1967, Recent carbonate sedimentation and diagenesis, Ambergris Cay, British Honduras. Ph.D. thesis, Rice Univ., Houston, Texas, 189 pp.

Finkel, H. J., 1959, The barchans of southern Peru. J. Geol., 67:614-647.

Friedman, G. M., and D. Gavish, 1971, Mediterranean and Red Sea (Gulf of Aquaba) beach rock. In (O. P. Bricker, ed.) Carbonate cements, pp. 13-16. Baltimore, Maryland. (Johns Hopkins Univ. Press).

Goldsmith, J. R., D. L. Graf, A. A. Chodos, O. I. Joensun, and L. D. McVicker, 1958, Relation between lattice constants and composition of the Ca-Mg carbonates. Am. Mineralogist, 43:84-101.

Goldsmith, J. R., D. L. Graf, and H. C. Hear, 1961, Lattice constants of the calcium magnesium carbonates. Am. Mineralogist, 46:453-457.

Hasselmann, K., W. H. Munk and G. MacDonald, 1963, Bispectra of ocean waves. Time Series Analysis, chapter 8, pp. 125-139, Wiley, New York.

Hendershott, M. C., 1973, Ocean tides. EOS Trans. Am. Geophys. Union, 54(2):76-86.

Hicks, B. B., and A. J. Dyer, 1970, Measurements of eddy-fluxes over the sea from an offshore oil rig. Quart. J. Roy. Meteorol. Soc., 96:523-528.

Hogben, N., and F. E. Lumb, 1967, Ocean wave statistics. D. R. Hillman and Sons, Ltd., Frome, England.

Hsu, S. A., 1971a, Wind stress criteria in eolian sand transport. J. Geophys. Res., 76:8684-8686.

Hsu, S. A., 1971b, Measurement of shear stress and roughness length on a beach. J. Geophys. Res., 76:2880-2885.

Hsu, S. A., 1972a, Boundary-layer trade-wind profile and stress on a tropical windward coast. Boundary-Layer Meteorol., 2:284-289.

Hsu, S. A., 1972b, Wind stress on a coastal water surface. Proc., 13th Coastal Engr. Conf., Vancouver, B. C., Canada, Am. Soc. Civil Engrs., 3:2531-2541.

Hsu, S. A., 1973, Computing eolian sand transport from shear velocity measurements. J. Geol., 81:739-743.

Hsu, S. A., 1974a, A dynamic roughness equation and its application to wind stress determination at the air-sea interface. J. Phys. Oceanog., 4:116-120.

Hsu, S. A., 1974b, On the log-linear wind profile and the relationship between shear stress and stability characteristics over the sea. Boundary-Layer Meteorol., 6:509-514.

Hsu, S. A., 1975, Wind stress on nearshore and lagoonal waters of a tropical island. Limnol. and Oceanog., 20:113-115.

Hsu, S. A., 1976, Determination of the momentum flux at the air-sea interface under variable meteorological and oceanographic conditions: further application of the wind-wave interaction method. Boundary-Layer Meteorol. (In press).

Hunkins, K., 1962, Waves on the Arctic Ocean.  J. Geophys. Res., 67(6):2477-2489.

Inman, D. L., C. G. Ewing, and J. B. Corliss, 1966, Coastal sand dunes of Guerrero Negro, Baja California, Mexico.  Bull. Geol. Soc. Am., 77:787-802.

Inman, D. L., and C. E. Nordstrom, 1971, On the tectonic and morphologic classification of coasts.  J. Geol., 79(1):1-11.

Johnson, D. H., 1970, The role of the tropics in the global circulation.  In (G. A. Corby, ed.) The global circulation of the atmosphere.  Quart. J. Roy. Meteorol. Soc., London, pp. 113-136.

Johnson, D. W., 1919, Shore processes and shoreline development.  John Wiley and Sons, New York, 584 pp.

Kadib, A. A., 1965, A function of sand movement by wind.  Tech. Rept. HEL-2-12, Univ. of California, Berkeley, 91 pp.

Kajiura, K., 1963, On the partial reflection of water waves passing over a bottom of variable depth.  Internat. Union Geodesy and Geophys. Monograph 24, Proc. Tsunami Meeting 1961, 10th Pacific Science Congr., Honolulu, Hawaii, pp. 206-230.

Kaye, C. A., 1959, Shoreline features and Quaternary shoreline changes of Puerto Rico.  U.S. Geol. Surv. Prof. Paper 317-B, 140 pp.

Kjerfve, B., 1973, Dynamics of the water surface in a bar-built estuary.  Unpublished Ph.D. thesis, Louisiana State Univ., Baton Rouge.

Kraus, E. B., 1972, Atmosphere-ocean interaction.  London (Oxford Univ. Press), 275 pp.

Land, L. S., 1971, Submarine lithification of Jamaican reefs.  In (O. P. Bricker, ed.) Carbonate cements.  Baltimore, Maryland (Johns Hopkins Univ. Press), pp. 59-62.

Lettau, H., 1967, Small- to large-scale features of boundary layer structure over mountain slopes.  Sect. 2, Proc., Symposium on Mountain Meteorology, Colorado State Univ., Fort Collins, Atmospheric Science Paper No. 122.

Lettau, K., and H. Lettau, 1969, Bulk transport of sand by the barchans of the Pampa de La Joya in southern Peru.  Zeit. fur Geomorph., 13:182-195.

Lowenstam, H. A., and S. Epstein, 1957, On the origin of sedimentary aragonite needles of the Great Bahama Bank. J. Geol., 65:364-375.

Mabesoone, J. M., 1964, Origin and age of the sandstone reefs of Pernambuco (Northeastern Brazil).  J. Sediment. Petrol., 34:7 5-726.

Mabesoone, J. M., 1971, Calcarios Recentes do litoral nordestino. Imprensa Univ., Natal, Estudos Sedimentologicos, 1:45-54.

Mabesoone, J. M., and P. N. Coutinho, 1970, Littoral and shallow marine geology of northern and northeastern Brazil.  Trab. Oceanogr. Univ. Fed. Pe., Recife, v. 12, 214 pp.

Matthews, R. K., 1966, Genesis of recent lime mud in southern Honduras. J. Sediment. Petrol., 36:428-454.

McCrea, J. M., 1950, On the isotopic chemistry of carbonates and a paleotemperature scale. J. Chem. Phys., 18:849-857.

Moore, C. H., Jr., 1973, Intertidal carbonate cementation, Grand Cayman, West Indies. J. Sediment. Petrol., 43:591-602.

Munk, W., 1949, Surf beats. Trans. Am. Geophys. Union, 39(6):849-854.

Munk, W., 1951, Ocean waves as a meteorological tool. In (T. F. Malone, ed.) Compendium of meteorology. Baltimore, Maryland (Waverly Press), pp. 1090-1100.

Munk, W., 1962, Long ocean waves. In (M. N. Hill, ed.) The sea, v. 1, pp. 647-663. New York-London (Interscience).

Nakamura, M., H. Shiraishi, and Y. Sasaki, 1966, Wave damping effect of submerged dike. Proc., 10th Conf. Coastal Engr., Tokyo, Japan, 1:254-267.

Pierson, W. J., and L. Moskowitz, 1964, A proposed spectral form for fully developed wind seas based on the similarity theory of S. A. Kitaigorodshkii, J. Geophys. Res., 69(24):5181-5190.

Priestley, C. H. B., 1959, Turbulent transfer in the lower atmosphere. Chicago (Univ. of Chicago Press), 130 pp.

Ramos, R. P. L., 1975, Precipitation characteristics in the northeast Brazil dry region. J. Geophys. Res., 80:1665-1678.

Roberts, H. H., S. P. Murray, and J. N. Suhayda, 1975, Physical processes in a fringing reef system. J. Mar. Res., 33:233-260.

Roll, H. U., 1965, Physics of the marine atmosphere. New York (Academic Press), 426 pp.

Russell, R. J., 1957, Caribbean beach rock observations. Zeit. fur Geomorph., NF v. 3, pp. 227-236.

Russell, R. J., 1969, South American marine energy. Tech. Rept. 73, Coastal Studies Inst., Louisiana State Univ., Baton Rouge, 31 pp.

Shinn, E. A., 1969, Submarine lithification of Holocene carbonate sediments in the Persian Gulf. Sedimentology, 12:109-144.

Sonu, C. J., 1972a, Field investigation of nearshore circulation and meandering currents. J. Geophys. Res., 77(18):3232-3247.

Sonu, C. J., 1972b, Comment on paper by Bowen and Inman, 'Edge waves and crescentic bars.' J. Geophys. Res., 77(33):6629-6631.

Sonu, C. J., S. P. Murray, S. A. Hsu, J. N. Suhayda, and E. Waddell, 1973, Sea breeze and coastal processes. EOS, Trans. Am. Geophys. Union, 54(9):820-833.

Suhayda, J. N., 1972, Experimental study of the shoaling transformation of waves on a sloping bottom.  Ph. D. dissertation, Univ. of California, San Diego, 106 pp.

Suhayda, J. N., 1974a, Determining nearshore infragravity wave spectra.  Preprints, International Symposium on Ocean Wave Measurement and Analysis, Sept. 9-11, 1974, New Orleans.

Suhayda, J. N., 1974b, Standing waves on beaches.  J. Geophys. Res., 79(21):3065-3071.

Sutton, O. G., 1953, Micrometeorology.  New York and London (McGraw-Hill), 333 pp.

Svasek, J. N., and J. H. J. Terwindt, 1974, Measurements of sand transport by wind on a natural beach.  Sedimentology, 21:311-322.

Taljaard, J. J., 1972, Synoptic meteorology of the southern hemisphere.  In (C. W. Newton, ed.) Meteorology of the southern hemisphere.  Meteorol. Monographs, 13(35):139-213.  Boston (Am. Meteorol. Soc.).

Trewartha, G. T., 1961, The earth's problem climates.  Madison (Univ. of Wisconsin Press), 334 pp.

Tricart, J., 1959, Problemes geomorphologiques du littoral oriental du Bresil.  Cahiers Oceanogr., 11:276-308.

Tucker, M. J., 1950, Surf beats:  sea waves of 1 to 5 minutes periods.  Proc., Roy. Soc. London, A, 202:565-573.

Ursell, F., 1952, Edge waves on a sloping beach.  Proc., Roy. Soc. London, A, 214: 79-97.

U.S. Department of Commerce, National Ocean Survey, 1975, Tide tables, east coast of North and South America.  Washington, D.C., (U.S. Government Printing office), 288 pp.

Waddell, E., 1973, The dynamics of swash and its implication to beach response.  Tech. Rept. 139, Coastal Studies Inst., Louisiana State Univ., Baton Rouge, 49 pp.

Walters, C. D., 1973, Atmospheric surface boundary layer wind structure studies on an Alaskan arctic coast during winter and summer seasons.  Unpublished M.S. thesis, Louisiana State Univ., Baton Rouge, 42 pp.

Walters, C. D., 1975, Drag coefficient and roughness length determinations on an Alaskan arctic coast during summer.  Boundary-Layer Meteorol., 8:235-237.

Weber, J. N., E. G. Williams, and M. L. Keith, 1964, Paleoenvironmental significance of carbon isotopic composition of siderite nodules in some shales of Pennsylvanian age.  J. Sediment. Petrol., 34:814-819.

Wiseman, Wm. J., Jr., J. M. Coleman, A. Gregory, S. A. Hsu, A. D. Short, J. N. Suhayda, C. D. Walters, and L. D. Wright, 1973, Alaskan Arctic coastal processes and morphology.  Tech. Rept. 149, Coastal Studies Inst., Louisiana State Univ., Baton Rouge, 171 pp.

Wright, L. D., and J. M. Coleman, 1973, Variations in morphology of major river deltas as functions of ocean wave and river discharge regimes. Bull. Am. Assoc. Petrol. Geologists, 57:370-398.

Wright, L. D., S. A. Hsu, N. H. Rector, and J. N. Suhayda, 1974, Preliminary reconnaissance of the coastal barriers of northeastern Brazil. Unpublished trip rept., Coastal Studies Inst., Louisiana State Univ., Baton Rouge.

Office of Naval Research
Geography Programs
Code 462
Arlington, Virginia 22217

Defense Documentation Center
Cameron Station
Alexandria, Virginia 22314

Director, Naval Research Lab
Attn: Technical Information
Officer
Washington, D.C. 20375

Director
Office of Naval Research Branch
Office
1030 East Green Street
Pasadena, California 91101

Director
Office of Naval Research Branch
Office
536 South Clark Street
Chicago, Illinois 60605

Director
Office of Naval Research Branch
Office
495 Summer Street
Boston, Massachusetts 02210

Commanding Officer
Office of Naval Research
 Branch Office
Box 39
FPO New York 09510

Chief of Naval Research
Asst. for Marine Corps Matters
Code 100M
Office of Naval Research
Arlington, Virginia 22217

NORDA Code 400
National Space Technology Lab
Bay St. Louis, MS 39520

Office of Naval Research
Operational Applications Div.
Code 200 Arlington, Virginia 22217

Office of Naval Research
Scientific Liaison Officer
Scripps Inst. of Oceanography
La Jolla, California 92038

Director, Naval Research Lab
Attn. Library, Code 2628
Washington, D.C. 20375

Commander
Naval Oceanographic Office
Attn. Library, Code 1600
Washington, D.C. 20374

Naval Oceanographic Office
Code 3001
Washington, D.C. 20374

Chief of Naval Operations
OP 987P1
Department of the Navy
Washington, D.C. 20350

Oceanographer of the Navy
Hoffman II Building
200 Stovall Street
Alexandria, Virginia 22322

Naval Academy Library
U.S. Naval Academy
Annapolis, Maryland 21402

Commanding Officer
Naval Coastal Systems Laboratory
Panama City, Florida 32401

Librarian
Naval Intelligence
 Support Center
4301 Suitland Road
Washington, D.C. 20390

Commanding Officer
Naval Air Dev. Center
Warminster, Johnsville
Pennsylvania 18974

Naval Ordinance Lab
White Oak
Silver Spring, Maryland 20910

Commanding Officer
Naval Civil Engineering Lab
Port Hueneme, California 93041

Officer in Charge
Environmental Prediction
 Research Facility
Naval Post Graduate School
Monterey, California 93940

Dr. Warren C. Thompson
Dept. of Meteorology and
 Oceanography
U.S. Naval Post Graduate School
Monterey, California 93940

Director
Amphibious Warfare Board
U.S. Atlantic Fleet
Naval Amphibious Base
Norfolk, Little Creek, Va. 23520

Commander, Amphibious Force
U.S. Pacific Fleet
Force Meteorologist
COMPHIBPAC CODE 25 5
San Diego, California 92155

Commanding General
Marine Corps Development and
 Educational Command
Quantico, Virginia 22134

Dr. A. L. Slafkosky
Scientific Advisor
Commandant of the Marine Corps
Code MC-RD-1
Washington, D.C. 20380

Defense Intelligence Agency
Central Reference Division
Code RDS-3
Washington, D.C. 20301

Director
Defense Mapping Topographic
 Center
Attn: Code 50200
Washington, D.C. 20315

Commanding Officer
U.S. Army Engineering
 Topographic Lab
Attn: ETL-ST
Fort Belvoir, Virginia 22060

Director
Coastal Engineering Res.
 Center
U.S. Army Corps of Engineers
Kingman Building
Fort Belvoir, Virginia 22060

Chief, Wave Dynamics Division
USAE-WES
P.O. Box 631
Vicksburg, Miss. 39180

Commandant
U.S. Coast Guard
Attn: GECV/61
Washington, D.C. 20591

Office of Research and
 Development
c/o DS/62
U.S. Coast Guard
Washington, D.C. 20591

National Oceanographic
 Data Center c/o D764
Environmental Data Services
NOAA
Washington, D.C. 20235

Assistant Director
Research and Development
National Ocean Survey
6001 Executive Boulevard
Rockville, Maryland 20852

Central Intelligence Agency
Attn: OCR/DD-Publications
Washington, D.C. 20205

Dr. Donald Swift
Marine Geology and
 Geophysics Laboratory
AOML - NOAA
15 Rickenbacker Causeway
Miami, Florida 33149

Dr. Mark M. Macomber
Advanced Technology Div.
Defense Mapping Agency
Naval Observatory
Washington, D.C. 20390

Ministerialdirektor
Dr. F. Wever
Rue/FO
Bundesministerium der
 Verteidigung
Hardthoehe
D-5300 Bonn, West Germany

Oberregierungsrat
Dr. Ullrich
Rue/FO
Bundesministerium der
 Verteidigung
Hardthoehe
D-5300 Bonn, West Germany

Dr. Yoshimi Goda
Director, Wave Research Div.
Port and Harbor Research Inst.
Ministry of Transportation
1-1 Nagase, 3 Chome
Yokosuka, 239 Japan

Mr. Tage Strarup
Defence Research Establishment
Osterbrogades Kaserne
DK-2100 Kobenhavn O, Denmark

Prof. Dr. Rer. Nat. H. G.
 Gierloff-Emden
Institut F. Geographie
Universitaet Muenchen
Luisenstrasse 37/III
D-800 Muenchen 2, West Germany

Prof. Dr. Eugen Seibold
Geol-Palaeontolog. Institut
Universitaet Kiel
Olshausenstrasse 4-60
D-2300 Kiel, West Germany

Dr. R. Koester
Geo.-Palaeontolog. Institut
Universitaet Kiel
Olshausenstrasse 40-60
D-2300 Kiel, West Germany

Prof. Dr. Fuehrboeter
Lehrstuhl F. Hydromechanik U.
Kuestenwasserbau
Technische Hochschule
 Braunschweig
Beethovenstrasse 51A
D-3300 Braunschweig
West Germany

Prof. Dr. Walter Hansen
Direktor D. Instituts f.
 Meereskunde
Universitaet Hamburg
Heimhuderstrasse 71
D-2000 Hamburg 13,
West Germany

Prof. Dr. Klaus Hasselmann
Institut F. Geophysik
Universitaet Hamburg
Schuleterstrasse 22
0-2000 Hamburg 13, West Germany

Prof. Dr. Nils Jerlov
Institute for Physical
 Oceanography
Kobenhavns Universitet
Haraldsgade 6
DK-2200 Kobenhavn, Denmark

Dr. Vernon W. Pidgeon
Dynex Consulting Company
1001 Kimberly Lane
Lynn Haven, Florida 32444

Dr. H. J. Schoemaker
Waterloopkundig Laboratorium
 Te Delft
61 Raam, Delft, Netherlands

Ir. M. W. Van Batenberg
Physisch Laboratorium TNO
Oude Waalsdorper Weg 63, Den Haag
Netherlands

Dr. Gordon E. Carlson
University of Missouri
Department of Electrical Engineering
Rolla, Missouri 65401

Mr. H. G. Tornatore
ITT Avionics
9140 Old Annapolis Road
Columbia, Maryland 21043

Prof. John D. Isaacs
University of California A-207
Institute of Marine Res.
La Jolla, California 92093

Mr. Donald A. Leonard
Computer Genetics Corporation
4 Lakeside Office Park
Wakefield, Massachusetts 01880

Dr. G. D. Hickman
Applied Science Technilogy, Inc.
19212 Plummer Drive
Germantown, Maryland 20767

ONR Scientific Liaison Group
American Embassy
Room A-407
APO San Francisco, CA 96503

Dr. Bernard Le Mehaute
Tetra Tech, Inc.
630 North Rosemead Blvd.
Pasadena, California 91107

Dr. Richard A. Davis, Jr.
Department of Geology
University of South Florida
Tampa, Florida 33620

Dr. William T. Fox
Department of Geology
Williams College
Williamstown, Mass. 01267

Dr. William S. Gaither
Dean
College of Marine Studies
Robinson Hall
University of Delaware
Newark, Delaware 19711

Dr. John T. Kuo
Henry Krumb School of Mines
Seeley W. Mudd Building
Columbia University
New York, New York 10027

Dr. Edward B. Thornton
Department of Oceanography
Naval Postgraduate School
Monterey, California 93940

Prof. C. A. M. King
Department of Geography
University of Nottingham
Nottingham, England

Dr. Douglas L. Inman
Scripps Institute of
 Oceanography
La Jolla, California 92037

Prof. Toshiyuki Shigemura
Civil Engineering Dept.
National Defense Academy
1-10-20 Hashirimizu
Yokosuka 239, Japan

Prof. Yuji Iwagaki
Civil Engineering Dept.
Kyoto University
9 Shimogamo Zenbucho,
 Sakyo-Ku
Kyoto, Japan

Prof. Kiyoshi Horikawa
Dept. of Civil Engineering
University of Tokyo
7-3-1, Hongo, Bunkyo-Ku
Tokyo 113, Japan

Dr. William W. Wood
Department of Geosciences
Purdue University
Lafayette, Indiana 47907

Dr. Alan W. Niedoroda
Director, Coastal Research
 Center
University of Massachusetts
Amherst, Mass. 01002

Dr. Benno M. Brenninkmeyer,
 S.J.
Dept. of Geology & Geophysics
Boston College
Chestnut Hill, Mass. 02167

Dr. Omar Shemdin
JPL-CALTECH
Mail Stop 183-501
4800 Oak Grove Drive
Pasadena, California 91103

Dr. Lester A. Gerhardt
Rennsselaer Polytechnic Inst.
Troy, New York 12181

Mr. Fred Thomson
Environmental Research Inst.
P.O. Box 618
Ann Arbor, Michigan 48107

Dr. J. A. Dracup
Environmental Dynamics, Inc.
1609 Westwood Blvd.
Suite 202
Los Angeles, Calif. 90024

Dr. Thomas K. Peucker
Simon Fraser University
Department of Geography
Burnaby 2, B.C., Canada

Dr. Bruce Hayden
Department of Environmental
 Sciences
University of Virginia
Charlottesville, VA 22903

Revised 10/27/77

## DOCUMENT CONTROL DATA - R & D

*(Security classification of title, body of abstract and indexing annotation must be entered when the overall report is classified)*

| 1. ORIGINATING ACTIVITY *(Corporate author)* | 2a. REPORT SECURITY CLASSIFICATION |
|---|---|
| Coastal Studies Institute ✓ <br> Louisiana State University <br> Baton Rouge, Louisiana 70803 | Unclassified |
| | 2b. GROUP <br> Unclassified |

3. REPORT TITLE

DOCUMENTATION AND ANALYSIS OF COASTAL PROCESSES, NORTHEAST COAST OF BRAZIL

4. DESCRIPTIVE NOTES *(Type of report and inclusive dates)*

5. AUTHOR(S) *(First name, middle initial, last name)*

Joseph N. Suhayda, S. A. Hsu, Harry H. Roberts, and Andrew D. Short

| 6. REPORT DATE <br> August 1977 | 7a. TOTAL NO. OF PAGES <br> 98 | 7b. NO. OF REFS <br> 87 |
|---|---|---|
| 8a. CONTRACT OR GRANT NO. <br> N00014-75-C-0192 <br> b. PROJECT NO. <br> NR 388 002 <br> c. <br> d. | 9a. ORIGINATOR'S REPORT NUMBER(S) <br> Technical Report No. 238 ✓ | |
| | 9b. OTHER REPORT NO(S) *(Any other numbers that may be assigned this report)* | |

10. DISTRIBUTION STATEMENT

Approved for public release; distribution unlimited.

| 11. SUPPLEMENTARY NOTES | 12. SPONSORING MILITARY ACTIVITY <br> Geography Programs <br> Office of Naval Research <br> Arlington, Virginia 22217 |
|---|---|

13. ABSTRACT

A multidisciplinary investigation was conducted during June and July 1975 to acquire data that would set a basic framework of the physical processes controlling morphology of the northeast coast of Brazil. Detailed field data were taken at two sites along the coast: Aracaju, Sergipe, and Suape, Pernambuco. Analysis of the data and long-term broad-scale data supplied by cooperating Brazilian agencies was conducted for two purposes: to delineate the physical processes and morphology of the coast and to investigate under field conditions the mechanics of specific important coastal processes.

The northeast coast of Brazil is located on the trailing edge of the South American continental land mass and consists of a broad coastal plain recently drowned by the Holocene rise in sea level. Long, linear depositional forms, barrier beaches, and stone reefs dot the coastline. The lithified stone reefs (beach-rock reefs) occur at various distances from the shoreline and greatly affect nearshore waves and currents; many small harbors along the coast result. At Aracaju the coastline was formed by a progradation process that has recently been reversed, so that dune migration and shoreline erosion are now occurring. The stone reefs were formed in a marine environment, and the cementation process may be continuing in several places contemporaneously. U

Physical processes affecting these morphologic features were studied in detail. Atmospheric shear velocity measurements indicate that the aerodynamic drag coefficient varies greatly from the offshore region, across the nearshore and beach environments, to the dune field. Beach dynamics are shown, by a study of the formation of an alongshore bar and accompanying processes, to depend greatly upon the action of long-period wave components in the surf zone. The stone reefs cause a decrease of up to 90 percent in wave heights as a result of induced breaking and wave reflection. The amount of decrease varies during a single tidal cycle from 50 percent to 90 percent. Circulation in back-reef lagoons varies greatly in pattern and intensity over a tidal cycle. U

| 14 KEY WORDS | LINK A | | LINK B | | LINK C | |
|---|---|---|---|---|---|---|
| | ROLE | WT | ROLE | WT | ROLE | WT |
| Northeast coast of Brazil | | | | | | |
| Coastal processes | | | | | | |
| Lithified stone reefs | | | | | | |
| Beach-rock barriers | | | | | | |

DD FORM 1473 (BACK)
1 NOV 65

S/N 0101-807-6821